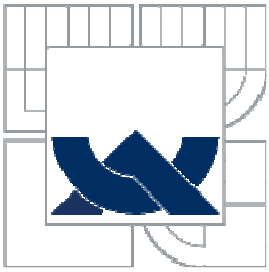

VYSOKÉ UČENÍ TECHNICKÉ V BRNĚ
BRNO UNIVERSITY OF TECHNOLOGY

FAKULTA CHEMICKÁ
CENTRUM MATERIÁLOVÉHO VÝZKUMU

FACULTY OF CHEMISTRY
MATERIALS RESEARCH CENTRE

FOTOGENERACE NÁBOJE V ORGANICKÝCH POLOVODIČÍCH

PHOTOGENERATION OF CHARGE CARRIERS IN ORGANIC SEMICONDUCTORS

DIZERTAČNÍ PRÁCE
PH. D. THESIS

AUTOR PRÁCE — Ing. PATRICIE HEINRICHOVÁ
AUTHOR

VEDOUCÍ PRÁCE — Prof. Ing. MARTIN WEITER Ph. D.
SUPERVISOR

BRNO 2014

Vysoké učení technické v Brně
Fakulta chemická
Purkyňova 464/118, 61200 Brno 12

Zadání dizertační práce

Číslo dizertační práce:	**FCH-DIZ0099/2013**	Akademický rok: **2013/2014**
Ústav:	Centrum materiálového výzkumu	
Student(ka):	**Ing. Patricie Heinrichová**	
Studijní program:	Fyzikální chemie (P1404)	
Studijní obor:	Fyzikální chemie (1404V001)	
Vedoucí práce	**prof. Ing. Martin Weiter, Ph.D.**	
Konzultanti:		

Název dizertační práce:

Fotogenerace náboje v organických polovodičích

Zadání dizertační práce:

Cílem práce je studium procesů fotogenerace elektrického náboje v organických polymerních polovodičích. Pozornost bude zaměřena na současné polymerní materiály s fotovodivými vlastnostmi, které jsou vhodné pro aplikaci v organické fotovoltaice. Procesy fotogenerace náboje v těchto materiálech budou studovány s využitím optických a optoelektrických metod, zejména metodami studia fluorescenčního zhášení v donor-akceptorových systémech polymer-fulerén. Dále budou z vybraných materiálů připraveny organické solární články a bude studována jejich fotovolatická účinnost a další parametry ve vztahu k použitým polymerním materiálům.

Termín odevzdání dizertační práce: 31.8.2014

Dizertační práce se odevzdává v děkanem stanoveném počtu exemplářů na sekretariát ústavu a v elektronické formě vedoucímu dizertační práce. Toto zadání je přílohou dizertační práce.

Ing. Patricie Heinrichová Student(ka)	prof. Ing. Martin Weiter, Ph.D. Vedoucí práce	prof. Ing. Miloslav Pekař, CSc. Ředitel ústavu

V Brně, dne 1.2.2013

prof. Ing. Martin Weiter, Ph.D.
Děkan fakulty

ABSTRAKT

S nástupem komerční výroby organických solárních článků roste i zájem o detailní poznání základních elektronových procesů souvisejících s fotogenerací náboje, které umožní dosáhnout vyšší účinnosti fotovoltaické konverze. Tato práce se zabývá studiem fotogenerace nosičů náboje v organických polovodičích, především v π-konjugovaných polymerních materiálech. První část práce popisuje současné poznatky o fotogeneraci nosičů náboje v polymerních solárních článcích. Následuje experimentální a výsledková část, která se věnuje studiu polymerních solárních článků připravených z elektron donorních polymerů MDMO-PPV, Tg-PPV, PCDTBT a PCBTDPP a elektron akceptorních derivátů fullerenu $PC_{60}BM$ a $PC_{70}BM$. Výsledky práce jsou rozděleny do tří hlavních částí: 1) studium přenosu náboje mezi elektron donorním a elektron akceptorním materiálem optickými metodami, 2) studium přenosu náboje mezi elektron donorním a elektron akceptorním materiálem optoelektrickými metodami a 3) vývoj organických solárních článků na flexibilních substrátech, zabývající se z velké části depozičními metodami tenkých vrstev funkčních materiálů.

ABSTRACT

The interest in the detail knowledge about elementary electronic processes during photogeneration of charge carriers, which allow achieving higher efficiency of organic solar cells, grows with advent of the commercial organic solar cells production. The thesis is focused on study of photogeneration of charge carriers in organic semiconductors, especially in π-conjugated polymer materials. First part of the thesis summarized state of the art in studies of photogeneration of charge carriers in polymer solar cells. Subsequent experimental and results part are focused on study of polymeric solar cells prepared from electron donor polymers MDMO-PPV, Tg-PPV, PCDTBT and PCBTDPP and electron acceptor derivates of fullerenes $PC_{60}BM$ and $PC_{70}BM$. Results of the thesis are divided in tree main parts: 1) study of charge transfer between electron donor and electron acceptor materials by

optical methods, 2) study of charge transfer between electron donor and electron acceptor materials by optoelectrical methods and 3) development of organic solar cells on flexible substrates. The last part is focused largely on deposition methods of active materials thin layer.

KLÍČOVÁ SLOVA

π-konjugované polymery, fullereny, absorpce světla, optoelektrické vlastnosti, fotogenerace nábojů, textilní solární články, organická fotovoltaika, přenos náboje, stavy s přenosem náboje, přenos energie

KEYWORDS

π-conjugated polymers, fullerenes, light absorption, optoelectrical properties, charge photogeneration, textile solar cells, organic photovoltaics, charge transfer, charge transfer states, energy transfer

HEINRICHOVÁ, P. *Fotogenerace náboje v organických polovodičích*. Brno: Vysoké učení technické v Brně, Fakulta chemická, 2014. 172 s. Vedoucí dizertační práce Prof. Ing. Martin Weiter, Ph.D.

PROHLÁŠENÍ

Prohlašuji, že jsem diplomovou práci vypracovala samostatně a že všechny použité literární zdroje jsem správně a úplně citovala. Diplomová práce je z hlediska obsahu majetkem Fakulty chemické VUT v Brně a může být využita ke komerčním účelům jen se souhlasem vedoucího diplomové práce a děkana FCH VUT.

.....

podpis studenta

Poděkování:

Poděkovaní patří mnoha lidem, zejména mému vedoucímu Prof. Martinu Weiterovi za vytvoření kvalitních podmínek pro doktorské studium a trpělivost při konzultacích disertační práce, dále pak Doc. Ivaylovi Zhivkovi a Doc. Martinu Valovi za odborné konzultace, Dr. Petru Dzikovi za přípravu tištěných tenkých vrstev, Doc. Ottu Salykovi za přípravu vakuově deponovaných vrstev, Ing. Veronice Schmiedové za elipsometrické měření a dalším členům týmu Organické elektroniky za dobrou spolupráci. A konečně i mému milému Kirimu a dědovi Heinrichovi za podporu.

CONTENT

1 INTRODUCTION

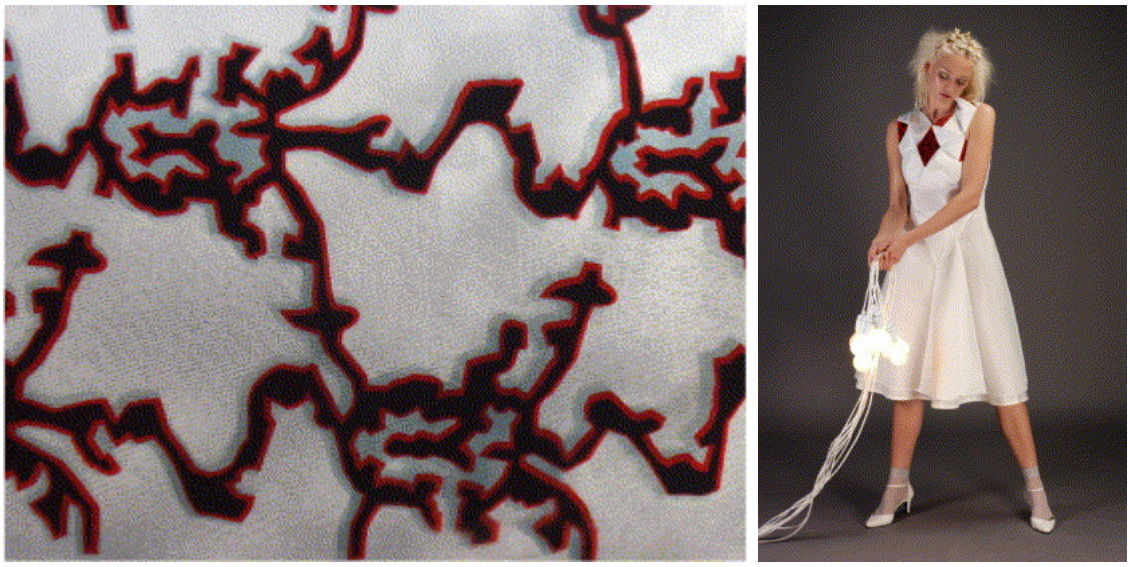

Fig. 1: Illustration photos of design proposals of textile solar cell implementation in clothes. Designed by Tine Hertz and Maria Langberg from Danmarks Designskole (Copenhagen, Denmark) [1]

Photovoltaic solar energy conversion is widely studied as one of the sources of renewable energy. Thin layer organic solar cells are alternative to silicon solar cells, and possess many desirable features, which silicon solar cells cannot offer. Organic solar cells are cheaper to production, easier to dispose at the end of life, can be made mechanically flexible, light transparent and can also work in the interiors thanks to their higher light absorption efficiency. On the other hand disadvantages of organic solar cells are the lower lifetime and lower energy conversion efficiency in comparison with the silicon solar cells.

Nevertheless, the interest in the development of organic solar cells grows with the possibility of their new applications. As one of many examples may serve the solar cells incorporation into textiles as *Fig. 1* and *Fig. 2* illustrate. These can be used for smart clothes, luggage, as energy source elements in houses or transportation vessels' interiors, etc.

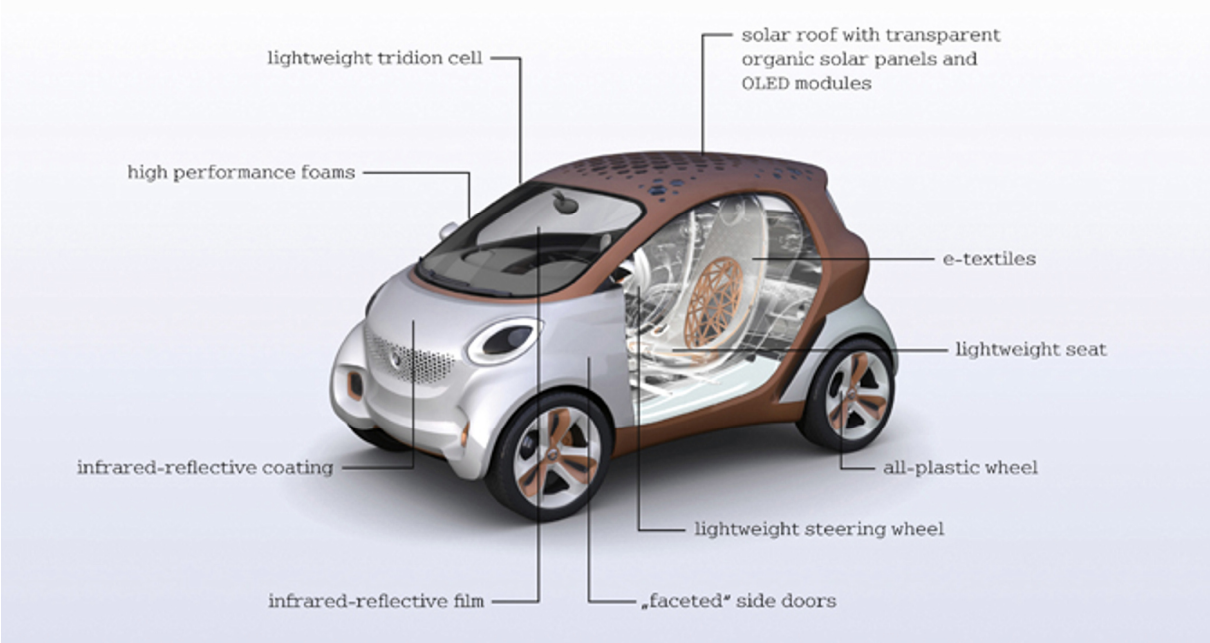

Fig. 2: Concept car using organic photovoltaic and other organic electronic devices [2].

Photogeneration efficiency of organic solar cells is currently achieving 10 % [3]. These data are coming as well from academic laboratories as from privately held companies. For example, we can mention companies such as Heliatek, GmbH; Mitsubishi Chemical, Co.; Polyera, Co.; Solamer Energy, Inc and other [4–6], who presented the most significant progress in organic photovoltaic development in the last four years. These facts show on the overall growing interest in commercial fabrication of organic solar cells and give the reasons, why we deal with research of organic solar cells.

1.1 Goals of the Thesis

This thesis is focused on:

- Basic research of photogeneration processes in polymeric solar cells primarily focused on study of charge transfer processes and charge transfer states.

- Applied research, focused on development of organic solar cell on textile substrates realized in the framework of FP7 project Dephotex.

1.2 Methodological Approach

Charge transfer and energy transfer processes were investigated by optical and optoelectrical methods to elucidate their contribution to photovoltaic phenomena in polymeric solar cells.

Fluorescence measurements were used for investigation of charge transfer and energy transfer processes. The results of fluorescence quenching experiments and detection of charge transfer states by measurement of near infrared fluorescence are presented.

Charge transfer states and their influence on photovoltaic conversion efficiency were further studied by optoelectrical methods: spectrally resolved photocurrent measurements and electroluminescence measurements.

The applied research focused on development of organic photovoltaic devices on textile substrate was realized in international cooperation with 15 European partners in the framework of the FP7 the project DEPHOTEX (NMP Theme – Nanosciences, Nanotechnologies, Materials & New Production Technologies). Dephotex project, research on photovoltaic textiles based on novel fibres was carried out for 3 years (since November 2008 to October 2011). This work involved primarily optimization of thin layers deposition and therefore this part of work is focused largely on comparison of properties of optoelectrical devices prepared by spin-coating, inkjet print and electrophoretic deposition.

2 ORGANIC SOLAR CELLS

2.1 Working Principle

Organic solar cells usually consists of an active layer, two transport layers for both types of charges and finally of electrodes. General scheme of organic photovoltaic cell is shown on *Fig. 3*.

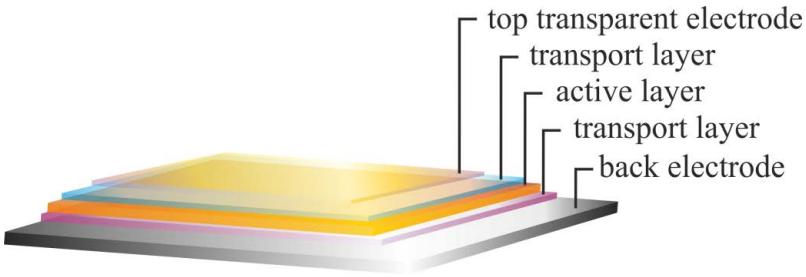

Fig. 3: general structure of organic solar cells which consist of active layer, charge transport layers and electrodes.

The charge carriers are generated in the active layer and then selectively transported by transport layers to the electrodes. One of the electrodes has to be transparent for light.

Electron donors

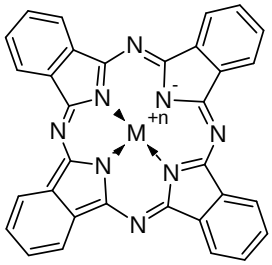

phtalocyanine

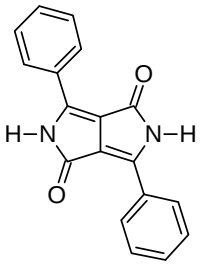

diphenyl-diketopyrrolo-pyrrole

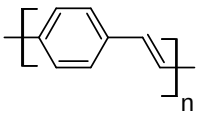

poly(para-phenylenevinylene)

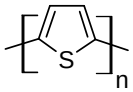

poly(thiophene)

Electron acceptors

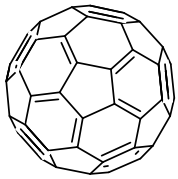

fullerene

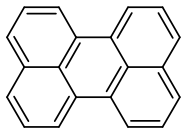

perylene

Fig. 4: Examples of electron donor and electron acceptor materials.

The active layer is consisting of electron donor and electron acceptor materials. Examples of some materials for organic photovoltaics are depicted in the *Fig.* 4. Both low-molecular and polymeric materials are studied. Low-molecular-weight materials have presented generally higher overall photo- and chemical stability while polymeric materials have shown better film-forming properties. Structures of active layers are illustrated on *Fig.* 5.

These materials may be arranged as bilayer structures (*Fig. 5A*) or as disordered blends in a single layer so called bulk heterojunction structure (*Fig. 5B*). There exist also possibilities of preparation of more assembled heterojunction structures [3] as presented in (*Fig. 5C*).

Fig. 5: Possible arrangement of electron donor and electron acceptor materials in active layer: A) bilayer, B) disordered bulk heterojunction and C) ordered bulk heterojunction.

Photogenerated free charge carriers are transported from the active layer through electron or hole transport layers to the respective electrodes. Transport layers are used for achieving the necessary lower energy barrier between active layer and electrodes. Hole transport layers is typically prepared from PEDOT:PSS (poly(3,4-ethylenedioxythiophene):poly(styrenesulfonate)). Alternatives of hole transport layer materials are for example graphen oxide [8], NiO [9], V_2O_5 [10], MoO_3 [11] etc. Electron transport layers can be created by TiO_2 [11], ZnO [12, 13] and others [14].

Electrodes are chosen according to their work function, i.e. to their ability to create electrical potential suitable for separation of electron-hole pairs. Frequently used materials are aluminium, silver and gold. One of the electrodes in the organic solar cell needs to be transparent for light, the generally utilized material is ITO (indium tin oxide). Further transparent

materials for electrodes are FTO (fluorine-doped tin oxide) or AZO (aluminium-zinc oxide) [15]. Unfortunately, electrodes from these materials present only limited mechanical flexibility. Moreover indium is considered to be a very rare element and not so easily available. For these reasons other transparent and more flexible materials are studied such as e.g. graphene [16, 17], thin layers of metals such as gold [18] or combined metals electrodes [19, 20] or metal grips [21, 22]. Consequently, organic electrodes are searched, in this case the PEDOT polymer [23–28] serves as transparent electrode.

All described layers of organic solar cells have to be well combined and optimized for achievement of high efficiency of photogeneration. This is generally a complex task and deep research of function principles of organic solar cells is necessary for development of high efficient devices. It is the reason, why following chapters deals with description of charge carriers photogeneration in polymer:fullerene solar cells, which are studied in the following thesis.

2.2 Charge Photogeneration

The primary process in organic solar cells is the conversion of incident solar energy to separated charge carriers. The process is complex and consists of series of sequential steps as illustrated *Fig. 6.*

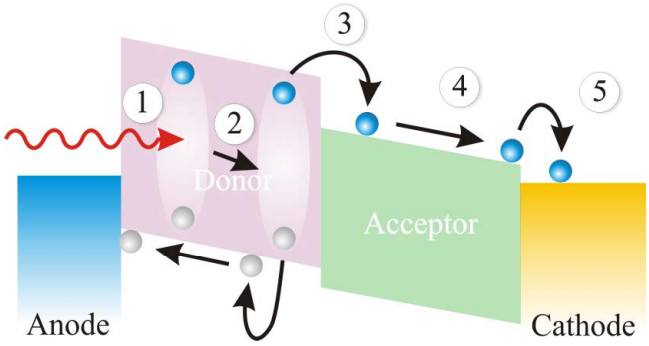

Fig. 6: Scheme of the charge photogeneration and transport processes in organic solar cell, where: 1 – photon absorption by electron donor, 2 – exciton migration to interphase of donor and acceptor, 3 – charge transfer between electron donor and acceptor with separation of free charge carriers, 4 – charge carriers transport to electrodes, 5 – charge carriers collection on electrode.

These steps are:

1) absorption of photon with energy $h\nu$ by electron donor D and generation of an exciton D^*

$$D \xrightarrow{h\nu} D^*, \quad (1)$$

2) exciton diffusion to electron donor and electron acceptor interphase $[D^*A]$

$$D^* + A \longrightarrow [D^*A], \quad (2)$$

3) charge transfer (CT) of electron from donor to acceptor resulting in generation of Coulombically bounded electron-hole pair $[D^{\bullet+}A^{\bullet-}]$ in CT state.

$$[D^*A] \longrightarrow [D^{\bullet+}A^{\bullet-}], \quad (3)$$

which has to be dissociated onto free charge carriers – hole on donor $D^{\bullet+}$ and electron on acceptor $A^{\bullet-}$,

$$[D^{\bullet+}A^{\bullet-}] \longrightarrow D^{\bullet+} + A^{\bullet-}. \quad (4)$$

4) carriers' transport,

5) collection of charge carriers on the electrodes.

Fig. 7 shows the energy diagram of each step of charge carrier photogeneration [29, 30]. The diagram illustrates exciton creation on electron donor molecule as an electron transition from singlet ground S_0 state to singlet excited S_1 after absorption energy νh, where ν is frequency of incident light and h is Planck constant. A triplet excited state T_1 is localized between energy level S_0 and S_1. Interaction between exciton and electron acceptor leads to hot charge transfer state (CT^*), which can thermally relax with kinetic constant k_{IC} to the lowest energy charge transfer state (CT). During the final step of photogeneration, free separated charge carriers (CS)

with energy level CS are created. Charge carriers can be excited into the CS^* state, as it is depicted in the diagram on the *Fig. 7*. There we speak about free hot charge carriers, which can thermally relax. The diagram shows creation of free charge carriers with kinetic constant k_{SC} from low CT state or with k_{SC}^* from hot CT^* state. Competing processes are not drawn in the diagram.

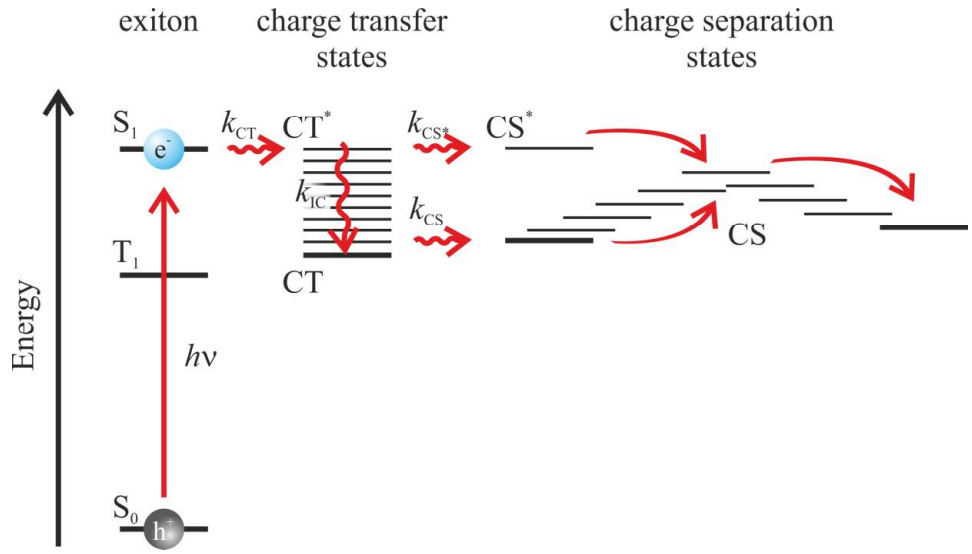

Fig. 7: Energy state diagram describing the photo-induced charge-carrier formation mechanism in an organic solar cell [29, 30].

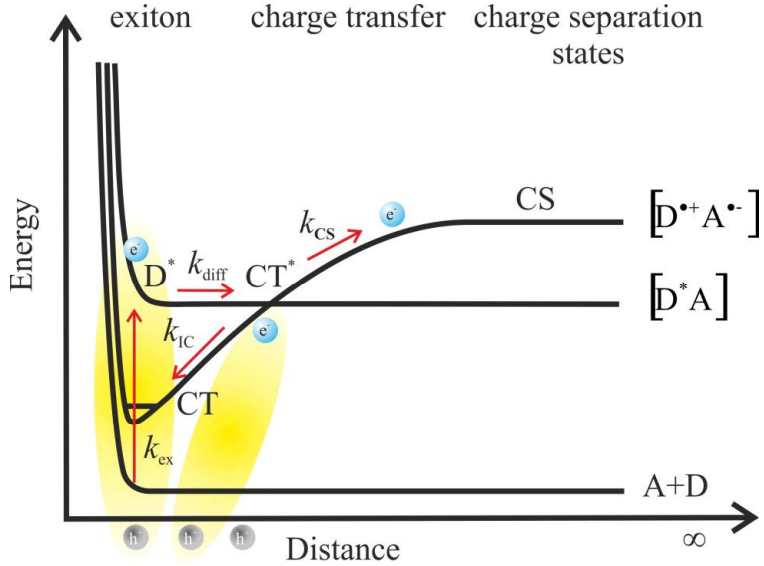

Fig. 8: Potential energy diagram for the species involved in charge photogeneration at donor acceptor interphase. Re-drawn according to [31].

The different graphical representation of charge photogeneration is depicted in the *Fig. 8* [30, 31]. This diagram sheds light onto the processes from the physical point of view in terms of energy and the charge distance. There is shown the exciton diffusion to electron acceptor interphase described via kinetic constant k_{diff} . Moreover, the diagram illustrates grow of the distance between electron and hole after their dissociation.

The individual steps of charge photogeneration are described in deeper details in the following chapters.

2.2.1 Photon Absorption and Exciton Formation

2.2.1.1 Molecular Level

The photoexcitation of a π-conjugated molecule by incident light generates a singlet excited state consisting of continuously Coulombically bonded electron-hole pair. This state is called a singlet exciton. The creation of long living geminate pairs is preferred process in the organic solid prior to fast free charge carrier generation, which is predominated in inorganic semiconductors. It is due to the low dielectric constants of organic semiconductors, the presence of significant electron-lattice (phonon) interaction and electron-electron correlation effect [32].

Energy needed for the generation of a molecule exciton by Franck Condon transition $\mathrm{S}_1 \leftarrow \mathrm{S}_0$ has to be equal or higher as the band gap E_{g}, which is defined by means of energy difference of the highest occupied molecular orbital (HOMO) and the lowest unoccupied molecular orbital (LUMO). This can be described by an equation:

$$E_{\mathrm{g}} \leq \frac{hc}{\lambda_{\mathrm{ex}}}, \tag{5}$$

where λ_{ex} is the wavelength of incident light, h is Planck constant and c is the speed of light. The band gap of polymers is influenced by conjugated length, which is usually smaller than the actual length of the polymer

backbone. It is caused by polymer chain conformations, which is result of many conditions: chains intermolecular interaction, polymer-solvent intermolecular interaction, the layer preparation conditions, post treatment, etc. [33–35].

The influence of polymer backbone length on the width of band gap was discovered by studying of oligomers with varying number of monomer units [34, 35]. Research of influence of polymer conformation and aggregation onto the band gap by means of the observations of optical properties were conducted too [36–39]. All the phenomena influencing band gap can be expressed by the term introduced by Roncali [40], which describes band gap energy E_g as a sum of energy contributions:

$$E_g = E_{bb} + E_{dist} + E_{sub} + E_{solv} + E_{cryst}, \quad (6)$$

where E_{bb} is the electronic transition energy of the unsubstantiated planar backbone, E_{dist} the hypsochromic (blue) energy shift induced by distortion from planarity in the equilibrium geometry, E_{sub} the energy shift induced by the positive/negative inductive or resonance effects of chemical substituents (in most cases a negative number), E_{solv} the bathochromic (red) solvent shift compared to the value in vacuum, and E_{cryst} the bathochromic shift induced by intermolecular interactions in the solid state.

Optical band gaps of conjugated polymers are often not well matched to the solar emission spectrum. Only partial fraction of solar radiation is absorbed, usually from the wavelength range from 400 nm to 650 nm. This fact is presented on the *Fig. 9*, showing absorption spectrum of the most studied conjugated polymers: MDMO-PPV (poly[2-methoxy-5-(3′,7′-dimethyloctyloxy)-1,4-phenylenevinylene]) with $E_g = 2.2$ eV and P3HT (poly(3-hexylthiophene-2,5-diyl)) $E_g = 1.9$ eV together with the AM 1.5 standard solar spectrum [29, 41]. For this reason low band gap polymers are synthesized and combined with higher band gap materials in tandem solar cells, such results have been already published for example in papers [45–47]. On other hand organic

semiconductors show high absorption coefficients in the 10^7 m^{-1} order. Therefore thickness of organic solar cells is usually in range of hundred nanometres, while thickness of silicon solar cells is a few micrometers [47].

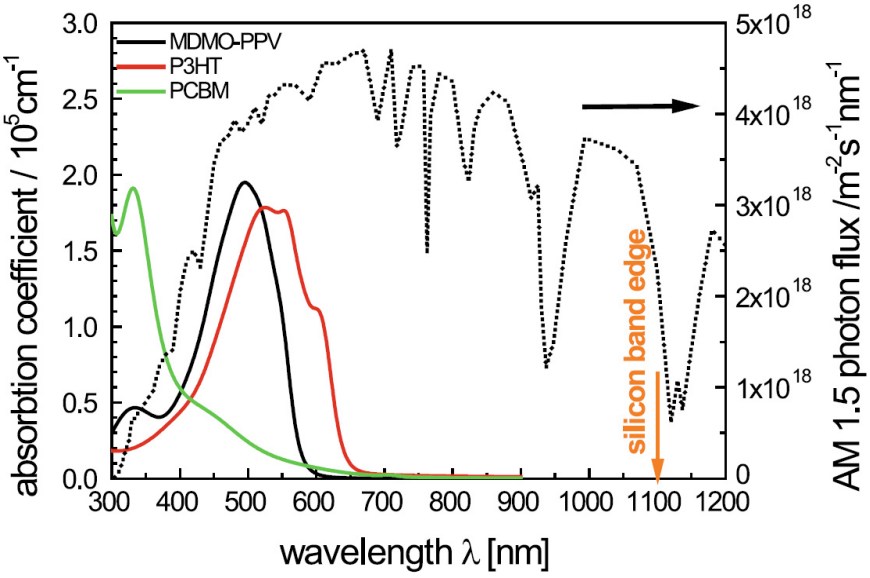

Fig. 9: Absorption coefficients of two conjugated polymers (MDMO-PPV and P3HT) and a fullerene derivative PCBM, which represent the most often studied polymer–fullerene systems, are shown together with the AM 1.5 standard of solar spectrum [41].

2.2.1.2 Thin Layers

Efficiency of the light absorption is also dependent on the layer thickness. Because layer thicknesses of functional materials usually vary between tens and hundreds of nm, light interference plays significant role on light absorption.

The situation is illustrated by *Fig. 10*, where the simple layer of material described as medium 1, which is incident on interface 1 by ray of light under the angle ϕ_0 is shown. Part of light is reflected. Reflection R_λ can be quantified employing Fresnel's equations [49]. The unreflected light travels to medium 1 at angle ϕ_1 according Snell's law. The light passing through the material absorbed according to term:

$$I = I_0 \exp(-\alpha d)\,, \tag{7}$$

where I_0 is initial intensity of light, α is absorption coefficient and d is distance. The rest of the light is again particularly reflected back to medium 1 under angle ϕ_1 on the next interface 2 and part of light is going through to the next optical medium 2 under angle ϕ_2 as transmitted light T_λ. The process is repeated until all the light is absorbed or transmitted from medium 1. Reflected light ray in medium 1 interferes with other rays.

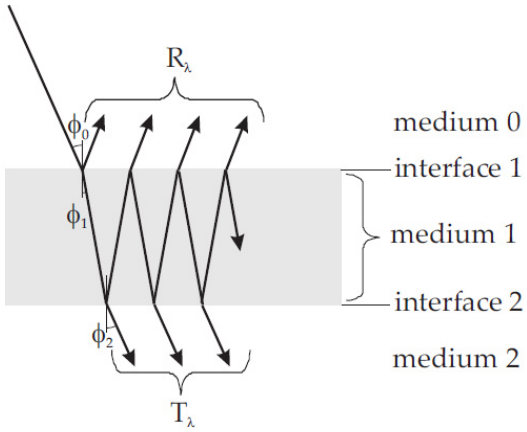

Fig. 10: Cross-section of a simple multilayer system containing two interfaces. The internally reflecting sub-rays are present. [49]

Since organic solar cells are usually prepared as multilayer ones, the optimization of layers' thicknesses is a more complex process, where the transfer matrix is used for the calculation of absorbed light amount [49]. The possible interference also leads to the dependence of light absorption efficiency on angle of incident light [50].

More works were focused on the optimization of light absorption in active layers [51, 52]. Remarkable results were published by Kim et al [53], when the authors used a thin layer of TiO_2 under the back Al electrode (see *Fig. 11*), as optical spacer which distributes maximum of light intensity to the active layer. This concept was also subjected to patent [54]. On the other hand, researchers such as Andersson et al. [55] opposed the utilization of optical spacer, while they calculated that the light absorption enhancement is negligible. However, some further materials were studied as optical spacers, e.g. ZnO_2 [56] or BCP (bathocuproine) [57].

Other ways of light absorption enhancement are studied in terms of using of scattering and light traps elements. The micro lenses [58], surface texturing [59], plasmon [60] and v-shape configuration [61] can be served as prospective examples.

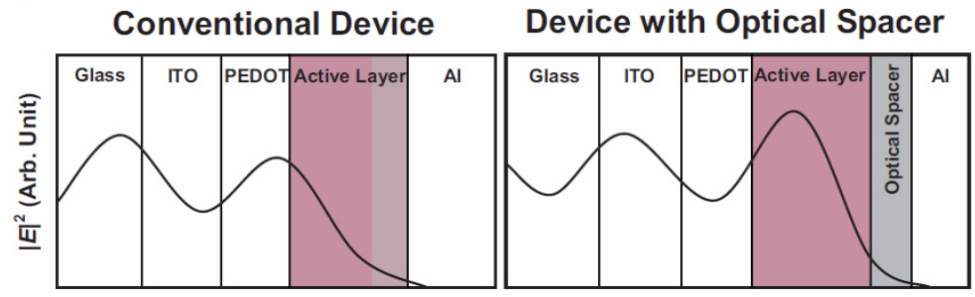

Fig. 11: Example of light absorption optimization of multilayer structure of organic solar cell utilizing optical spacers, which shifts maximum of light intensity (expressed as squared optical electric field strength $|E^2|$ represented by curve from PEDOT layer to active layer) [53].

Theoretical model combining optical and electrical approach for organic solar cells' active layers both with classical or inverted geometry and of tandem solar cells was published by Kotlarski and Blom [62]. The maximization of light absorption by the active layer itself does not guarantee the solar cell efficiency. Correct localization of charge generation in the active layer is also tremendously important due to the often unbalanced charge transports, which can lead to accumulation of slower charge carriers in active layer and therefore to recombination [62].

2.2.2 Excitons

Absorption of light by polymeric donors leads to single exciton formation, the strongly bonded electron-hole pair called Frenkel exciton. These excitons are delocalized only over a few monomer units [63]. According to theoretical and experimental investigations of Knupfer et al. [64], the size of polymeric excitons is corresponding to the conjugated length. The polymeric excitons are usually localized in the intra-molecular scale [65], however some cases of interchain excitons were reported too [66].

Exciton binding energy varies between 0.5 eV and 1 eV [67, 68] and is proportional to the electron-hole Coulomb attraction *E*:

$$E = \frac{e^2}{4\pi\varepsilon_0\varepsilon_r\langle r\rangle}, \tag{8}$$

where *e* is elementary charge, ε_0 is the permittivity *in vacuo* and ε_r the relative permittivity of material, relatively low for organic materials ($\varepsilon_r \approx 2$–4) and $\langle r\rangle$ is the hole-electron distance.

Typical lifetime of excitons in π-conjugated polymers lies between 100 ps and 1 ns [30]. During exciton existence, it can diffuse ideally through material on the interphase of donor and acceptor in the solar cell. Since excitons are neutral species, their motion is independent on the electric field. The diffusion length of excitons in conjugated polymers varies between 5 nm and 14 nm [69]. As well as the exciton life time and the diffusion length are dependent on the polymer conformation driven by layer morphology, impurities presence, etc. [70, 71].

Excitons may be relaxed by radiative transitions, which means by fluorescence emission.

$$S_1 \rightarrow S_0 + h\nu \tag{9}$$

This exciton extinction is considered to be an important phenomenon, because the study of fluorescence allows the observation of exciton lifetime, processes as exciton separation by charge transfer between donor and acceptor [72–74] and exciton diffusion [69, 75]. Electron-hole pair binding energy can be experimentally determined by measurement of photoluminescence quenching by electric fields [76].

Quantum yield of fluorescence ϕ_f quantifies the efficiency of fluorescence intensity. It is defined as the ratio of the number of photons emitted to the

number of photons absorbed and can be described by means of kinetic constants [77]:

$$\phi_f = \frac{k_r}{k_r + k_{nr}}, \tag{10}$$

where k_r is kinetic constant of radiative decay of excitons and k_{nr} is kinetic constant of non-radiative decay of excitons. Reciprocal value of k_r is the natural lifetime of exciton, which the exciton performs in the absence of non-radiative processes; else the exciton lifetime τ is equal:

$$\tau = \frac{1}{k_r + k_{nr}}. \tag{11}$$

Non-radiative pathways can be classified according to their dependence on excitation intensity [63]. In the first step there exist excitation intensity independent pathways [77, 78].

- Internal conversion

$$S_1 \rightarrow S_0 + \text{heat} \tag{12}$$

In most cases excitons decay this way due to the phonon interaction to the ground state. Characteristic time of the process is from 10^{-11} to 10^{-9} s. This process can be suppressed by cooling of the samples.

- Intersystem crossing

$$S_1 \rightarrow T_1 \tag{13}$$

Intersystem crossing is a spin forbidden transfer which leads to long living triplet excitons. Characteristic time constant of the process varies between 10^{-10} and 10^{-8} s. Energy of the phosphorescence light is typically 0.7 eV lower compared to the energy of fluorescence light [79].

- Exciton dissociation to a charge pair:

$$S_1 \rightarrow S_0 + h^+ + e^- . \quad (14)$$

This process leads to direct charge generation in a pristine material. Separated charges are long-living, in the range of milliseconds and seconds. Anyway, direct photogeneration process is the less probable pathway for organic materials due to the strong Coulomb attraction between hole and electron in such a material as it was described above.

- Energy and charge transfer

These processes are thoroughly described in the following chapters, because they are essential for photovoltaic conversion of organic solar cells.

There exist also exciton decay pathways dependent on excitation intensity. Following processes are occurred when excitons are accumulated [63]:

- Singlet-singlet exciton annihilation

$$S_1 + S_1 \rightarrow S_0 + S_1^* , \quad (15)$$

or

$$S_1 + S_1 \rightarrow S_0 + e + h , \quad (16)$$

or

$$S_1 + S_1 \rightarrow T_1^* + T_1^* , \quad (17)$$

- Singlet-triplet exciton annihilation

$$S_1 + T_1 \rightarrow S_0 + T_1^* \quad (18)$$

- Triplet-triplet exciton annihilation

$$T_1 + T_1 \rightarrow S_0 + T_1^* \quad (19)$$

or

$$T_1 + T_1 \rightarrow S_0 + S_1^* \quad (20)$$

Exciton-exciton annihilation leads to the singlet or triplet exciton in higher vibronic-electronic state, which can decay radiatively. These processes result in observation of delayed fluorescence or phosphorescence [64].

Observation of delayed luminescence may be also caused by some other processes than exciton-exciton annihilation. For example the triplet-triplet annihilation was studied in contrast to the delayed fluorescence coming from recombined charge carriers [83]. The authors noted, that delayed fluorescence in thin layer of conjugated polymer is more possibly observed from charge carrier recombination than from triplet-triplet annihilation while in single chain it is *vice versa*. Moreover, delayed fluorescence coming from charge carriers' recombination can be decayed by electric field unlike from the delayed fluorescence from triplet-triplet annihilation [83].

Exciton-exciton annihilation also allows studying the diffusion length of the excitons as it was presented by Lewis et al. [87], when the authors observed change of exciton lifetime depending on the excitation density.

- Exciton-free charge carriers interaction

$$S_1 + \left(h^+, e^-\right) \rightarrow S_0 + \left(h^+, e^-\right)^* \quad (21)$$

In case of the insufficient transport of charge carriers to electrode, the charge carriers may collide with excitons, so they may be bimolecular quenched.

2.2.2.1 Energy Transfer

Energy transfer is caused by a quencher, which can be represented by chemical or structural defect.

$$S_1 + Q \rightarrow S_0 + Q^* \quad (22)$$

This effect was observed between donor and acceptor, when fluorescence of acceptor is detected instead of charge transfer and generation of charge carriers [30, 80].

Energy transfer can be realized by irradiative or non-irradiative pathway. Irradiation mechanism is caused by reabsorption of fluorescence emission of donor by acceptor and doesn't affect donor exciton lifetime. Non-irradiative energy transfer causes shorter donor exciton lifetime. There are two described mechanisms of non-radiative energy transfer: Förster resonance energy transfer and Dexter exchange energy transfer.

According to the Förster's theory [81] energy transfer rate is given by kinetic constant k_{ET}:

$$k_{ET} = \left(\frac{R_{RET}}{R} \right)^6 \tau_0^{-1}, \tag{23}$$

where τ_0 is the sum of radiative and non-radiative decay constants of the excited donor molecule in the absence of an acceptor, R is radius between donor and acceptor and R_{RET} is the Förster's radius, which can be predicted by equation:

$$R_{RET} = \left(\frac{9000 f^2 \ln 10}{128 \pi^5 N_A n_0^4} \phi_D \Omega \right)^{1/6}, \tag{24}$$

where f^2 is an orientational factor. In general case its value is 2/3. Term ϕ_D is a fluorescence yield of the donor, n_0 is the refraction index of environment (in solution it is of solvent), N_A is Avogadro's constant and Ω is spectral overlap integral between donor and acceptor, because mechanism assumes presence of dipole-dipole interaction of donor and acceptor. Its value is given by integral:

$$\Omega = \int \frac{\sigma_{fluor}^D(\nu) \alpha(\nu)}{\nu^4} d\nu, \tag{25}$$

where $\sigma^{D}_{fluor}(\nu)$ is the intersection of normalized fluorescence spectrum of donor with normalized absorption spectrum of acceptor (see example on *Fig.* 12). The term $\alpha(\nu)$ represents molar absorption coefficients of acceptor in $M \cdot cm^{-1}$ units. The integral is calculated over light energy expressed by wavenumbers in cm^{-1}.

Energy transfer is also possible in the triplet excited state. Kinetics of the process is described by the Dexter theory [81] based on overlapping of orbitals. The Dexter energy transfer occurs over a donor and acceptor distance shorter as the Förster energy transfer. The distance needs to be in order of 0.5 to 1 nm, which is one order of magnitude less as for Förster energy transfer. Electrons exchange mechanism is expected, when acceptor gives less energetic electron to donor and receives more energetic electron of donor [63].

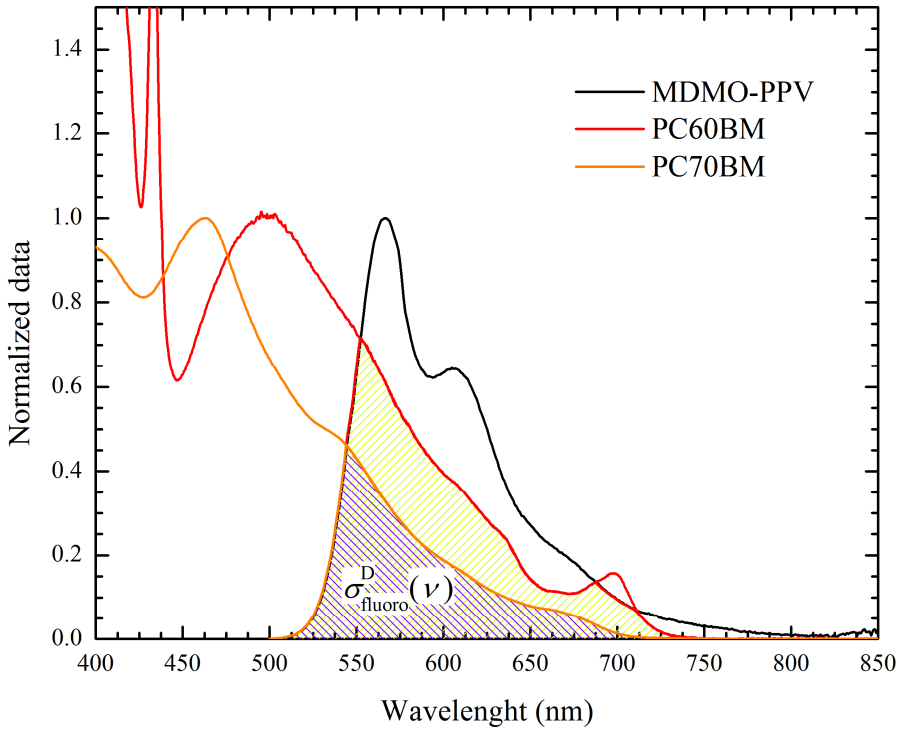

Fig. 12: Spectral overlap $\sigma^{D}_{fluor}(\nu)$ between normalized fluorescence spectrum of MDMO-PPV and normalized absorption spectra of two types of fullerene acceptors $PC_{60}BM$ and $PC_{70}BM$.

Energy transfer contributes to photovoltaic effect by several ways. First exciton diffusion is realized through multiple Förster energy transfer [81, 82] and next energy transfer can contribute to charge transfer, when foregoes to hole transfer from ground states of acceptor to ground states of donor [85]. This mechanism represents an alternative photogeneration process, which was experimentally confirmed [83].

2.2.3 Charge Transfer

Charge transfer (CT) between exited electron donor and electron acceptor is the one of many possible pathways of excitons extinction as it was summarized before. The kinetics and dynamics of the process was described by Marcus' theory [88] of semi-classical non-adiabatic electron transfer. This theoretical approach expects the intimately mixture of donor and acceptor phases, which involves electron transfer in femtosecond time scale [30]. Femtosecond kinetics of charge transfer process was observed by ultrafast transient absorption measurements [89–91]. For this reason, the thermodynamically irreversible model of charge transfer is assumed [94].

The theory considers the reactant and product potential energy surface as the two intersecting harmonic oscillators as *Fig. 13* shows. Q labelled axis represents the reaction coordinate and axis E is energy. The reactant, excited donor-acceptor pair, has to achieve the intersection point representing the energy level and nuclear configuration necessary for the isoenergetic electron transfer. The activation energy barrier $\Delta G^{\dagger}$ is proportional to Gibbs free energy ΔG° and reorganization energy λ according to term:

$$\Delta G^{\dagger} = \frac{(\lambda + \Delta G^{\circ})^2}{4\lambda}. \tag{26}$$

The reorganization energy λ is the dissipative heat, which is realised after charge transfer, due to reorganization of donor and acceptor molecules geometry in equilibrium geometry after changes of their electronically

structures. Reorganization energy is given by inner λ_i and outer λ_o contributions.

$$\lambda = \lambda_i + \lambda_o \,. \tag{27}$$

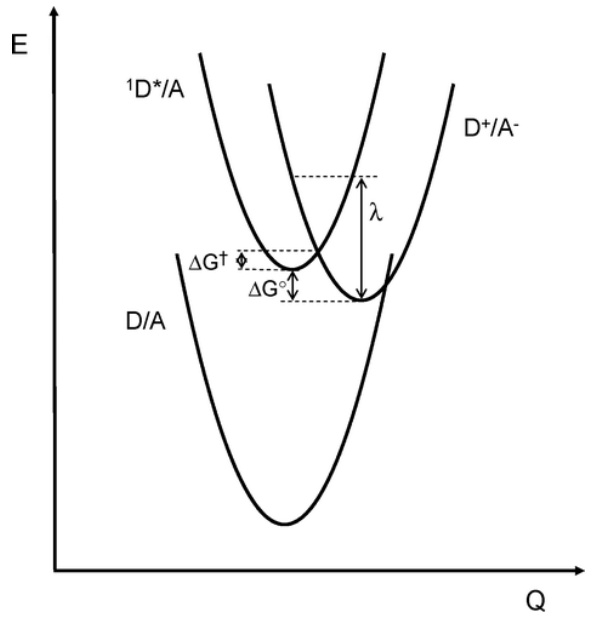

Fig. 13: Marcus' theory approaches onto electron transfer. The plot illustrates potential energy surface of donor-acceptor system labelled by D/A, of photoexcitated system $^1D^*/A$ and system after electron transfer D^+/A^-. $\Delta G°$ is Gibbs free energy, $\Delta G^\dagger$ is the energy activation barrier and the point of intersection between the two surfaces and λ is the reorganization energy [30].

Inner contribution λ_i corresponds to intramolecular reorganization and can be determined by Huang-Rhys factor S_i, which describes electron-vibration (phonon) coupling.

$$\lambda_i = S_i \hbar\omega_i \,, \tag{28}$$

where $\hbar\omega_i$ is the energy of vibration mode. Other way of λ_i determination is the calculation from absolute electron energy values of donor and acceptor [92].

λ_o term is the reorganization energy of surround due to electronic and nuclear polarization and/or relaxation of the surrounding medium, e.g. contribution from solvent. This term is valid also for organic crystals due to

van der Waals weak interaction among organic molecules. Its value can be predicted by equation:

$$\lambda_o = \left(\frac{1}{R_D} + \frac{1}{R_A} 2 \sum_A \sum_D \frac{q_A q_D}{r_{DA}} \right) \left(\frac{1}{\varepsilon_{op}} - \frac{1}{\varepsilon_s} \right) \frac{e^2}{2} . \quad (29)$$

e is transferred charge, ε_{op} is optical dielectric constant of the medium, R_D and R_A are the effective radii of donor and acceptor. Values of both λ_i and λ_o are usually of the same order of magnitude [92].

Gibbs free energy $\Delta G°$ can be approximated by the difference between the ionization energy of the donor I_D and the electron affinity of acceptor A_A according to Rehm-Weller equation

$$\Delta G° = I_D - E_{gap\,D} - A_A - \frac{e^2}{4\pi\varepsilon r_{AD}} . \quad (30)$$

$E_{gap\,D}$ is the energy of band gap for $S_0 \rightarrow S_1$ transition of donor, r_{AD} is radius between donor and acceptor, ε is the static permittivity of surround [7, 93].

If the reorganization energy λ is equal to the Gibbs free energy $\Delta G°$ then the value of the rate of electron transfer will be maximal and polymer solar cells will then work optimally according to the theory [94].

The rate constant of electron transfer k_{eT} can be determined in terms of a Fermi's Golden rule [95] type of analysis:

$$k_{eT} = \frac{2\pi}{\hbar\sqrt{4\pi\lambda kT}} |V|^2 \exp\left(-\frac{(\lambda + \Delta G°)^2}{4\lambda kT} \right), \quad (31)$$

where the matrix element $|V|^2$ refers to the electronic coupling between the reactant and product states and it is poorly determinable for unordered blends of materials. Strong coupling denotes the adiabatic limit [30, 94].

Electron-hole pair in CT state is still Coulombically bonded by energy from about 0.1 to 0.5 eV [30, 96]. This is still more than an order of magnitude larger than the thermal energy at the room temperature (kT at 300 K = 0.025 eV), however lower than the binding energy of excitons (0.5–1 eV) [67, 68].

CT state is a long living state. In case of PPV:$PC_{60}BM$, the lifetime of CT state was observed from microseconds to milliseconds orders depending on temperature [97]. For this reason it is spoken about the metastable charge transfer complex CTC [48, 98–99], with ground state CT and excited hot state CT*. Energy of CT states, given by the difference energy of donor HOMO level and acceptor LUMO level, are theoretically of the maximal values of open circuit voltage V_{OC} of organic solar cell with donor – acceptor system. Experimental value of V_{OC} is usually lower by correction factor ranging from 0.3 to 0.5 V due to recombination processes [48, 99]. Numerous models for prediction of V_{OC} from E_g and CT state [90, 100–104] were presented.

2.2.3.1 CT States and Their Experimental Observation

Similar as excitons on donor or acceptor molecule, excited CT states can be deactivated by several pathways (see *section* 2.2.2 *Excitons*). Extinction pathways of CT states are illustrated by *Fig. 14*. Dissociation of CT states in free charge carriers is the most desirable, because contributes to photovoltaic conversion. If CT states cannot be dissociated during their life time, they will be geminately recombined [48]. The loss process is either non-radiative or has a very low emission energy [70, 99, 100].

Example of fluorescence emission spectrum of CT states is presented in *Fig. 15* [70], where the energy of excited levels S_1 of donor (MDMO-PPV) and of acceptor ($PC_{60}BM$) molecules and energy level of CT states compared with measured fluorescence spectrum are shown. Emission peak with maximum energy about 1.3 eV (adequate to ≈ 955 nm) is the fluorescence of CT states.

Since the fluorescence emission of CT states is very weak, the CT states are investigated by methods based on studies of fluorescence quenching [73,

74, 83, 84]. This method is indirect and quenching can be simultaneously caused by other processes, for example by energy transfer [83, 85].

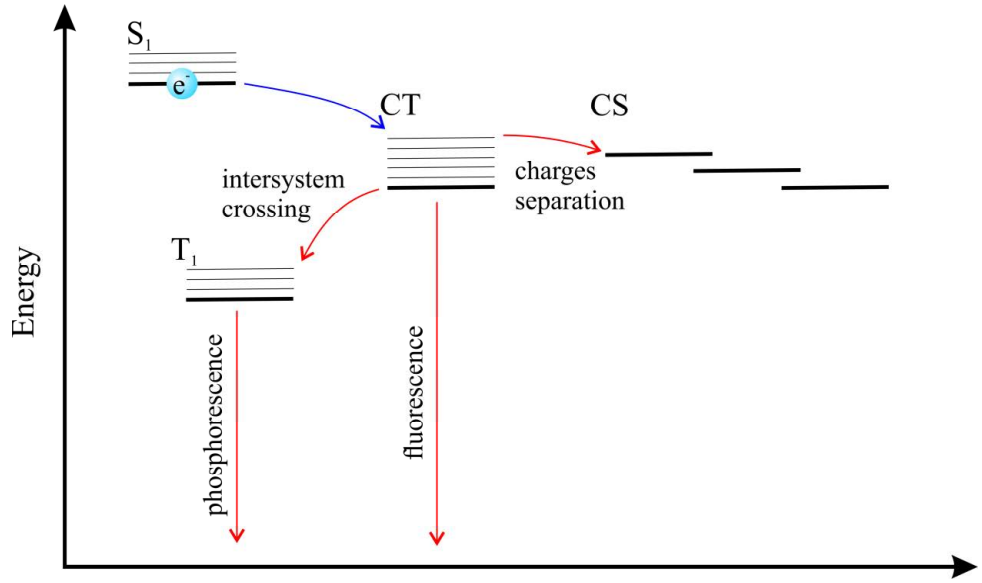

Fig. 14: Scheme of extinction pathways of CT excited state.

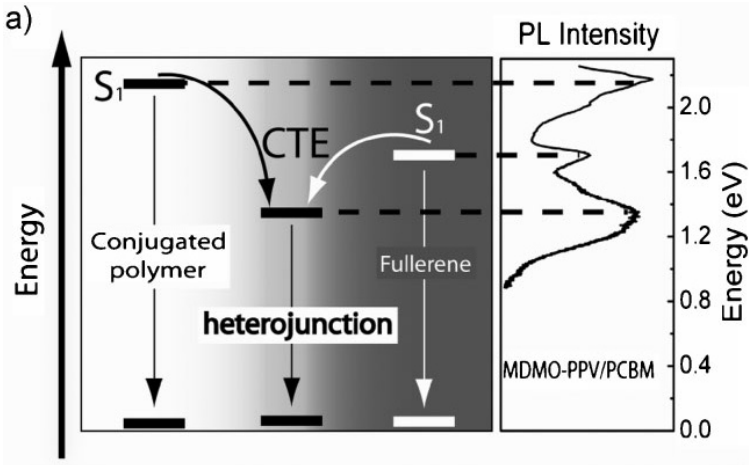

Fig. 15: Fluorescence emission spectrum of MDMO-PPV:$PC_{60}BM$ blend compared with energy levels of excited states of compounds and CT state [70].

Futher recombination process can take place trough electron transfer from CT state to triplet excited state T_1 of donor or acceptor. Such process is possible if triplet state performs smaller energy than the CT state [99].

Emissions spectra of CT states can be also observed by electroluminescence measurements on solar cells devices, as shown in *Fig. 16* [104, 105]. Electroluminescence is caused by bimolecular recombination of charge carriers injected in diode devices through electrodes. According to Tvingstedt, K. et al. [105], recombination takes place on the interface of donor and acceptor of heterojunction devices. The observed spectrum is thus created only by emission of CT states and not by pristine material, like in the case of fluorescence spectrum, which is the superposition of all emission states.

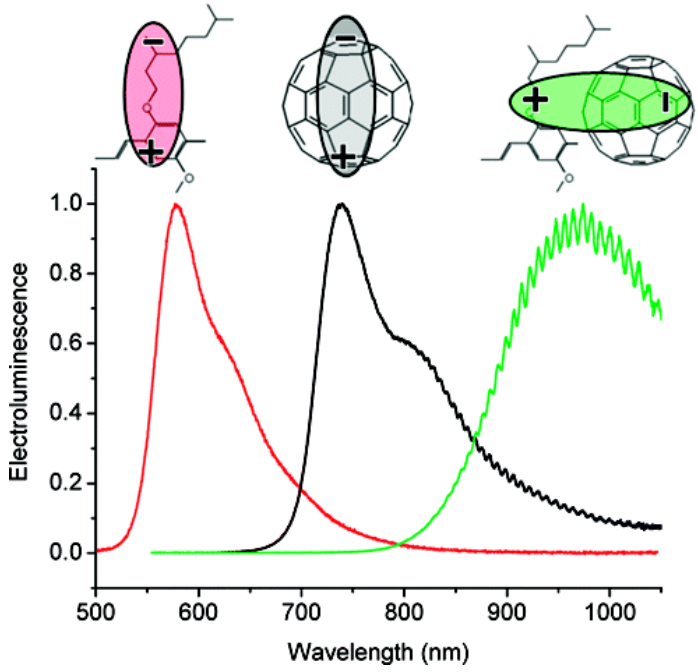

Fig. 16: Electroluminescence spectra of electron donating material MDMO-PPV, of electron accepting material $PC_{60}BM$ and of CT state formed as the result of interaction between both materials [105].

Further way to research the CT states is to investigate the CT ground states. In this context it is spoken about charge transfer complexes (CTC). Vandewal et al. [99] reported observation of CTC ground states band in external quantum efficiency (EQE) spectra obtained from Fourier-transform photocurrent spectra measurements. The example of EQE spectra is depicted in the left part of the *Fig. 17*, where spectra of MDMO-PPV, $PC_{60}BM$ and their blends are shown. The right part of the *Fig. 17* shows absorption

coefficients spectra which demonstrate very low absorption coefficient of CTC states [99].

Absorption coefficients of CTC were determined using photothermal deflection spectroscopy by Goris et al. [108]. Photothermal deflection spectroscopy is a very sensitive technique of measurements based on a local heating of the sample, which is caused by absorbed light of a given wavelength. Presented absorption spectra of MDMO-PPV, $PC_{60}BM$ and their blends (see *Fig. 17* on right) are very similar to EQE spectra described in previous paragraph. As further example of CTC absorption study, the work of Parashchuk et al. could be considered. The authors studied the absorption spectra of MEH-PPV (poly[(2-methoxy-5-(2′-ethylhexyloxy)-1, 4-phenylenevinylene]) and TNF (2, 4, 7-trinitro-fluorene-9-one) blend in thin layers and solutions [106].

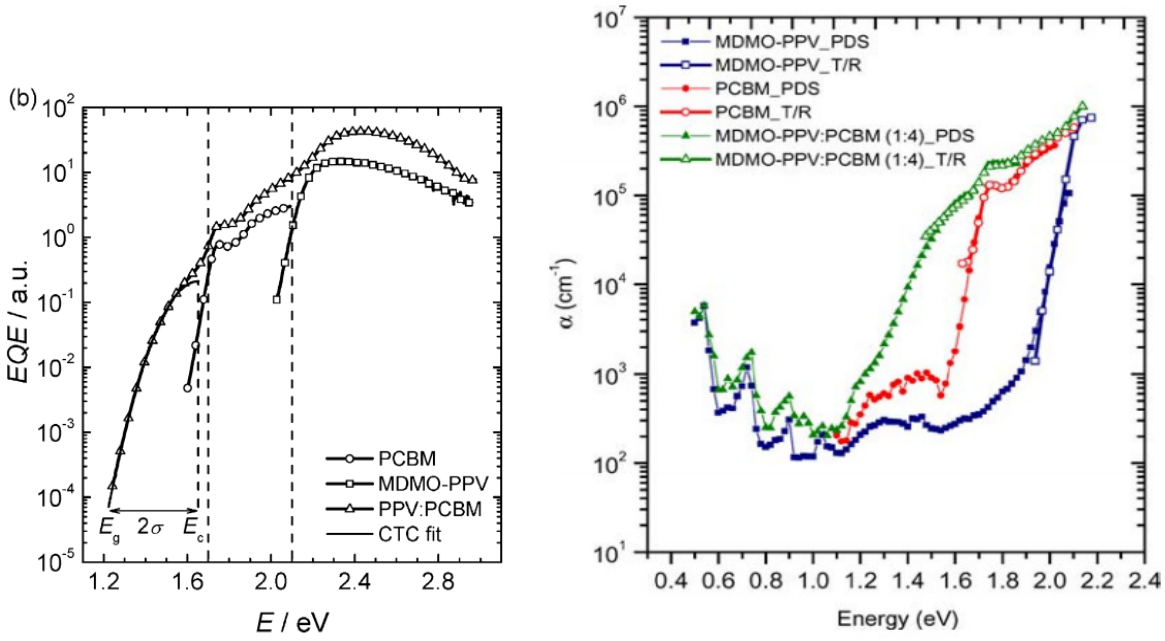

Fig. 17: On left: EQE spectra of MDMO-PPV, $PC_{60}BM$ and MDMO-PPV:$PC_{60}BM$ blend which shows low energy band of CT state [99]. On right: Absorption coefficients spectra of MDMO-PPV, $PC_{60}BM$ and MDMO-PPV:$PC_{60}BM$ blend which shows low energy band of CT state [107].

More complex investigation of CTC was reported by Benson-Smith et al. [107]. Authors studied poly(fluorene) polymers (TFMO, PFO, F8BT) blended with $PC_{60}BM$ employing the fluorescence quenching experiments, low energy

fluorescence measurements, photothermal deflection absorption studies, constant photocurrent method measurements and AFM (atomic force microscopy). They also compared results with equivalent observation on blend of MDMO-PPV:$PC_{60}BM$ and P3HT:$PC_{60}BM$ from other authors, see *Table 1*. However the table does not contain information about low energy emission of MDMO-PPV:$PC_{60}BM$ and P3HT:$PC_{60}BM$ blends. Such results were published two years later (2009) by Hallermann et al. [70] and *Table 1* is supplemented by this information.

Hallerman et al. [70] found correlation between the presence of low energy absorption caused by presence of CTC and efficiency of photocurrent generation. Similar correlation is valid between CTC low energy fluorescence and photocurrent generation. Moreover there is also important influence of ionization potentials of polymers on the efficiency of CTC dissociation, when high value of ionization potential acts against charge carrier dissociation.

Table 1: Summary of CT observation on different polymers and PCBM blends by PDS and PL measurements in contribution with morphology of layers, polymer ionization potential and photocurrent generation observation. Table is taken from source [107] and supplemented with results of [70] .

Polymer Film	**Low energy absorption (PDS)**	**Emission > 800 nm (PL)**	**Cluster in Morphology**	**Ionization potential (eV)**	**Photocurrent generation**
P3HT:$PC_{60}BM$	Yes	Yes	Yes	4.9	good
MDMO-PPV:$PC_{60}BM$	Yes	Yes	Yes	5.0	good
TFMO:$PC_{60}BM$	Yes	Yes	No	5.2	good
PFO:$PC_{60}BM$	No	No	Yes	5.8	poor
F8BT:$PC_{60}BM$	No	No	No	5.9	poor

CTC ground states may be also studied by the Raman spectrometry, which allows simultaneous investigation of the changes of molecular structure in CTC as was showed by Bruenvich et al. [109], when the charge transfer complex established between MEH-PPV and TNF was researched. The authors stated that polymer chain is planarized in CTC, but conjugated length stays unchanged [110].

2.2.4 Dissociation of the Geminated Pair

The last step of free charge carrier photogeneration is the dissociation of the geminated pair in the charge transfer state.

Strong indication for the existence of a bound electron-hole pair in polymer:fullerene blends is the field and temperature dependence of the photocurrent at the reverse bias [111].

Onsager-Braun theory [112, 113] is the most used theory for description of the electrical field-dependent charge dissociation of electron-hole pair into the free charges. The probability of dissociation of bounded electron-hole pair is given according to the model:

$$P(T,E,a) = \frac{k_D(E,T,a)}{k_D(E,T,a) + k_F}, \tag{32}$$

where k_F is the recombination rate constant of geminate pair assisted mainly by phonon-assisted non-radiative recombination [97]. k_D (E, T, a) stands for the rate constant of dissociation of an exciton at the donor acceptor interphase dependent on electrical field E, temperature T and initial donor-acceptor radius a as follows:

$$k_D = k_R \frac{3}{4\pi a^3} e^{-E_B/kT} \left[1 + b + \frac{b^2}{3} + \frac{b^3}{18} + \frac{b^4}{180} + \ldots \right], \tag{33}$$

where E_B is the binding energy, k is the Boltzmann constant and b is defined by equation:

$$b = \frac{e^3 E}{8\pi\varepsilon_r\varepsilon_0 k^2 T^2}, \tag{34}$$

where e is the elementary charge, ε_r is relative permittivity and ε_0 is permittivity of vacuum.

The model assumes the recombination of free charges through the establishing of the reverse CT state which can be dissociated or recombined

again [48]. The Onsager-Braun theory is however limited due to the not-accounting of the energetic or spatial disorders as well as the presence of hopping transport and in the lack of experimental proof of model predicted strong temperature dependence of dissociation [48]. For this reason, more other models and derivatives of Onsager-Braun model were reported [114]–[140]. There exists also concept of free charge carriers' generation from hot CT states [141].

2.3 Materials for Organic Solar cells

In previous chapters, the physical-chemical principles of organic solar cells function were described and it was shown that many processes (e.g. light absorption, charge transfer, etc.) need to happen in an efficient way to really gain a working OSC. Organic materials for photovoltaics can be chemically modified according to requirements resulting from models of organic solar cells function, but in many cases these modifications cause also unwanted properties like lesser stability, lower electrical conductivity, etc. In the following subsections examples of solved issues as well as the trends in search for novel highly efficient materials are reviewed.

2.3.1 Electron Donating Polymers

π-conjugated polymers are creating a broad group of electron donating materials. Electrical properties of polymers were studied already in the 1970's, when it was discovered that certain conjugated polymers, notably poly(sulphur nitride) and poly(acetylene), could be made highly conducting in the presence of dopants like iodine [117]. Alan J. Heeger, Alan MacDiarmid a Hideki Shirakawa described the nature of polymer conductivity and in 2000 they have been awarded by the Nobel Prize for this work [121]. As a next generation of conjugated polymers, the polyaromatic polymers emerged, such as the most known P3HT (poly(3-hexyl-thiophene)) and PPV (poly(*p*-phenylene vinylene), which are used as reference material in research until now.

The conductivity of polymers is driven by a number of factors. Delocalization of conjugated bonds is absolutely essential, but delocalization of bonds through the whole polymeric chain is impossible due to rotation of monomer units around bonds, as *Fig. 18* shows. Polymeric chain twisting causes grow of band gap energy compared to band gap energy of absolutely planar chain.

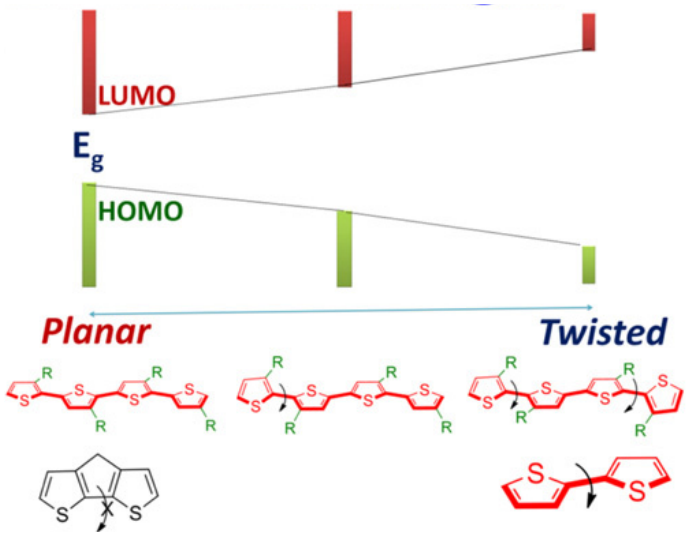

Fig. 18: Influence of chain rotation on the band gap energy E_g *[122].*

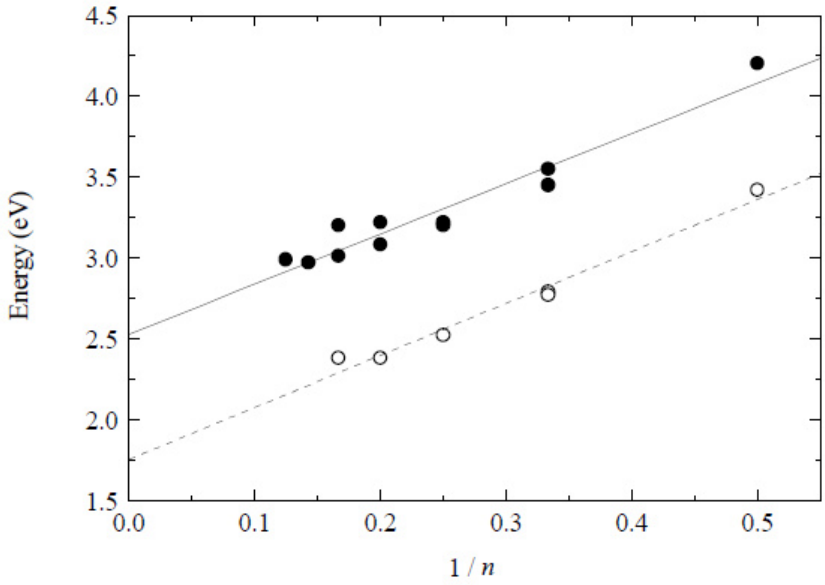

*Fig. 19: Dependence of absorption and emission maxima of oligo(*p*-phenylene vinylene) on the reciprocal value of phenylene rings number shows decrease of band gap with the chain growth [118].*

For the description of chain conformation, the concept of effective conjugated length is introduced, which describes the mean length of conjugated part of polymer chain. Effective conjugated length can be determined from optical properties of oligomers with varying number of monomer units as it was already presented [118]. The example of experimental data is shown in the *Fig. 19*, where dependence of absorption and emission maxima of oligo(*p*-phenylene vinylene) on reciprocal value phenylene rings number is plotted. Achieving a certain number of monomer units, oligomers tend to stop being planar and their band gap stays constant. Absorption and emission peaks possition are not changed, only the changes in spectra shape are observed; mainly the vibronic structure of spectra is smoothed [32].

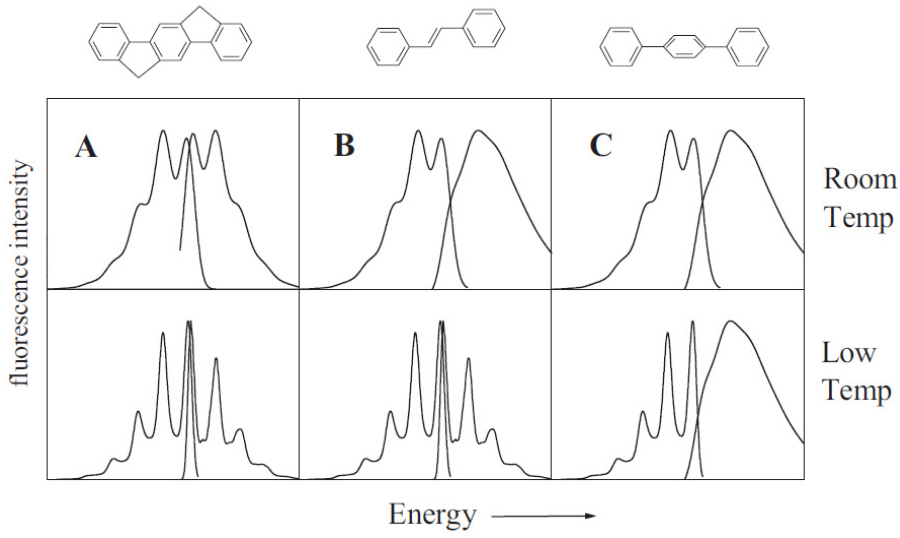

Fig. 20: Three types of molecules and shapes of their absorption and emission spectra. A type is molecule with rigid structure. B type represents the rigid structure in excited state and after cooling in ground state as well. C type is shown for molecule without rigid equilibrium geometry [119].

Fluorescence spectra of polymers are usually vibronically resolved while absorption spectra are more often non-resolved. It is caused by better orderliness of polymers' excited states, when chain torsion is suppressed by getting shorter bond of exciton [119]. Situation is illustrated by *Fig. 20*, where three types of molecules with shapes of their absorption and emission spectra are presented. A type is a molecule with rigid structure. B type represents the rigid structure in excited state and after

cooling in ground state as well. C type stands for the molecule without rigid equilibrium geometry.

The exciton diffusion into the lowest excited energy states during the exciton's lifetime is considered also to be a reason of that emission spectra of polymers are structured by vibronic modes [82].

The torsion of chain and breach of its planarity can be caused also by bulky side groups, which are introduced from various reasons. For example alkyl and alcoxy groups are generally introduced to increase the solubility of polymer in organic solvents. There can be demonstrated that influence of substituents can be destructive for the chain planarity as well as it can contribute to better planarity, see *Fig. 21*. Alcoxy group allows the creation of hydrogen bonds between the oxygen atom and vinylene carbon atom, which contribute to the chain planarity, while alkyl group acts only by steric effect against chain planarity [120].

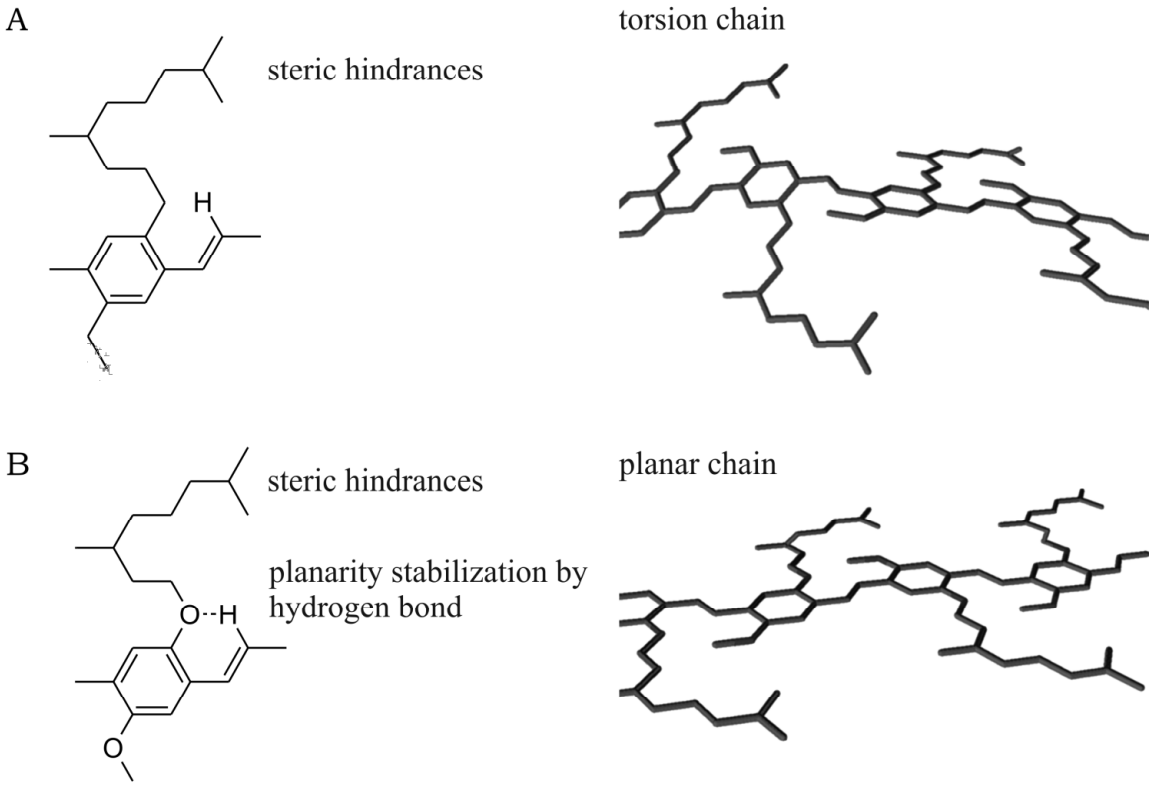

Fig. 21: Planarization of soluble PPV polymeric chains by hydrogen bond.

These groups can reduce not only the chain planarity, but may loosen the bulk polymer structure and interrupt intermolecular interactions, which decrease the material electrical conductivity [122].

The other way how to modify a conjugated polymer chain is to add the electron withdrawing side groups. This modification contributes to chain planarity and changes affinity to electrons (see *section 2.3.1.1*). Halogens (F, Cl) and cyano– groups are the most common electron withdrawing substituents [120].

Polyaromatic polymers unfortunately possess many undesirable characteristics, such as low material stability, relatively broad optical band gap (large than 2 eV), low dielectric constant, low electrical conductivity and others, which prevent high efficiency and long lifetime of organic solar cells made of these polymers [48]. Therefore, high attention is focused on searching of new and improved donor polymers for construction of more efficient organic solar cells.

The current trend is the syntetization of low band gap π-conjugated polymers. There are two ways to achieve low the band gap in polymers:

1. *Conversion of a polyaromatic chain into a conjugated system with an enhanced quinoid character*, which causes more rigid structure of polymer chain and therefore greater effective conjugated length [122]. Difference in electronic form of aromatic and quinoid moiety is showed on *Fig. 22*, where their structure energies is plotted. The quinoid form presents higher energetic structure and therefore lower stability as the aromatic one. For achieving the stabilized quinoidal forms, there are condensed aromatic structures synthesized, such as isothianaphthene and further analogies (see right side of the *Fig. 22*).

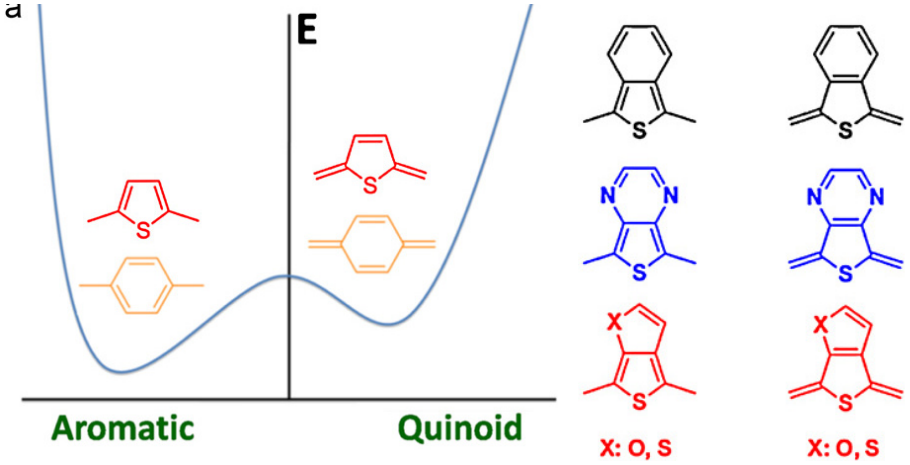

Fig. 22: Schematic presentation of the non-degenerate fundamental energy for the aromatic and quinoid resonance forms (left) and typical heterocyclic moieties used for the stabilization of the quinoid form (right) [122].

Using of poly(isothionaphthene) (with band gap only 1 eV) and some of its derivatives in OPV were referred, but photovoltaic efficiencies of devices were generally poor (less than 0.5 %) [44]. Despite this fact, these types of monomer units are usually incorporated in alternating copolymers, which form the next group of low band gap polymers.

2. *Synthesis of donor-acceptor alternating copolymers* [122] is the most preferred way to achieve the electron donating polymer for photovoltaics.

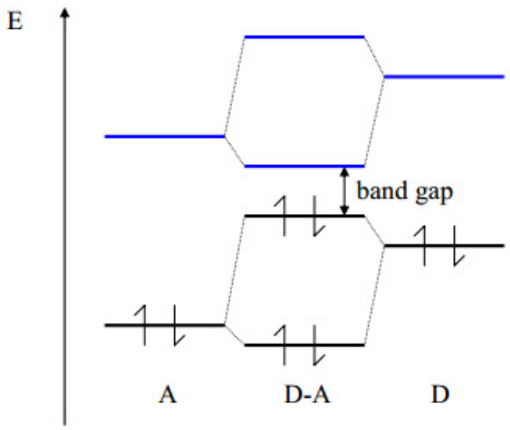

Fig. 23: Effective band gap of alternating donor-acceptor units in polymeric chain is achieved by mixing of their orbitals [44].

Intramolecular charge transfer between donor and acceptor monomer in chain takes place and creates new energetic levels [44], as *Fig. 23* shows, with low band gap. Similarly to previous case, copolymer chains are more planar.

Examples of typical electron donor monomer units incorporated in copolymers are thiophenes, pyrroles or fluorenes. Electron acceptor units can be represented by benzothiadiazole, diketopyrrolopyrole and other molecules, which can be modified by electron withdrawing groups (such as –CN, $–NO_2$ and others) for the amplification of electron accepting properties [44, 123].

There exist a whole series of donor-acceptor alternating copolymers, as shown by the published overviews, for example [44, 122, 123, 126]. *Table 2* summarizes the high efficient solar cells prepared from donor-acceptor alternating copolymers. The highest photovoltaic conversion efficiency of these devices ranges from 7 to 9 %. *Fig. 24* shows chemical structures of polymers listed in *Table 2*.

Table 2: Examples of high efficient photovoltaic heterojunction devices prepared from currently studied co-polymers. Classical structure stands for device structure ITO/PEDOT/active layer/metal electrode, inverted structure means: ITO/MoO_3/active layer/ZnO_2/metal electrode

Device	Active materials	Efficiency	Active area	Reference
Classical structure				
	PBnDT-DTffBT:$PC_{60}BM$	7%	0.12 cm²	Zhou (2011) [127]
	PilTVT:$PC_{60}BM$	7.09%		Jung and Jo (2014) [128]
	PBDTTT-C-T: $PC_{70}BM$	7.6 %	0.1 cm²	Huo (2011) [129]
	PTB7:$PC_{70}BM$	8.24 %	0.09 cm²	He et al. (2012) [129]
	PDPP3TaltTPT: $PC_{70}BM$	8 %	0.09 cm²	Hendriks et al. (2013) [131]
	PDPP3T:$PC_{70}BM$	7.1 %	0.09 cm²	Hendriks et al. (2013) [131]
	PDPPTPT:$PC_{70}BM$	7.4 %	0.09 cm²	Hendriks et al. (2013) [131]
Inverted structure				
	PTPD3T:$PC_{70}BM$	7.72 %		Guo et al. (2013) [132]
	PBTI3T:$PC_{70}BM$	8.42 %		Guo et al. (2013) [132]
	PTB7:$PC_{70}BM$	9.21 %	0.16 cm²	He et al. (2012) [130]

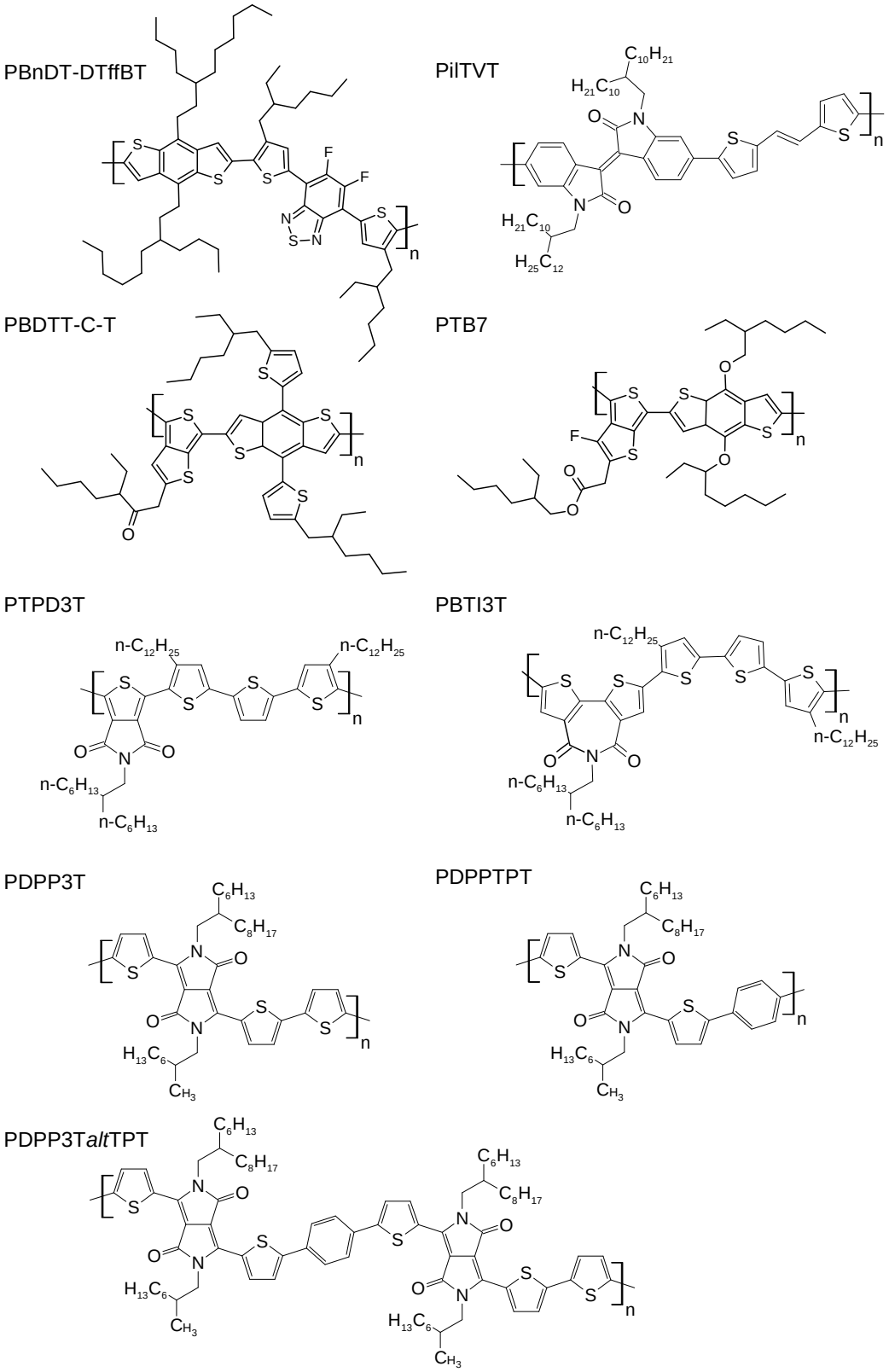

Fig. 24: Structures of electron donor materials, which provide the most efficient organic solar cells.

2.3.1.1 Properties of Selected Polymers

This section introduces properties of following electron donating π-conjugated polymers studied in this thesis:

a) polyaromatic polymers – MDMO-PPV and Tg-PPV,

b) donor-acceptor alternating copolymers with internal charge transfer states – PCDTBT and PCBTDPP,

Full chemical systematic names are introduced in *Table 3* and chemical structures in *Fig. 25* respectively. These polymers were chosen for wide spectrum of optical and electrical properties which allowed the study of photogeneration processes in these polymers in rather general way.

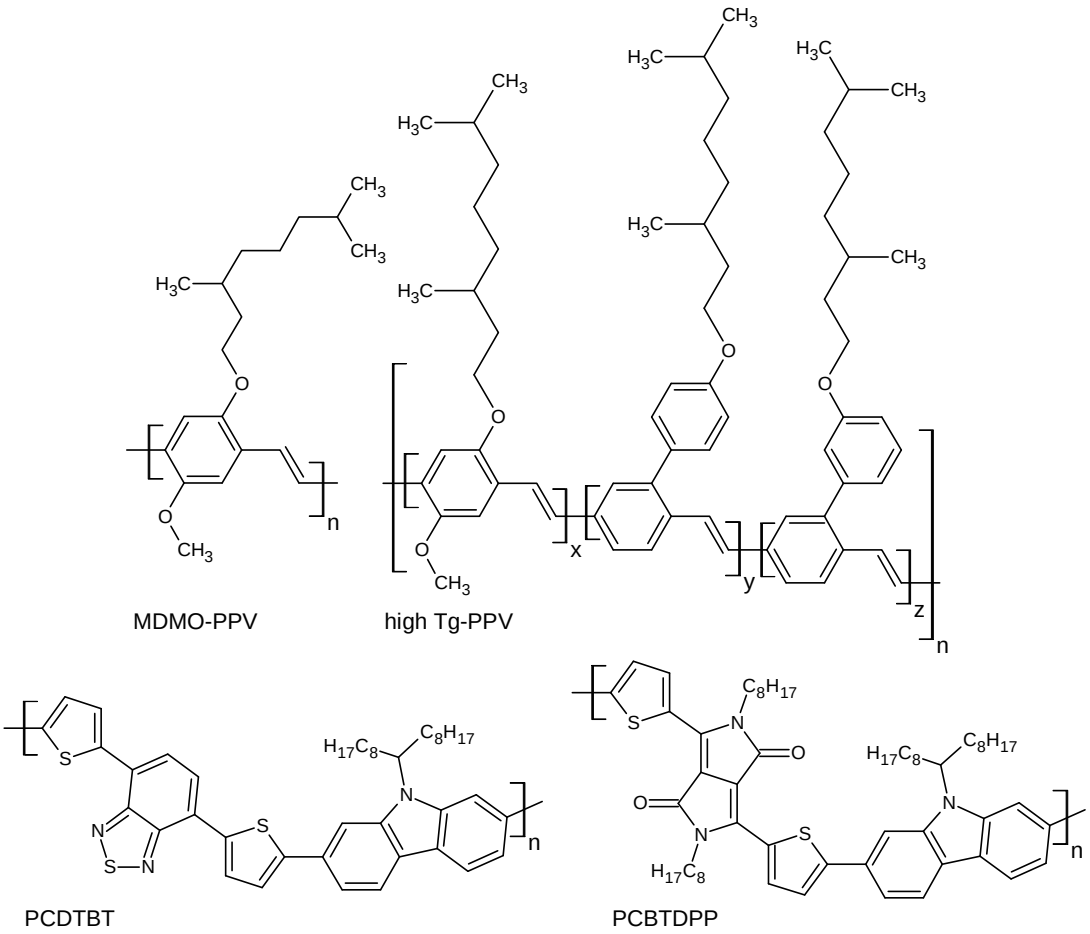

Fig. 25: Studied electron donating polymers. For systematic names see Table 3.

Table 3: Full chemical names of the studied polymers

Material name	Formula
MDMO-PPV	poly[2-methoxy-5-(3′,7′-dimethyloctyloxy)-1,4-phenylenevinylene]
Tg-PPV (commercial name PDO-123)	triblock copolymer of poly[2-methoxy-5-(3′,7′-dimethyloctyloxy)-1,4-phenylenevinylene], poly{2-[4′-(3′′,7′′-dimethyloctyloxy)-1′,4′-phenyl]-1,4-phenylenevinylene} and poly{2-[3′-(3′′,7′′-dimethyloctyloxy)-1′,4′-phenyl]-1,4-phenylenevinylene)}
PCDTBT	poly[*N*-9′′-hepta-decanyl-2,7-carbazole-*alt*-5,5-(4′,7′-di-2-thienyl-2′,1′,3′-benzothiadiazole)
PCBTDPP	poly[*N*-9′-heptadecanyl-2,7-carbazole-alt - 3,6 - bis (thiophen-5-yl) - 2,5-dioctyl - 2,5-dihydropyrrolo[3,4-]pyrrole-1,4-dione]

The derivatives of poly(*p*-phenylenevinylene) MDMO-PPV and Tg-PPV represent polyaromatic polymers. MDMO-PPV is frequently used as model electron donor material for organic electronics, since its properties are well described. It was also chosen as a reference for experiments in this work. Tg-PPV copolymer is characteristic by high glass transition temperature T_g = 138 °C [99, 143] against MDMO-PPV with T_g = 45 °C [99]. Higher T_g ensures better stability of morphology in blends with fullerenes and thus better stability of photovoltaic devices [143, 144]. Nevertheless, Tg-PPV is commercially supplied preferably as electroluminescent material for organic light emitting diodes (OLED) [145]. It is so due to its high energy band gap (see *Table 4*), which prevents to utilize the red light to photovoltaic phenomenon. Values of HOMO and LUMO energy levels for both polymers are summarized in *Table 4* and were used to evaluation of experiments.

Table 4: Energetic properties of the studied π-conjugated polymers.

Material	E_{HOMO} (eV)	E_{LUMO} (eV)	E_g (eV)	Source
MDMO-PPV	−5.2	−3.1	2.10	Veldman et al. [99]
Tg-PPV	−5.2[b]	≈ − 2.9	2.26[a]	Vandewal et al. [99]
PCDTBT	−5.5	−3.6	1.85	Park et al. [149]
PCBTDPP	−5.4	−3.9	1.60	Aïch et al. [150]

[a] Estimated from point of overlap of thin film absorption and emission spectra.
[b] $E_{HOMO} = E_{LUMO} - E_g$

The other studied polymers PCDTBT and PCBTDPP belong to donor-acceptor altering copolymers group. PCDTBT seems to be nowadays a popular material for photovoltaic applications due to its low band gap (see *Table 4*) which allows red light absorption and also due to its good electrical conductivity. PCDTBT:fullerene based photovoltaic devices achieved almost 6% photogeneration efficiency [148]. Simultaneously, photovoltaic devices prepared from this material showed long lifetime: "*6.2 years, assuming 5.5 h of one-sun intensity per day*" [153]. PCBTDPP is relatively new low band gap (only 1.6 eV see *Table 4*) material with high electrical conductivity and strong red light absorption. On other hand, the highest known efficiency of photovoltaic devices prepared from PCBTDPP was only 2.5 % [152]. For comparison, *Table 5* summarizes the best published properties of photovoltaic devices prepared from studied polymers. Similar photovoltaic structures were prepared and characterized in this work.

Table 5: Properties of photovoltaic devices prepared on ITO/PEDOT:PSS and with top Al electrode from studied polymers and fullerenes.

Devices	j_{SC} (mA cm^{-2})	V_{OC} (V)	*FF* (%)	μ (%)	Source
MDMO-PPV:$PC_{60}BM$ 1:4	5.25	0.82	61	2.5	Shaheen et al.[153]
MDMO-PPV:$PC_{70}BM$ 1:4	7.6	0.77	51	3.0	Wienk et al. [146]
Tg-PPV:$PC_{60}BM$ 1:4	3.1	0.82	40	1.0	Vandewal et al. [99]
Tg-PPV:$PC_{70}BM$	-	-	-	-	-
PCDTBT:$PC_{60}BM$ 1:4	6.92	0.89	63	3.6	Blouin et al. [147]
PCDTBT:$PC_{70}BM$ 1:4	10.3	0.88	63	5.8	Ossila [148]
PCBTDPP:$PC_{60}BM$ 1:3	5.2	0.85	37	1.6	Huo et al. [152]
PCBTDPP:$PC_{70}BM$ 1:3	8.02	0.76	40	2.45	Jo et al. [151]

2.3.2 Electron Acceptors

Unlike to donor materials, there is only limited number of types of acceptor materials available, because the designing of acceptor molecules is more complicated. Both small molecules and polymers can serve as electron acceptors. Common electron acceptor material is usually represented by

polycondensed aromatic compounds, allotropic modification of carbon (fullerenes, nanotubes, graphene) or other π-conjugated materials modified with strong electron withdrawing substituents (halogens, cyano group, nitro group).

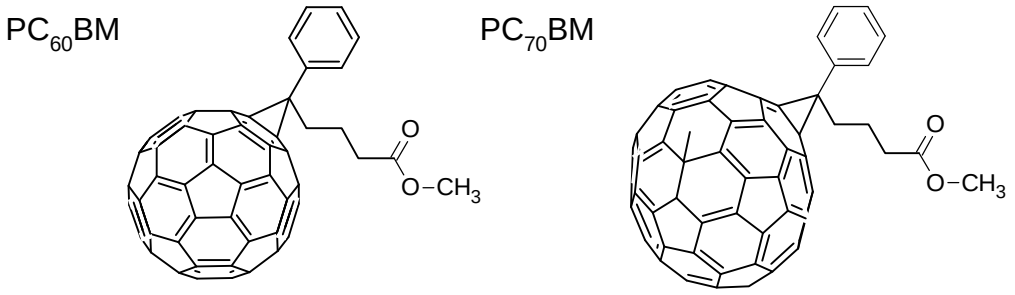

Fig. 26: Dominantly used electron acceptors in organic photovoltaics are soluble derivatives of C_{60} and C_{70} fullerenes.

The fullerenes are the widely investigated group of electron acceptors; especially soluble derivates $PC_{60}BM$ ([6,6]-phenyl-C_{61}-butyric-acid-methyl ester) and $PC_{70}BM$ ([6,6]-phenyl-C_{71}-butyric-acid-methyl ester) (see *Fig. 26*). Fullerenes are highly electronegative and therefore they act as strong oxidants in chemical reactions [123]. Fullerenes are ably to accept more than one electron in their structure. The example of cyclic voltammetry characteristics of C_{60} and its soluble derivative $PC_{60}BM$ on the *Fig. 27* shows possibility of reduction of these structures by means of four electrons [133]. Fullerenes' accepting capacity is also driven by side groups, which are introduced not only for increasing of their solubility, but also to ensure the better assembly of fullerene in blend with donor material and consequently better interaction [134].

Table 6: Energy level of HOMO and LUMO orbitals of the studied fullerenes

Material	E_{HOMO} (eV)	E_{LUMO} (eV)	E_g (eV)	Source
$PC_{60}BM$	−6.08	−4.38	1.70	Veldman et al. [99]
$PC_{70}BM$	−6.0	−4.3	1.70	Park et al. [149]

Moreover, fullerenes are due to low energy of band gap electron conducting materials [136]. The example of electron energy levels of $PC_{60}BM$ and $PC_{70}BM$ are summarized in *Table 6*. Under the specified conditions, fullerenes

crosslink in blend with donor polymer and this introduces the effective charge carrier transport to electrodes [125].

Nevertheless, fullerenes present also a few disadvantages. Mainly their synthesis and purification is expensive [138]. Further, their electron energy levels are not fully compatible with all donor materials [122].

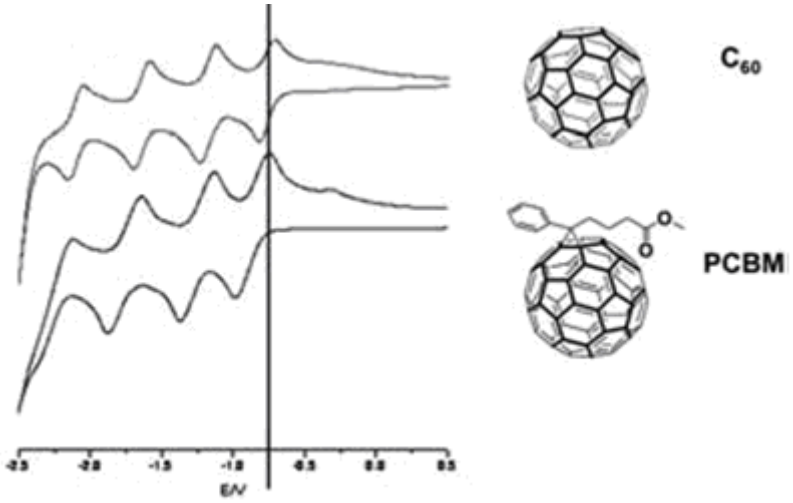

Fig. 27: Cyclic voltammetry plots of C_{60} and its soluble derivative PCBM shows the reduction possibility by to four electrons [133].

Therefore, one of most crucial problems of collateral organic photovoltaics is the development of new electron acceptor materials [138, 139]. Design of new acceptors is usually the first approach in research focused on fitting the energy levels of HOMO and LUMO so that the levels involve efficient charge transfer from the donor as it is illustrated on *Fig. 28*. The scheme shows that greater differences between LUMO energy levels of donor and acceptor is important for charge carriers photogeneration, where energy difference E_d of 0.3 eV is considered as sufficient for efficient charge separation [135]. Simultaneously, energy difference between LUMO of acceptor and HOMO of donor drives the open-circuit voltage V_{OC} of photovoltaic devices. Low band gap of the electron donor is limiting factor for the V_{OC} value, since the E_d value needs to stay at certain minimum value for the sustaining of the efficient exciton dissociation.

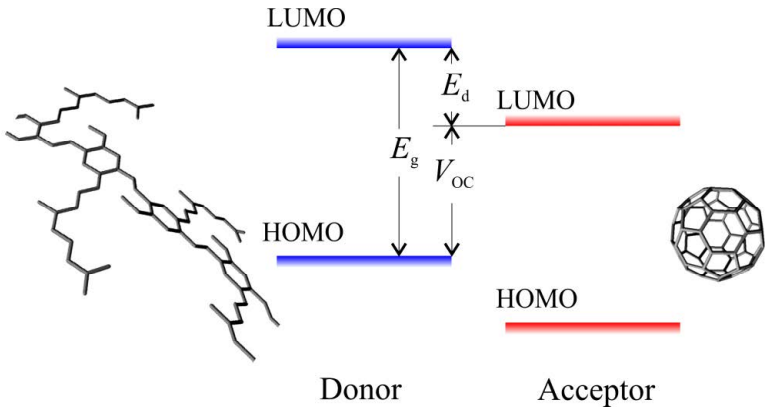

Fig. 28: Difference of energy levels E_d of donor LUMO and acceptor LUMO drives the charge transfer. Voc is given by the difference between energy of donor HOMO and acceptor LUMO.

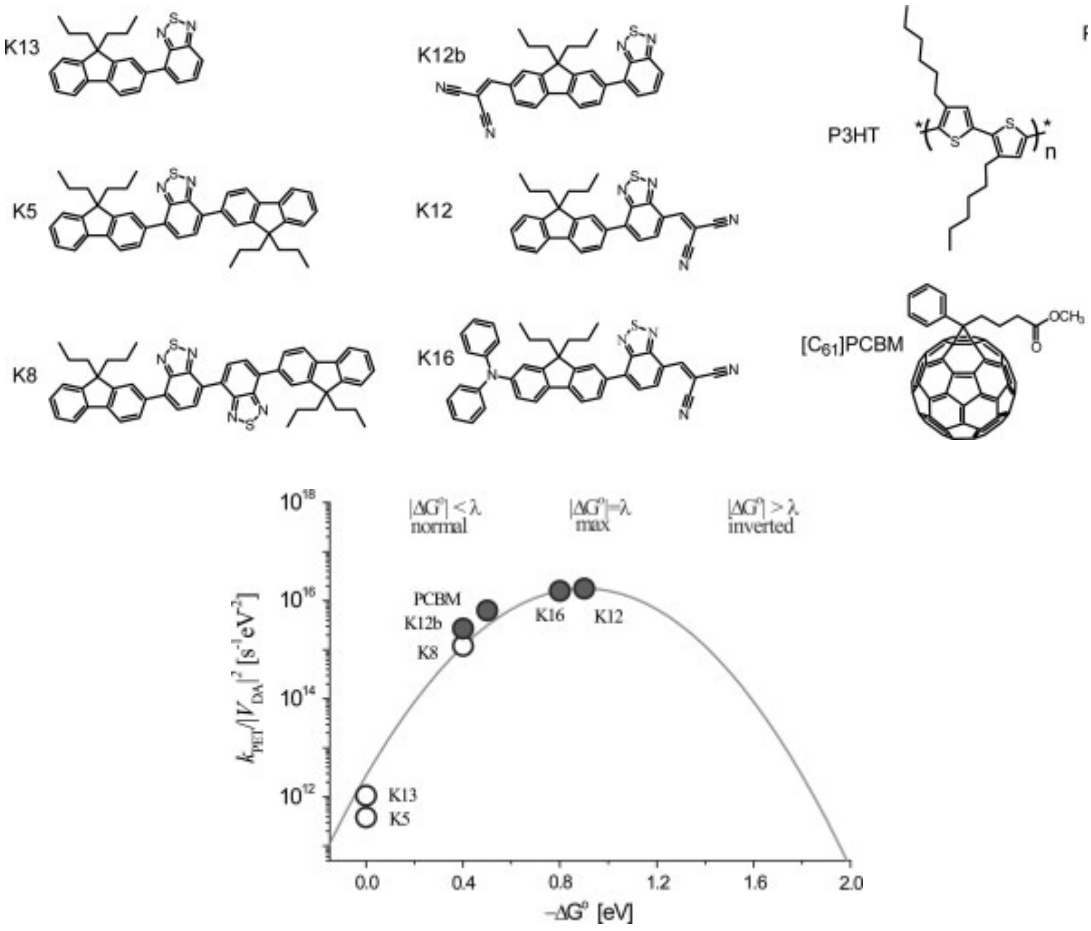

Fig. 29: Application of Marcus theory to search of ideal electron acceptor for selected donor material. In this case authors Schwenn et al. studied series of acceptors combined with P3HT [93].

Charge transfer is described by Marcus theory, see *section 2.2.3*. This theory is practically applicable in search of new electron accepting molecules which was demonstrated for example by Schwenn et al. [93]. Series of molecular

structures proposed as electron acceptors for P3HT polymer as electron donor have been studied (see *Fig. 29*). Cyclic voltammetry was employed to determinate the ionization potentials and electron affinities of molecules and data were used to calculation of reorganization energies and Gibbs free energies of charge transfer. Results are shown on *Fig. 29,* where two compounds, K12 and K16, seem to be theoretically better acceptors as the most used electron acceptor PCBM.

Unfortunately, the authors did not present solar cells prepared from these materials. As was already explained, efficient charge transfer is not a guaranty of high solar cells efficiency; because the acceptor has to also allow efficient electrons transport in active layer.

Treat et al [124] presented a methodology, how to control the miscibility of electron donor polymers and fullerene derivatives modified with side groups. Authors found relationship between miscibility of fullerene derivatives and electrical properties, when high miscibility caused small polymer-rich and fullerene-rich domains in layer morphology, which are important for transport of photogenerated charge carriers.

2.4 Summary

The physical principles of charge carrier photogeneration in organic solar cells were described as well as principles of design of organic photovoltaic devices. Understanding of these principles is necessary for basic research of photogeneration processes as well as for the development of novel devices.

Special attention was paid to description of charge transfer process, charge transfer states and their experimental observations, because the following presented experiments and results are significantly built on this knowledge.

In connection with photovoltaic devices design, current trend in design of new π-conjugated polymers and electron accepting materials were described. With regard to this knowledge the materials for experiments were chosen and their selected properties were described.

3 EXPERIMENTAL PART

This section deals with description of used materials, sample preparations, and with characterization methods used in experiments focused on photogeneration processes.

3.1 Materials

Two different types of electron donating π-conjugated polymers were studied:

1. polyaromatic polymers - MDMO-PPV, Tg-PPV,
2. donor-acceptor alternating copolymers with internal charge transfer states – PCDTBT and PCBTDPP.

Properties of polymers were described in *section 2.3.1.1.* Selected physical parameters are summarized in *Table 7.*

Table 7: Selected physical properties of the studied polymers

Material name	Properties
MDMO-PPV	solid, M_n = 23 000 g·mol^{-1}. T_g = 45 °C, electron donor, $\mu = 10^{-7}$ cm^{2}V^{-1}s^{-1} [185]
Tg-PPV (commercial name PDO-123)	solid, M_n = 340 000 g·mol^{-1}, polydispersity index 5.15, T_g = 138 °C, electron donor [145]
PCDTBT	solid, M_n = 16700 g·mol^{-1}, polydispersity index 2.01, electron donor, $\mu = 10^{-3}$ cm^{2}V^{-1}s^{-1} [147]
PCBTDPP	solid, $M_n \approx$ 25000 g·mol^{-1}, electron donor, $\mu = 2 \cdot 10^{-2}$ cm^{2}V^{-1}s^{-1} [150]

Two frequently studied derivatives of fullerenes were used as electron acceptors: $PC_{60}BM$ and $PC_{70}BM$. Chemical structures were already shown in *Fig. 26* in the *section 2.3.1.1,* where properties of fullerenes were presented.

Polymers MDMO-PPV, PCBTDPP and fullerene $PC_{60}BM$ were supplied by Sigma Aldrich Co., Steinheim, Germany, Tg-PPV by Merck KGaA, Darmstadt, Germany and PCDTBT and fullerene $PC_{70}BM$ by Ossila Ltd, Sheffield, United Kingdom.

During preparation of OSC structures several additional materials were used. PEDOT:PSS was used as transport layer in OSC structure for improved of holes collection by ITO electrode. Used suspensions came from different suppliers, who delivered a variety of suspensions differing by the PEDOT and PSS ratio, which controls properties of final transport layer. More details about used PEDOT:PSS suspensions are summarized in *Appendix No 1.*

Silver paint paste Spi 05003AB (SPI Supplies® Inc., West Chester, PA, USA) and Carbon paint paste Spi #05006AB were used for completion of OSC devices prepared on textiles.

3.2 Samples

In order to study of the photogeneration processes in above mentioned polymers, two types of samples were prepared:

a) Samples for optical measurements –thin films and solutions of studied pristine materials or blends.

b) Samples for optoelectrical measurements – prepared samples of the general structure substrate/electrode/transport layer/active layer/electrode. Example of samples is shown on *Fig. 30*.

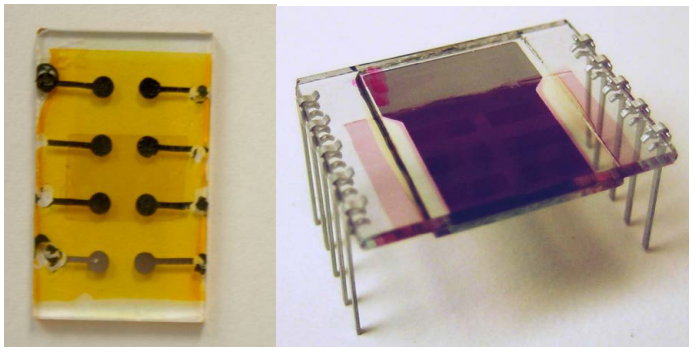

Fig. 30: Laboratory photovoltaic devices: A – prototype prepared in ordinary laboratory under ambient conditions, B – encapsulated prototype made on Ossila company substrate under controlled conditions in glovebox.

3.2.1 Sample Preparation Conditions

The samples were in many cases prepared in ordinary chemical laboratory under ambient atmosphere, room temperature (25 °C), atmospheric pressure and without special requirements against the presence of dust (standard conditions). In November 2012 new class C clean rooms (clean lab) have been opened in our faculty. The clean lab is equipped with MB-200B MBRAUN gloveboxes (M. Braun Inertgas-Systeme GmbH, Garching, Germany), see *Fig. 31*. Gloveboxes allow the preparation of samples in nitrogen atmosphere with minimal content of oxygen and water (less than 0.1 ppm). Amount of dust in glovebox is also reduced due to tidiness of clean lab. Samples prepared in glovebox were encapsulated by epoxy resin (EE1 Encapsulation epoxy, Ossila) and glass for their protection. Epoxy resin was cured for 30 min under ultraviolet light.

Fig. 31: Left: clean lab with gloveboxes for organic electronic devices preparation. Right: preparation of samples under standard conditions.

3.2.2 Solutions

Solutions for spectroscopic measurements were prepared under standard laboratory conditions. The molar concentration of polymer dissolved in chlorobenzene was $0.36 \cdot 10^{-5}$ mol·dm^{-3} spectroscopic units (SPUN). SPUNs represent the part of the polymer chain where the singlet excited state (exciton) is located [158] and, thus, determine the spectral properties of the

polymer. The length of the PPV-based polymer SPUN (MDMO-PPV and Tg-PPV) was estimated from the comparison of fluorescence emission maximum $\lambda_{PL\ max}$ with published values for PPV oligomers of various length [156]. The SPUN length was estimated on seven monomer units for both of the polymers. The PCDTBT SPUN was used according to the work of Gieseking et al. [157] and, for PCBTDPP, an analogous structural unit was assigned. The SPUNs in these polymers are constituted by a carbazole unit accompanied by one thienyl and one benzothiadiazol unit from each side in the case of PCDTBT, and by one thienyl and one diketopyrrolopyrrole unit from each side of the carbazole moiety in the case of PCBTDPP. The calculated molar weights M_{SPUN} are summarized in *Table 8,* together with molar weight of monomers M_u for comparison.

Table 8: Molecular weight of polymers monomeric units M_u and of polymers spectroscopic units M_{SPUN}.

Material	M_u ($g \cdot mol^{-1}$)	M_{SPUN} ($g \cdot mol^{-1}$)
MDMO-PPV	288.42	2018.94
Tg-PPV	455.67	3189.69
PCDTBT	702.04	918.32
PCBTDPP	926.41	1397.05

Polymer solutions were modified by addition of fullerenes. Fullerene concentrations varied from $1 \cdot 10^{-5}$ mol·dm^{-3} to $1 \cdot 10^{-3}$ mol·dm^{-3}.

3.2.3 Solid Samples

3.2.3.1 Substrates and Pre-Treatment for Deposition

Optical measurements of thin films were realized on glass slides or quartz glass slides (Herasil® 102, Heraeus Quarzglas Co., Kleinostheim, Germany) which were pre-treated by ultrasonic cleaning in following baths:

1) Detergent Neodisher (Miele, Inc., NJ, USA) or NaOH solution (5%), 10 min,

2) deionized (Milli-Q) water, 20 min,

3) acetone (p. a.) and/or isopropyl alcohol (a. p.), 10 min.

Glasses were finally pre-treated by other solvent like chloroform, if it was required to successful deposition of the thin films.

The organic solar cell structures were prepared on various kinds of substrates according to experimental plan. Research of photogeneration processes was realized on samples prepared on glass substrates with ITO (indium tin oxide) electrode. ITO is transparent for light with wavelength larger than 350 nm. Substrates were supplied by Sigma Aldrich or Ossila companies.

Occasionally, the shape of ITO electrode was modified by bleaching in mixture of HCl with elementary zinc. The shape was determined by a mask from a common transparent office tape. Substrates with ITO were cleaned by the very same procedure as glasses for optical measurements.

PET foils with ITO or textiles with various electrodes were employed during the development of flexible solar cells. PET foils with ITO were supplied by Sigma Aldrich. Other suppliers of ITO PET foil were Cener (Centro Nacional de Energías Renovables Fundación CENER-CIEMAT Sarriguren (Navarra), Spain) and Centi (Vila Nova de Famalicão Portugal) research centres. These substrates were pre-treated by the same procedure as the glass substrates, but without using of ultrasonic cleaning.

Textile substrates were composed from fabric (poly(ester); PES), smoothing layer for compensation of fabric roughness and electrode. Structure of conductive textile substrate is depicted on *Fig. 32*.

The smoothing layers were made from poly(urethane), silicone, latex (Tubicoat B40) or Licocene® B. Electrodes were made from silver, aluminium, carbon or ITO.

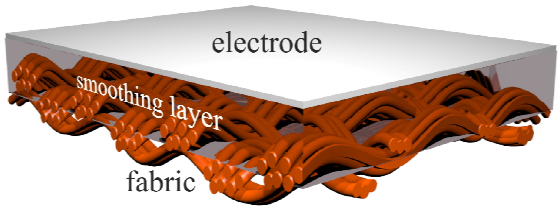

Fig. 32: Textile substrates consisting of fabric, smoothing layer and metal electrode.

Textile substrates were supplied by partners of the DEPHOTEX project. For information see *Table 9*, where fourteen examined types of textile substrates are summarized. These substrates were pre-treated before solar cells structures deposition only by oxygen plasma due low stability against solvents, if it was required.

Table 9: Fourteen types of studied textile substrates, which were used for preparation of textile solar cells.

Textile substrate	Supplier	Smooth layer	Electrode
CIAS Ain AgPES Lico	AIN*	Licocene® B	Ag
CIAS Ain AgPES Tubi	AIN	Tubicoat B40 latex	Ag
CIAS Ain AlO-AlPES pu	AIN	poly(urethane)	AlO-Al
CIAS Ain AlPES pu	AIN	poly(urethane)	Al
CIAS Ain AlPES sil	AIN	silicone	Al
CIAS Ain AlO-AlPES sil	AIN	silicone	AlO-Al
CIAS Ain 037-Al	AIN	poly(urethane)	Al
DTNW carbon textile	DTNW‡	carbon	C
CETEMMSA MST Al	CETEMMSA†	poly(urethane)	Al
Al fabric	DTNW	nothing	Al
Centi AI textile Al	Centi	poly(urethane)	Al
Cener Depho-037-01-ITO	Cener	poly(urethane)	ITO
PES Ag screen printed	CETEMMSA	poly(urethane)	Ag
PES ITO	Cener	poly(urethane)	ITO

*Ain, Asociación de la Industria Navarra, Cordovilla Pamplona, Spain

‡DTNW, Deutsche Textilforschungszentrum Nord-West e.V. Land der Ideen, Deutschland

†CETEMMSA technological centre, Barcelona, Spain,

3.2.3.2 Deposition Methods

Thin films deposition methods were selected according to solubility of materials in solvents and the substrate stability.

Insoluble materials were deposed by vacuum deposition. Materials were sublimated in initial vacuum $2 \cdot 10^{-4}$ Pa. Depositions were performed in the U311B Tesla vacuum evaporator (Tesla, Opočno,Czech Republic) or in the glovebox in MB-ProVap-5 vacuum deposition chamber from MBRAUN, see *Fig. 33*. These methods were used for preparation of Al and Au electrodes.

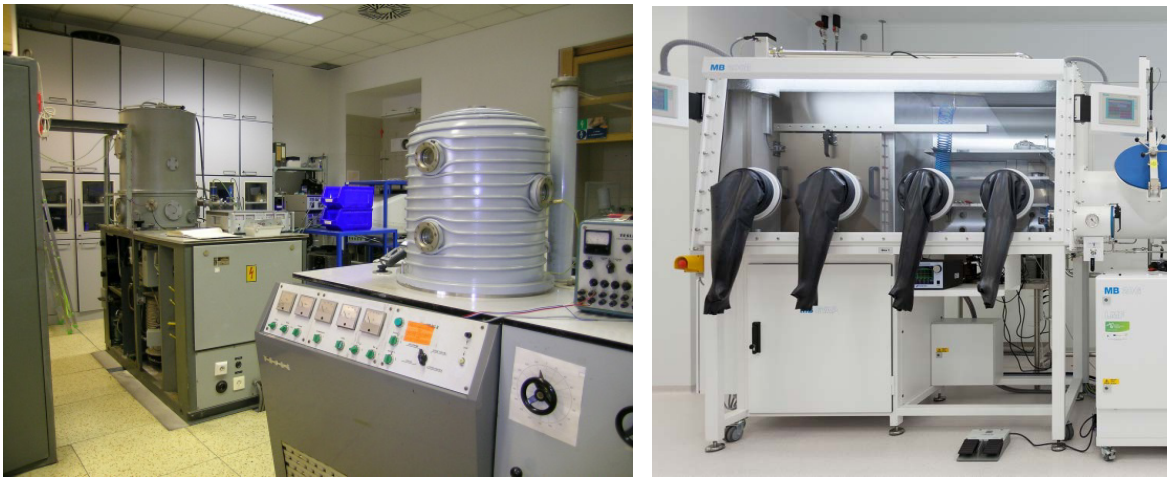

Fig. 33: Vacuum deposition chambers: Left U311B Tesla, right MB-ProVap-5 MBRAUN situated in glovebox.

The studied polymers and fullerenes are well soluble in organic solvents such as chlorobenzene, chloroform, toluene and others, therefore thin films of these materials were prepared by spin-coating. This most used laboratory thin layer deposition method was used for deposition of transport layers of PEDOT:PSS as well.

Spin-coatings were realized utilizing the spin-coater KW-4A CHEMAT Technology or the MB-SC-200 MBRAUN spin-coater in-built in glovebox.

Photoactive materials were deposed from chlorobenzene solutions usually at 1000 rpm. Material concentration varied according to behaviour during deposing and desired final coating thicknesses, for details see *Appendix No 2.* PEDOT:PSS was deposed from purchased water suspension at 5000 rpm.

Apart from spin-coating, alternative deposition methods from solutions were studied – the inkjet printing and electrophoretic deposition.

Inkjet printing was performed by means of the Dimatix Materials Printer DMP-2800 (Fujifilm Holdings Co., Valhalla, NY, U.S.A.) Material inks were prepared from standard solutions for spin-coating, where their film-forming properties were adjusted using cyclohexanone and toluene [158]. This method was applied for preparation of Tg-PPV, Tg-PPV:$PC_{60}BM$ and PEDOT thin films. Deposition was realized at standard laboratory conditions.

Electrophoretic deposition was applied only in the case of Tg-PPV polymer. Thin layers were prepared from Tg-PPV suspension of a concentration of $7.74 \cdot 10^{-3}$ $g \cdot dm^{-3}$. Suspension was prepared from solution of Tg-PPV in toluene by precipitation with acetonitrile, toluene:acetonitrile ratio was 42.5 % of acetonitrile, see *Appendix No* 3. Deposition was realized under constant current conditions in the range of 0.060 to 0.150 mA by means of Keithley 2410 Source Meter (Keithley Instruments Inc., Cleveland, OH, U.S.A.). The value of the current controls the rate of deposition. Time of deposition varied between 30 and 60 s and influenced the final film thickness. Films of Tg-PPV were prepared on glass substrates covered with ITO electrode purchased from Sigma-Aldrich. Deposition was performed under standard laboratory conditions.

3.2.3.3 Post-Treatment

Thin layers were treated by thermal annealing for modification of morphology and for elimination of residual solvent in layer. Annealing was realized in vacuum oven in standard laboratory conditions or on hot plate in glovebox under nitrogen atmosphere. Duration and temperature of annealing were chosen according to the material. Conditions used are summarized in *Appendix No 2.Table B*.

3.3 Experimental Methods

3.3.1 Optical Characterization

3.3.1.1 Absorption Study in UV-VIS and Near IR

Absorption spectra of samples were measured both in solutions and in thin layers employing Varian Cary Probe 50 UV-VIS spectrometer (Agilent Technologies Inc., Santa Clara, CA, U.S.A.). Solutions were studied in Hellma QS 10 mm quartz cuvette (Hellma GmbH, Mühlheim, Germany). Thin layers were prepared on quartz glass slides (see *section 3.2 The Samples*).

Molar absorption coefficients $\alpha(\lambda)$ of pristine materials were determined from measurements of dependence of absorbance spectra $A(\lambda)$ of solutions on the material concentration c (1.10^{-5} to 6.10^{-5} mol·dm^{-3}) [77]:

$$\alpha(\lambda) = \frac{A(\lambda)}{cl}, \tag{35}$$

Term l is optical path of cuvette.

3.3.1.2 Fluorescence Study in UV-VIS and Near IR

Fluorescence was investigated both in solutions and in thin layers. Solutions were studied in quartz cuvettes with an optical path of 10 mm. Thin layers were prepared on quartz glass slides (see *section 3.2 The Samples*).

Fluorescence spectra were measured utilizing both Thermo Spectronic Aminco Bowman AB-2 fluorescence spectrometer (Thermo Fisher Scientific Co., Waltham, MA, U.S.A.) and Horiba Jobin Yvon Fluorolog (Horiba Jobin Yvon S.A.S., Chilly Mazarin, France) equipped with IR detector (800–1200 nm) and with integration sphere for absolute fluorescence quantum efficiency measurement [154].

The material solution concentrations for fluorescence quantum yield measurements were adjusted to a level of light absorption equal to 0.1 in a

10 mm cuvette. Thickness of thin films of pristine materials was higher than 100 nm.

Fluorescence lifetime was processed from time resolved fluorescence data obtained utilizing the Horiba Jobin Yvon Fluorocube device for time correlated single photon counting (TCSPC) measurements. Fluorescence lifetime was calculated from experimental data by means of the specialized software DAS6, provided by the company Horiba Jobin Yvon.

3.3.2 Mechanical Characterization of Thin Layers

The thicknesses of prepared layers were measured by means of Dektak XT mechanical profilometer (Bruker AXS GmbH; Karlsruhe, Germany) with stylus of 12.5 μm diameter and applied pressure from 3 to 5 g. Profilometer was also employed for investigation of layers' surface roughness.

Thin layers morphology (crystallinity, materials distribution and others) and quality in micrometre range were checked by the optical microscope Nikon Eclipse E200 (Nikon Corp., Tokyo, Japan).

3.3.3 Optoelectrical Characterization of OSC

3.3.3.1 Photovoltaic Efficiency characterization

The current voltage measurements of opto-electrical devices were executed by means of picoampermeter Keithley 6478, electrometer Keithley 6517A or source meter Keithley 2601B (Keithley Instruments Inc., Cleveland, OH, U.S.A.). Data were collected by computer software (National Instruments LabView) via GPIB (National Instruments, Austin, TX, U.S.A.) or USB interface.

Non-encapsulated samples were placed in the VPF-475 cryostat (Janis Research Company Inc., Wilmington, MA, U.S.A.) at 10^{-4} Pa at laboratory temperature. Large area samples and encapsulated samples were measured at ambient conditions.

Current voltage characteristics were measured for samples both in dark and under irradiation. Xenon lamp LSH502 LOT Oriel (LOT-Oriel Co., Darmstadt, Germany) and solar simulator LS0916 LOT Oriel (see *Fig. 34*) were used as light sources. Intensity of incident light varied from 1 to 10 $mW \cdot cm^{-2}$ in case of xenon lamp LSH502 and was controlled by irradiance meter X97 Gigahertz-Optik with radiometric detector head RW-3703-4 for UV-VIS range (Gigahertz-Optik GmbH, Trkenfeld, Germany).

Fig. 34: left: Reference silicon solar cell; right: Solar simulator LS0916 LOT Oriel.

The solar simulator LS0916 LOT Oriel class AAA provides defined light source according to standard AM 1.5g [160]. Incident light intensity was 100 $mWcm^{-2}$ and was controlled by calibrated reference silicon cell RR200O from ReRa systems (ReRa Solutions BV; Nijmegen, Netherlands), see *Fig. 34*. For further specification about reference cell see [161].

3.3.3.2 Spectrally resolved Photocurrent Measurement

Spectrally resolved electrical response was assessed using a combined apparatus consisting of: picoampermeter Keithley 6478, xenon lamp LSH502 LOT Oriel, monochromator MSH101 LOT ORIEL, photometric head SiQE120 RaRe Solutions connected to picoampermeter Keithley 485. Data were collected by National Instruments LabView software via GPIB interface

(National Instruments, Austin, TX, U.S.A.). Apparatus scheme is sketched on the *Fig. 35*.

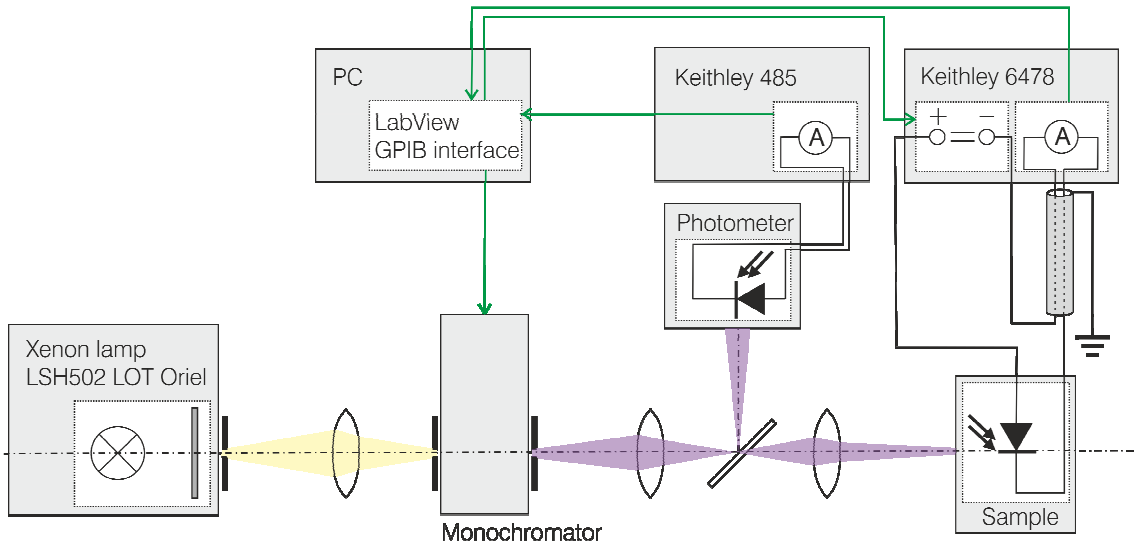

Fig. 35: Scheme of apparatus for spectrally resolved photocurrent measurement.

The wavelength of light was selected by monochromator in the range from 350 nm (limit given by the absorption edge of ITO) to 850 nm (limit given by monochromator construction). The monochromatic beam was divided in two beams in the ratio of 91.6 % of light intensity to sample and 8.6 % of light intensity to photometric head. This allowed simultaneous measuring of both incident light intensity and photocurrent response from the sample. Integral incident light intensity was set up to 1 mW/cm^2 and measurements were provided at zero applied voltage on sample. Picoampermeter Keithley 6478 allowed measured currents in the range from 10^{-12} to 10^{-2} A.

3.3.3.3 Electroluminescence

Intensity of electroluminescence was detected by the R3896 photomultiplier (Hamamatsu Photonics K.K., Iwata, Japan) with spectral response from 185 to 900 nm. Photomultiplier head was connected to high-voltage power supply Hamamatsu C9525. For further specification see [162]. This measurement was usually realized simultaneously with dark current voltage characteristic.

Qualitative assessment of electroluminescence was involved by spectra measurements. Electroluminescent spectra were captured by Shamrock SR-303i-B Andor (Andor Technology plc., Belfast, North Ireland) equipped by iCCD istars DH740-18U-03 Andor camera.

4 RESULTS AND DISCUSSION

In this chapter presents the results of experiments focused on studies of photogeneration of charge carriers in polymer semiconductors, as well as the applied research focused on the preparation of flexible polymer solar cells on textile substrates realized in our group within the European FP7 project DEPHOTEX.

These results are presented in three sections:

1. Optical studies of photogeneration processes – present the research of charge transfer and energy transfer between donor and acceptor in solutions and thin films by fluorescence spectrometry.

2. Detection and studies of CT states by optoelectrical methods – OSC devices were characterized by current voltage characteristics, spectrally resolved photocurrent measurements and electroluminescence measurements to assess the influence of charge transfer states on photogeneration efficiency.

3. Textile OSC application – this last section present results of experiments focused on preparation of thin films by different deposition methods: spin-coating, electrophoretic deposition and inkjet printing. Based on these findings the textile organic solar cells were proposed.

4.1 Optical Methods for Study of Photogeneration Processes

This chapter is focused on study of charge transfer and resonance energy transfer processes by fluorescence spectrometry. In particular, the studies of fluorescence quenching and the analysis of fluorescence emission in near infrared region caused by relaxation of excited CT states are utilized. In order to find suitable donor-acceptor pairs, the several studies based on

optical methods were realized, subsequently several parameters of photovoltaic devices prepared from these materials were estimated.

4.1.1 Optical Parameters of Pristine Materials

The detailed knowledge of optical spectra and optical parameters of the studied materials is necessary for evaluation of fluorescence quenching. Therefore their spectral characteristics, fluorescence quantum yield and fluorescence lifetime measurements are introduced. These experiments were realized both in solutions and thin films of pristine studied materials.

4.1.1.1 Optical Properties of Materials in Solutions

Absorption and fluorescence spectra of MDMO-PPV, Tg-PPV, PCDTBT, PCBTDPP, $PC_{60}BM$ and $PC_{70}BM$ diluted in chlorobenzene are shown on *Fig. 36.* Their absorption maxima $\lambda_{ABS\ max}$ and emission maxima $\lambda_{PL\ max}$ are listed in *Table 10.* These values are completed by molar absorption coeffi-

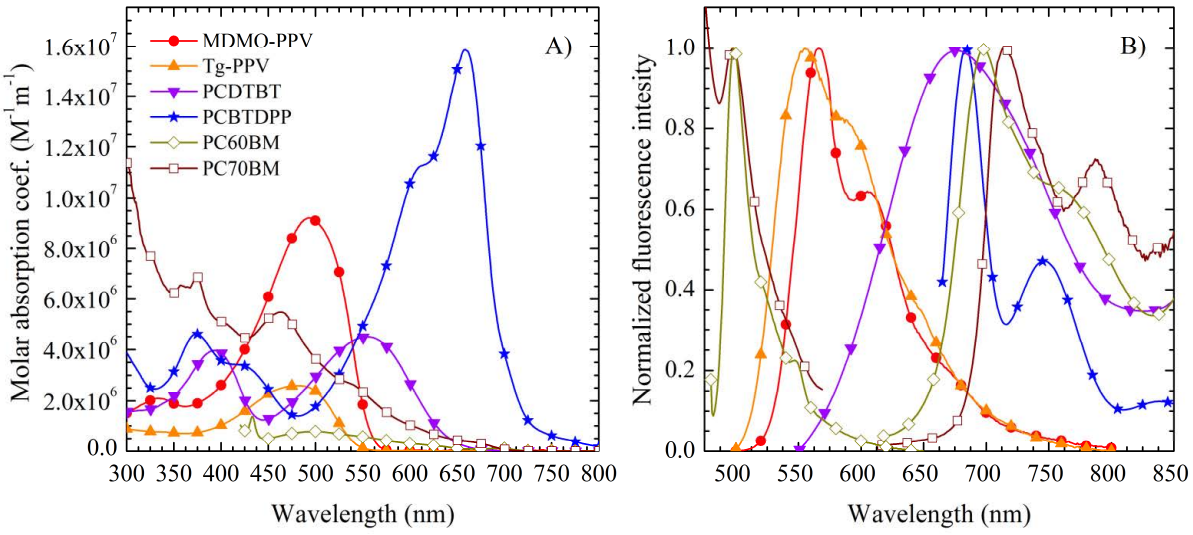

Fig. 36: Molar absorption coefficient spectra of MDMO-PPV (circles), Tg-PPV (triangles), PCDTBT (rotated triangles), PCBTDPP (stars), $PC_{60}BM$ (empty rhombus) and $PC_{70}BM$ (empty squares). B) Normalized fluorescence spectra of these materials.

cients at absorption maximum ε_{max}, which were determined from absorption spectra as described in *section 3.3.1.1*. In addition, the fluorescence lifetimes τ measurements at $\lambda_{PL\ max}$ and fluorescence quantum yields ϕ measurement were determined and are summarized in *Table 10*. These parameters are used for evaluation of fluorescence quenching processes.

Table 10: Optical parameters of studied materials in chlorobenzene solution: wavelength of absorption maximum $\lambda_{ABS\ max}$, molar absorption coefficient at absorption ε_{max}, wavelength of fluorescence maximum $\lambda_{PL\ max}$, fluorescence lifetime τ and fluorescence quantum yield ϕ.

Material	$\lambda_{ABS\ max}$ (nm)	ε_{max} (10^6 mol^{-1}dm^{3}m^{-1})	$\lambda_{PL\ max}$ (nm)	ϕ (%)	τ (ns)
MDMO-PPV	495	9.2	566	41 ± 2	0.376 ± 0.012
Tg-PPV	478	2.6	555	61 ± 6	0.629 ± 0.004
PCDTBT	574	4.5	685	36 ± 3	3.26 ± 0.02
PCBTDPP	660	15.8	685	40 ± 6	1.57 ± 0.02
$PC_{60}BM$	498	0.2	711	-	-
$PC_{70}BM$	463	2.4	694	-	-

Fig. 36 shows that emission spectra of polymers are overlapped by absorption spectra of fullerenes. Fluorescence spectra of PPV polymers (MDMO-PPV and Tg-PPV) exhibit larger spectral overlap with absorption spectra of fullerenes than that of the new alternating copolymers (PCDTBT and PCBTDPP). This implies that fluorescence spectra of polymers in blends with fullerenes are distorted by re-absorption of fluorescence by fullerenes and co-absorption of both materials. Therefore spectra were corrected according to the method published by Zheng et al. [74]. The spectral overlap between donor and acceptor indicates also possibility of presence of resonance energy transfer as will be shown further.

Fluorescence spectra of fullerenes exhibit green and red emission as shown in *Fig. 36.* This observation is consistent with the previous observations [164, 166]. Fluorescence intensity of fullerenes was significantly smaller than that of the polymers. The red emission is important for detection of CT states, because CT and fullerenes fluorescence spectra can be overlapped each other.

4.1.1.2 Optical Properties of Thin Films

The optical properties of thin films were characterized in similar way describe above. *Fig. 37* shows absorption and fluorescence spectra of thin films prepared from studied materials. Optical parameters were evaluated and are summarized in *Table 11*. Fluorescence lifetime and fluorescence quantum yield of studied polymers were determined (for experimental detail see *section 3.3.1.2*). Absorption coefficients of fullerenes were determined by ellipsometry. This was realized in teamwork with Ing. Schmiedová who presented the related complex optical data on international conference [165].

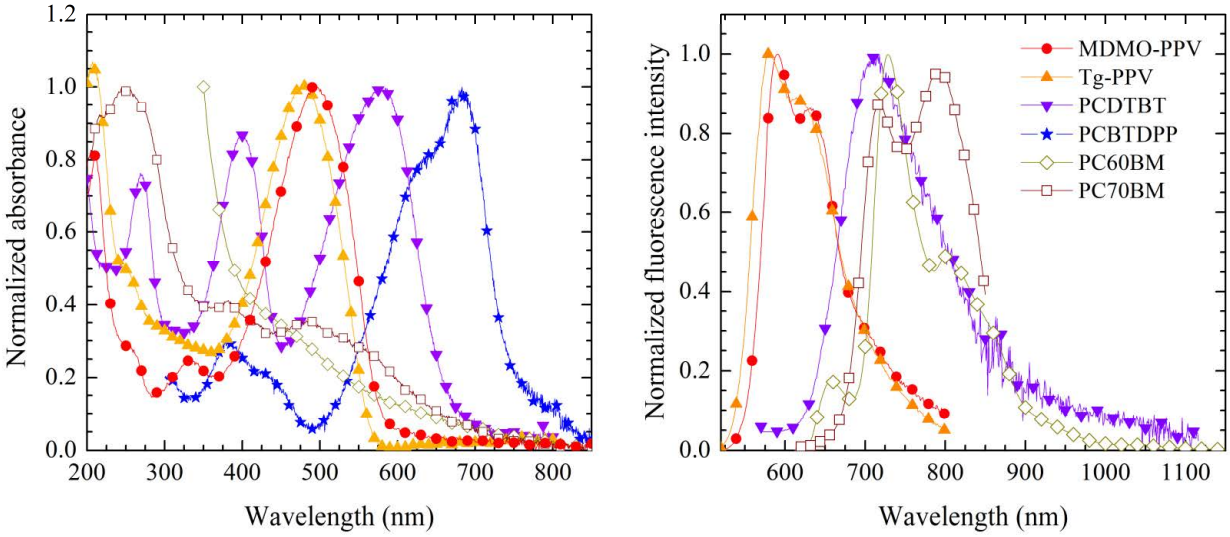

Fig. 37: Normalized absorption and emission spectra of thin films of pristine materials.

Table 11: Optical parameters describing properties of polymer thin layers $\lambda_{ABS\ max}$ –wavelength of absoption maximum, α_{max} – absorption coefficient at absorption maximum, $\lambda_{PL\ max}$ – wavelength of fluorescence maximum, φ – fluorescence quantum yield, τ – fluorescence lifetime

Material	$\lambda_{ABS\ max}$ (nm)	α_{max} ($10^6 m^{-1}$)	$\lambda_{PL\ max}$ (nm)	ϕ (%)	τ (ns)
MDMO-PPV	495		590	10.4 ± 0.5	0.28
Tg-PPV	480		580	9.9 ± 0.5	0.36
PCDTBT	580		712	7 ± 1	4.5
PCBTDPP	685		0	0	0
$PC_{60}BM$	475	8.57	727		
$PC_{70}BM$	495	13.1	717		

Spectra of all the investigated materials in thin films exhibit bathochromic shifts (about 10 nm in average) in comparison with spectra of solutions introduced in *section 4.1.1*. This effect could be attributed to the closer distance between molecules in thin films, which results in significant decrease of fluorescence quantum yields. While fluorescence quantum yield of studied polymers in solutions is about 45 % in average, fluorescence quantum yield of thin layers decreases bellow 10 %. PCBTDPP thin layer is even non-fluorescent.

4.1.2 Fluorescence Quenching

The charge transfer and energy transfer processes between polymers and fullerenes were studied in details by fluorescence quenching. Initially, the studies were realized in solution, as the results can be evaluated by standard fluorescence quenching models based on Stern-Volmer equation and Perrin equation. Based on gained results, the studies were extended on thin layers to achieve a deeper insight to the interaction of electron donor and electron acceptor in photovoltaic devices. The bellow described results of fluorescence quenching experiments in solutions have been published in *Chemical Physics Letters* [163], which is attached as *Appendix No 4.,* the results of the thin film studies are prepared for publication in the same journal.

4.1.2.1 Fluorescence Quenching in Solutions

Fig. 38 shows plots of the fluorescence emission spectra of each polymer (SPUN concentration $0.36 \cdot 10^{-5}$ mol·dm^{-3}) and its blends with $PC_{60}BM$ or $PC_{70}BM$ (both concentration $1 \cdot 10^{-4}$ mol·dm^{-3}). These spectra verify the fluorescence quenching effect caused by fullerenes and show that $PC_{70}BM$ is more effective quencher than $PC_{60}BM$.

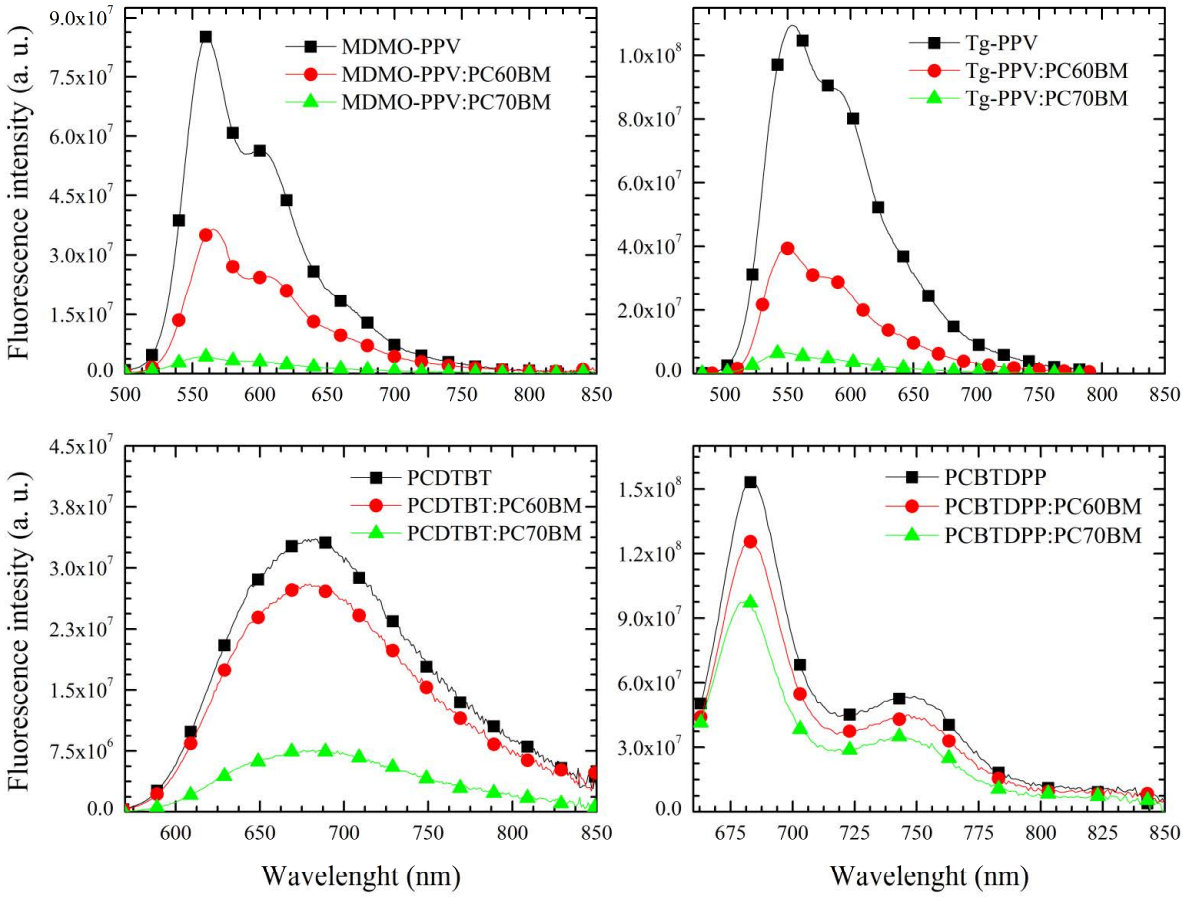

Fig. 38: Emission spectra of pristine polymer solutions (squares), polymer solutions with $1 \cdot 10^{-4}$ mol·dm^{-3} $PC_{60}BM$ (circles) and with same concentration of $PC_{70}BM$ (triangles).

In order to explore the influence of the charge transfer and energy transfer on fluorescence quenching, experiments were carried out with fullerene concentrations varying from $1 \cdot 10^{-5}$ mol·dm^{-3} to $1 \cdot 10^{-3}$ mol·dm^{-3}. Polymers were excited at their absorption maxima.

The quenching efficiency was evaluated from the dependence of the ratio between the fluorescence intensity of pristine polymer and the fluorescence intensity of polymer mixed with fullerenes (PL_0/PL) on quencher (fullerene) concentration [Q].

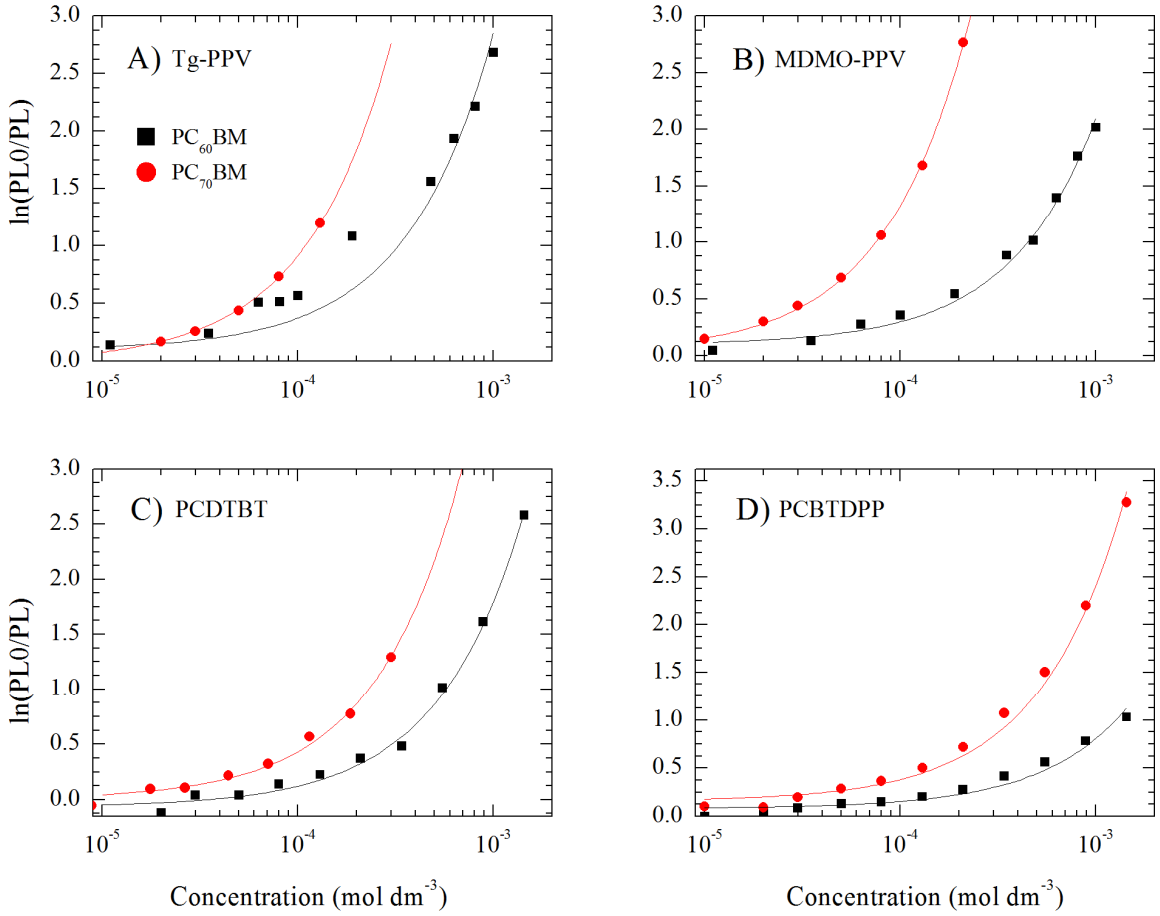

Fig. 39: Perrin plots of relative fluorescence decay of different polymers A) Tg-PPV B) MDMO-PPV C) PCDTBT D) PCBTDPP on concentration of $PC_{60}BM$ (squares) and $PC_{70}BM$ (circles).

The dependencies are shown in *Fig. 39*, where fullerene concentration is plotted in a logarithmic scale, because the characterization was performed over a broad concentration range exceeding two orders of magnitude. These results correspond well to the model of the static quenching [77] and were evaluated according to the Perrin equation:

$$\frac{PL_0}{PL} = \exp(K[Q]), \tag{36}$$

where K is the equilibrium quenching constant. The Perrin model expects that quenching is possible if the distance between the exciton and quencher is smaller than radius R_{eff} [77]. The values of quenching sphere radius R_{eff} were calculated:

$$K = \frac{4}{3}\pi R_{eff}^3 N_A . \quad (37)$$

N_A in the equation stays for Avogadro's constant. The calculated equilibrium quenching constants K are summarized in *Table 12* as well as the radius of action sphere R_{eff} calculated from K. As shown in *Table 12*, the values of R_{eff} significantly differ according to the used fullerene acceptor ($PC_{60}BM$ vs. $PC_{70}BM$) and the type of polymer.

Table 12: Gibbs free energy ΔG of the charge transfer between the electron donating polymer and $PC_{60}BM$ and $PC_{70}BM$ electron acceptors, the calculated Förster critical distance R_{RET}, the experimental values of quenching equilibrium constant K calculated from the Perrin plots, and radius R_{eff} of the Perrin action sphere.

Fullerene	Polymer	ΔG (eV)	Ω (mol·dm^{-3}m^{-2})	R_{RET} (nm)	K (mol^{-1}dm^3)	R_{eff} (nm)
$PC_{60}BM$	MDMO-PPV	– 1.28	$1.96 \cdot 10^{-11}$	8.5 ± 0.4	1900 ± 50	9.1 ± 0.1
	Tg-PPV	–1.44	$2.70 \cdot 10^{-11}$	10 ± 1	2380 ± 150	9.8 ± 0.2
	PCDTBT	– 0.73	$2.49 \cdot 10^{-11}$	8.7 ± 0.8	1690 ± 50	8.8 ± 0.1
	PCBTDPP	– 0.50	$0.86 \cdot 10^{-11}$	7 ± 1	740 ± 50	6.6 ± 0.1
$PC_{70}BM$	MDMO-PPV	– 1.20	$1.55 \cdot 10^{-10}$	12 ± 1	6500 ± 600	13.7 ± 0.5
	Tg-PPV	– 1.36	$2.20 \cdot 10^{-10}$	14 ± 1	9300 ± 500	15.4 ± 0.5
	PCDTBT	– 0.70	$1.40 \cdot 10^{-10}$	12 ± 1	4300 ± 100	12.0 ± 0.1
	PCBTDPP	– 0.40	$0.42 \cdot 10^{-10}$	10 ± 1	2400 ± 70	9.8 ± 0.1

The obtained values of K and R_{eff} also reveal that the fluorescence quenching of PPV polymers is more pronounced than that of copolymers PCDTBT and PCBTDPP. It was also found that the values of K noticeably correlate with the degree of polymer fluorescence and fullerene absorption overlap. This correlation suggested that fluorescence quenching can be caused by Förster resonance energy transfer. Förster critical distance R_{RET} at which the probability of RET is equal to 50 %, was determined according to the equation:

$$R_{RET} = \left(\frac{9000 f^2 \ln 10}{128 \pi^5 N_A n_0^4} \phi_D \Omega \right)^{1/6}, \quad (38)$$

where f^2 is the orientational factor (for randomly orientated transition dipoles in systems [77], it is equal to 2/3), ϕ_D is the fluorescence yield of the donor, n_0 is the refractive index of the solvent, N_A is Avogadro's constant and Ω spectral overlap integral. Values of Ω was calculated by numerical integration of intersection of polymer fluorescence and fullerene absorption spectra. The calculated values of Ω and R_{RET} are listed in *Table 12*.

There is clear evidence that the Förster critical distance R_{RET} (obtained from the spectral analysis of RET efficiency) reaches similar values to these obtained from the analysis of the Perrin model of static quenching R_{eff}. This proves that the observed fluorescence quenching can be fully explained by RET.

Simultaneously, kinetic and thermodynamic conditions for charge transfer in studied solution were verified. Thermodynamic conditions for CT are fulfilled according to values of Gibbs energy ΔG (see *Table 12*) calculated by using of Rehm-Weller equation [77]:

$$\Delta G = I_D - A_A - E_g - \frac{e^2}{\varepsilon d}, \tag{39}$$

where I_D is the ionization energy of the donor and can be approximated by the HOMO energy of the donor, A_A is the electron affinity of the acceptor and can be approximated by the LUMO energy of the acceptor, and E_g is the band gap of the donor. The last term expresses the interaction of the D-A pair with the solution, where e is the elementary charge, ε is the permittivity of the environment, and r_{AD} is the distance between the donor and the acceptor. This term can be neglected in the first approach, because its contribution is small (about 10^{-2} eV) [77]. Nevertheless significant contribution of charge transfer to fluorescence quenching was not considered, because there are the kinetic limits given by long distances between molecules in solutions (expected distance between donor and acceptor for CT is smaller than 1 nm [77]).

In summary, it was shown that resonance energy transfer plays a dominant role with respect to fluorescence quenching under the conditions when π-conjugated polymers and fullerenes are separated at such distance that direct contact and electron exchange is not possible. This was concluded on the basis of the similarity between the Förster critical distance R_{RET} obtained from the spectral analysis of RET efficiency and the R_{eff} values obtained from the analysis of the Perrin model of static quenching. Resonance energy transfer is more pronounced for $PC_{70}BM$, as it has a higher absorption coefficient compared to $PC_{60}BM$.

4.1.2.2 Fluorescence Quenching in Thin Layers

In order to understand the charge photogeneration processes in active layers of organic photovoltaic devices, fluorescence quenching in thin layers of MDMO-PPV and Tg-PPV blended with $PC_{60}BM$ were studied. Blends were excited at absorption maximum of polymers. Fluorescence spectra of MDMO-PPV with various content of $PC_{60}BM$ (from 0 to 50 %wt.) are shown on *Fig. 40 A*. Mutual comparison of fluorescence spectra for different concentration of $PC_{60}BM$ revealed that only 0.8 % mass fraction of $PC_{60}BM$ causes decay of polymer fluorescence intensity *PL* to 50 %. This indicates high efficiency of fluorescence quenching of MDMO-PPV polymers by $PC_{60}BM$ in thin layers. Comparable fluorescence intensity decay was observed in case of Tg-PPV blended with $PC_{60}BM$. The PCDTBT, PCBTDPP polymers were not included in this study.

Efficiency of the fluorescence quenching was evaluated from dependences of ratio $\ln(PL_0/PL)$ (fluorescence intensity of non-quenched polymer divided by intensity of fluorescence at given quencher concentration) on the mass fraction of $PC_{60}BM$ w. The dependencies are plotted for both polymers on *Fig. 40 B*.

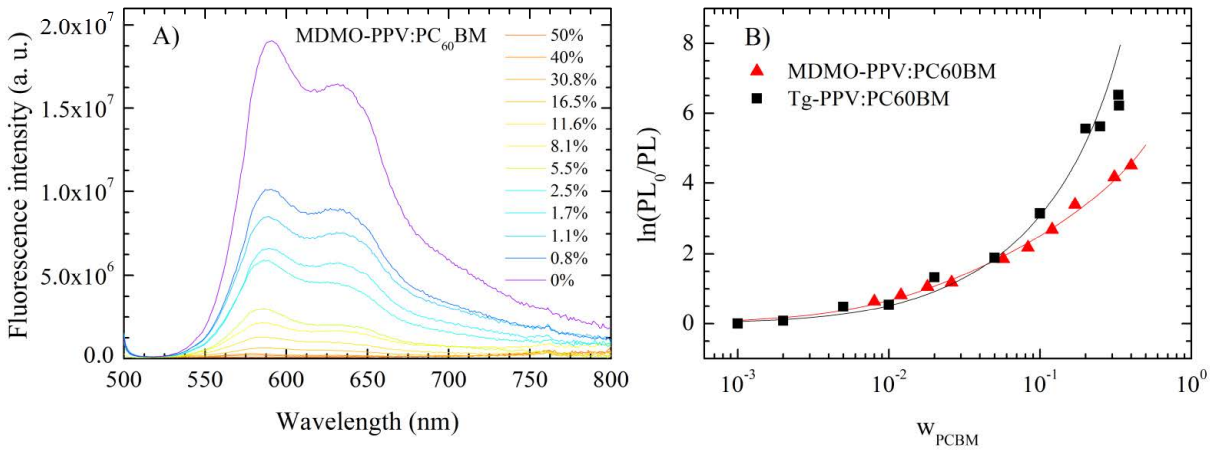

Fig. 40: A) Fluorescence spectra of MDMO-PPV with varying concentration of $PC_{60}BM$. B) Qualitative evaluation of fluorescence quenching efficiency.

The detailed analysis of the dependencies shows that the experimental data cannot be fitted by linear or single exponential function corresponding to the Stern-Volmer or Perrin equations respectively. However the data can be fitted with an exponential growth function, where the pre-exponential factor linearly depends on concentration. This suggests that combined model for static and dynamic quenching can be suitable for description of studied phenomena. The model is derived from Stern-Volmer and Perrin equations [77]:

$$\frac{PL_0}{PL} = [1 + K_2 c]\exp(K_1 c). \tag{40}$$

K_1 is the equilibrium constant for static quenching, which can be used for calculation of quenching sphere radius R_{eff}, as described in previous chapter. K_2 is quenching equilibrium constant for dynamic quenching equal to:

$$K_2 = k_{\text{diff}}\,\tau_0\,, \tag{41}$$

where τ_0 is fluorescence lifetime in absence of quencher and k_{diff} is kinetic constant for exciton diffusion. The value of k_{diff} is given by diffusion length L, collisional encounters efficiency f and collision radius R_c:

$$k_{\mathrm{diff}} = 4\pi R_{\mathrm{C}} \frac{L^2}{\tau_0} N_{\mathrm{A}} f. \tag{42}$$

This quenching model is validated for solutions, where concentration of quencher is expressed by molar concentration *c*. However, it is necessary to modify the equation in case of thin films, when molar concentration is expressed by mass fraction *w*:

$$c = \frac{w\rho(w)}{M_{\mathrm{A}}}, \tag{43}$$

where ρ is mass density of layer and varies with mass fraction of quencher in layer [167]. For the first approach, ρ was estimated from mass density of pristine components ρ_{A} (mass density of acceptor) and ρ_{D} (mass density of donor):

$$\rho(w) = \frac{\rho_{\mathrm{A}}}{w + (1-w)\dfrac{\rho_{\mathrm{A}}}{\rho_{\mathrm{D}}}}. \tag{44}$$

Based on the literature search, the density value ρ_{A} = 1.7 kg·dm^{-3} [168] was used. Simultaneously, ρ_{D} = 0.91 kg·dm^{-3} published for MDMO-PPV [169] was used for both PPVs as the mass density of Tg-PPV was not found in the literature. Therefore the mass density of Tg-PPV was expected similar to MDMO-PPV for the first approximation.

Based on *Eqs*. (39) and (42), the equation describing fluorescence quenching in thin films can be written in final form:

$$\ln\frac{PL_0}{PL} = \frac{K_1}{M_{\mathrm{A}}} w\rho(w) + \ln\left[1 + \frac{K_2}{M_{\mathrm{A}}} w\rho(w)\right]. \tag{45}$$

This model together with *Eq*. (43) was used for analysis of studied phenomena in particular for determination of quenching constants K_1 and K_2 presented in *Table 13*.

It is generally expected that quenching is caused by Förster resonance energy transfer as well as by charge transfer with kinetics driven by exciton diffusion [83]. For verification of this assumption, the quenching sphere radii R_{eff} was calculated from static equilibrium constant K_1 and diffusion kinetic constants k_{diff} from K_2. The kinetic constants k_{diff} were also used for estimation of collision radii R_C, where the exciton diffusion length was estimated to 6 nm. This value was published for pristine MDMO-PPV [82]. The resulting values of k_{diff}, R_{eff} and R_C are summarized in *Table 13*.

Table 13: Parameters describing fluorescence quenching

	MDMO-PPV	Tg-PPV
K_1 (M^{-1})	1.4 ± 0.3	4.2 ± 0.6
R_{eff} (nm)	0.8 ± 0.2	1.2 ± 0.2
R_{RET} *(nm)*	2.1 ± 0.1	2.0 ± 0.1
K_2	74 ± 6	90 ± 20
τ_0 (s)	$(2.8 \pm 0.3)\cdot10^{-10}$	$(3.7 \pm 0.6)\cdot10^{-10}$
k_{diff} (s^{-1})	$(2.7 \pm 0.4)\cdot10^{11}$	$(2.5 \pm 0.7)\cdot10^{11}$
L (nm)	6 ± 1[a]	6 ± 1[a]
R_C (nm)	0.5 ± 0.2	0.7 ± 0.2

a) Diffusion length of MDMO-PPV exciton determined by Scully et al.[168]

The values of quenching sphere radius R_{eff} were found 0.8 nm for MDMO-PPV and 1.2 nm for Tg-PPV respectively. These values are lower than Förster critical distances R_{RET} determined from spectral overlaps (for details see *Appendix No 5.*) to be 2 nm for both polymers, see *Table* 13. This value of R_{RET} is consistent with published value for MDMO-PPV:$PC_{60}BM$ by Scully et al. [168]. Simultaneously, R_{eff} of Tg-PPV was found to be higher than 1 nm, which is the highest excepted distance for charge transfer [77]. Therefore, R_{eff} can be attributed to the weighted averages of the radii describing both quenching processes over the probability of occurrence.

In case of collision radius R_C, the obtained values are well aligned with the distance for the CT rather than for RET, as the calculated values are smaller than 1 nm. On the other hand, R_{RET} is generally greater than R_{CT} and therefore exciton can achieve earlier the suitable distance for energy transfer

during the diffusion rather than for charge transfer. This indicates that average value of exciton diffusion length can be smaller than the used value taken from literature. Finally, R_C value can be considered as the weighted average radii of both quenching processes as it was noted in case of R_{eff}.

In summary, the detailed analysis of fluorescence quenching for the study of electron processes (charge transfer and energy transfer) related to the charge carries photogeneration in photovoltaic devices was presented.

It was shown that experimentally obtained dependencies of fluorescence intensities on fullerenes concentration can be evaluated by standard models for fluorescence quenching (Stern-Volmer and Perrin equations), which was modified with respect to the expression of fullerene amount in thin layers by mass fraction *w*. The obtained quenching constants were deeply analyzed in order to identify the presence of charge transfer and energy transfer. Thus, the studies allows to obtain information (range of dynamic and static quenching) which can help to optimize active layer morphology (materials domain size) for achievement of high photogeneration efficiency of charge carries in polymeric photovoltaic devices.

4.1.3 Emission of CT States

As it was described in *section 2.2.3.1,* that charge transfer states can be studied by fluorescence spectrometry in near infrared region. Herein, the fluorescence spectra of studied polymere:fullerene blends and identification of emission bands of CT states, which provided direct information of band gap energy of CT states are presented.

Fluorescence emission from CT states was studied in solution as well as in thin layers. The polymer:fullerene blends were excited at absorption maximum of polymer materials (see *Table 10* and *Table 11*). It was observed that solutions of polymers mixed with fullerenes did not showed any new emission peaks in the near infrared region in comparison with pristine materials spectra. Absence of these peaks is independent confirmation that

resonance energy transfer from polymers to fullerenes was dominant fluorescence quenching process as described in *section 4.1.2.1*.

However, in case of thin layers, new emission peaks in comparison with pristine materials were observed in the near infrared range. The spectra are plotted on *Fig. 41*. The layers of pristine fullerene show the fluorescence peak in the near infrared range too.

Fullerene spectra were analyzed and used for reconstruction of the spectra of blends and to identification of CT emission peaks. The positions of CT peaks were predicted using the empirical relation for CT band gap according to Veldman et al. [99]:

$$E_{CTlteo} = E_{\mathrm{LUMO\ A}} - E_{\mathrm{HOMO\ D}} + 0.29\ \mathrm{eV}, \tag{46}$$

Calculated E_{CTteo} values are summarized in *Table 14* together with positions of new emission peaks maxima E_{PLCT}, obtained from the spectra analysis.

Table 14: Comparison of theoretical values of charge transfer energy states and energy at emission peak maxima of polymer:fullerene blends.

Sample	E_{CTteo} (eV)	E_{PLCT} (eV)
MDMO-PPV:$PC_{60}BM$	1.11	≈1.34
MDMO-PPV:$PC_{70}BM$	1.19	≈1.36
Tg-PPV:$PC_{60}BM$	1.11	≈1.33
Tg-PPV:$PC_{70}BM$	1.19	
PCDTBT:$PC_{60}BM$	1.36	1.28
PCDTBT:$PC_{70}BM$	1.44	1.29
PCBTDPP:$PC_{60}BM$	1.41	1.26
PCBTDPP:$PC_{70}BM$	1.49	1.28

PPV blends revealed their dominant emission E_{PLCT} at 1.4–1.5 eV. These values correspond rather to the published maximum for phosphorescence of fullerenes [99] than to the emission from CT states. Emissions of CTs are roughly estimated around 1.35 eV. Determined energy (E_{PLCT}) is still 0.14 eV higher in average than calculated values E_{CTteo}.

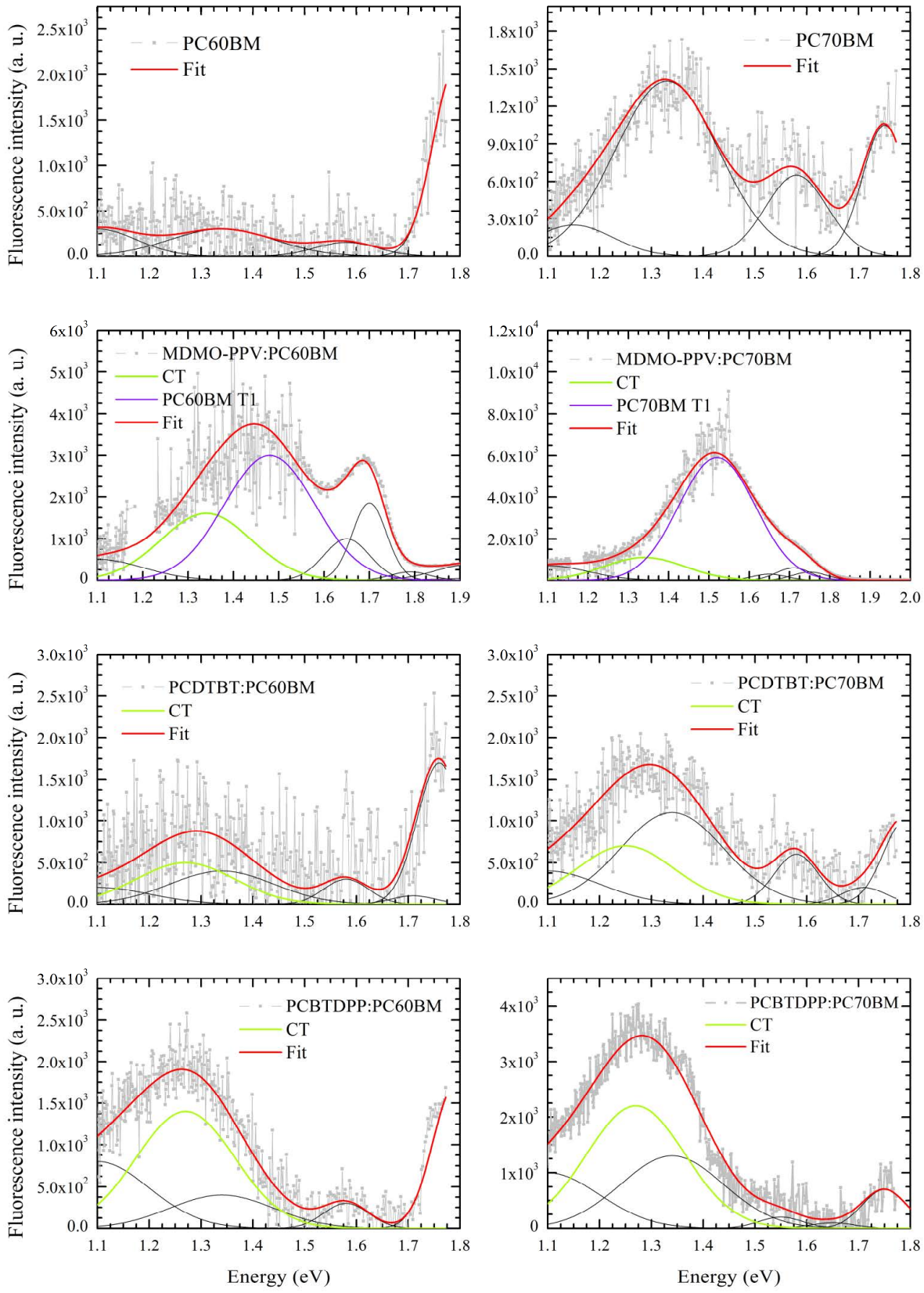

Fig. 41: Photoinduced emission of thin layers of fullerenes and polymer:fullerene blends in near infrared range.

PCDTBT and PCBTDPP copolymers blends showed near infrared emission maxima in average at about 0.2 eV lower than it was predicted by theoretical calculations. This is in accordance with the fact that the emission maximum is red shifted by the reorganization energy [170]. Nevertheless, the spectrum of PCDTBT:$PC_{70}BM$ is very similar to spectrum of pristine $PC_{70}BM$. Pristine PPVs as well as PCDTBT are fluorescent emitting materials in thin layers, therefore emission of CT states may be overlapped by enhanced emission of fullerenes, due to resonance energy transfer from polymers. Therefore, identification of CT emission peaks is hindered.

In case of PCBTDPP, the resonance energy transfer on fullerenes is not expected due to the absence of PCBTDPP fluorescence. Therefore, fullerenes in blends with PCBTDPP can be excited only by direct light absorption. Moreover, absorption maximum of PCBTDPP lies at 1.73 eV. This is very near to the absorption edge of fullerenes since their absorption is at this light energy negligible in comparison to PCBTDPP. Thus detected near infrared emission peaks from PCBTDPP:fullerenes blends are most likely originating from charge transfer states.

In summary, weak fluorescence of CT states were observed on thin films of the studied blends. Despite the co-emission of fullerenes and CT states, the positions of CT states emission maxima were determined based on spectra analysis. More straightforward results were obtained for PCBTDPP:PCBM thin layers, because polymer PCBTDPP is non-fluorescent in thin films and have smaller optical band gap than fullerenes, which allow excitation of polymer without simultaneous excitation of fullerenes.

4.1.4 Determination of Photovoltaic Devices Properties

The modelling of photovoltaic parameters can be used for estimation of suitability of new donor or acceptor materials for application in photovoltaic devices. Therefore this section is focused on utilization of optical spectra of studied polymer:fullerenes blends for estimation of photovoltaic devices parameters, in particular open circuit voltage V_{OC} and short current

density j_{SC}. These parameters are usually estimated from molecular energy levels (energy of band gap, HOMO and LUMO levels) of used materials [177]. Both approaches to modelling of photovoltaic devices parameters were utilized and obtained parameters were compared with parameters of real devices.

4.1.4.1 Determination from Molecular Energy Levels

The values of V_{OClim} were calculated as difference of HOMO energy level of polymer (donor) and LUMO energy level of fullerene (acceptor):

$$V_{OClim} = E_{LUMO\ A} - E_{HOMO\ D}\ . \tag{47}$$

It presents the theoretical maximal value of V_{OC} and therefore this quantity is marked V_{OClim}. Calculated values are summarized in *Table 15*.

Short current density j_{SC} was estimated through the Shockley-Queisser limit model [173, 174]:

$$j_{SC} = q\int_{E_1}^{E_2} \phi_{Sun}(E)a(E)dE\ , \tag{48}$$

where a is absorptance of the layer and is expected equal to 1 for all the absorbed energies. ϕ_{Sun} is photon flux of Sun and was calculated from Sun light intensity spectrum defined by standard AM 1.5G. Integral upper limit E_2 was determined by absorption edge of ITO (350 nm) and lower limit E_1 by band gap of polymer.

The Shockley-Queisser limit model expects that all the absorbed photons contribute to photocurrent generation. An external quantum efficiency EQE is equal to 1 above the absorption edge of donor and is equal to 0 under the absorption edge, respectively. This is the reason why this model is not fully appropriate for organic materials, which does not exhibit sharp absorption edge [174]. Values of j_{SC} calculated by this way represent the maximal value and can be again considered as limit. Therefore, this calculated short current density is marked j_{SClim} as summarized in *Table 15*.

The calculated values can be more realistic, if the value of j_{SClim} will be multiplied by the expected mean value of EQE, as it is realized for example in The Ossila Scharber Calculator [177].

Table 15: Comparison of estimated values of short current density j_{SC} and open circuit voltage V_{OC} estimated from optical parameters with values determined on real photovoltaic devices.

	According to energy levels		**According to optical spectra**		**Literature data***	
Device	j_{SClim} **(mA/cm²)**	V_{OClim} **(V)**	j_{SCa} **(mA/cm²)**	$V_{OCteofl}$ **(V)**	j_{SC} **(mA/cm²)**	V_{OC} **(V)**
MDMO-PPV:PC_{60}BM 1:4	13	0.82	12	0.87	5.3	0.82
MDMO-PPV:PC_{70}BM 1:4	13	0.90	20	0.89	7.6	0.77
Tg-PPV:PC_{60}BM 1:4	10	0.82	10	0.86	3.1	0.82
Tg-PPV:PC_{70}BM 1:4	10	0.90	17			
PCDTBT:PC_{60}BM 1:4	18	1.07	13	0.81	6.9	0.89
PCDTBT:PC_{70}BM 1:4	18	1.15	15	0.82	10.3	0.88
PCBTDPP:PC_{60}BM 1:3	23	1.12	12	0.79	5.2	0.85
PCBTDPP:PC_{70}BM 1:3	23	1.20	14	0.81	8.0	0.76

*for reference see *Table 5*.

4.1.4.1 Determination from Spectral Characteristics

At this approach, the values of V_{OC} were determined from energy of maximum of emission peak of CT state. Veldman et al. [99] described relation between energy of charge transfer state E_{CT} and open circuit voltage V_{OC} by empirical term:

$$V_{OCteo\,fl} = E_{CT} - 0.47\ \text{eV}. \tag{49}$$

Open circuit values calculated by this way is marked $V_{OCteofl}$ and calculated values are shown in *Table 15*.

Values of j_{SCa} were calculated by Shockley-Queisser limit model (*Eq.* (48)), where absorptance a was calculated from experimental obtained absorbance A:

$$a(E) = 1 - 10^{-A(E)}. \tag{50}$$

In solar cells devices, the incident light, which was not absorbed during transmission through thin layers, is reflected back by the aluminium electrode. Thus, the reflection allows higher absorption. This contribution was taken into account by means of multiplication of absorbance by two. This is only a rough simplification according to the description in *section 2.2.1* and it was deeper analysed for example in work [178]. The spectra were integrated from 350 nm to absorption edge. Obtained values of j_{SCa} are summarized in *Table 15.*

4.1.4.1 Models Comparison

Table 15 summarizes values of j_{SC} and V_{OC} calculated from both energy levels and optical spectra, and real values of V_{OC} and j_{SC} published in literature.

There is one significant difference between j_{SClim} and $j_{SCa:}$ Values of j_{SCa} include the contribution of light absorption by fullerenes and therefore better reflect the difference between $PC_{60}BM$ and $PC_{70}BM$. On other hand j_{SCa} values are dependent on layer thickness, which control light absorption as well as losses of photogeneration efficiency due to the recombination of charge carriers during charge transport. Therefore, direct comparison with the data from the literature is not straightforward even if the influence of EQE will be included. Still, the values of j_{SCa} demonstrate that the modelled short current density from the absorption spectra are more realistic than the values modelled from the band gap energy, because it reflects the contribution of both donor as well as acceptor materials.

Values of both calculated open circuit voltages are better comparable between each other. While V_{OClim} values predicted photovoltaic devices with V_{OC} greater than 1 V, $V_{OCteofl}$ values saturate at 0.82 V. These values are in good agreement with published experimental V_{OC} values.

In summary, the estimation of j_{SC} and V_{OC} of organic heterojunction photovoltaic devices from optical spectra of used electron donor and electron acceptor materials blends was presented. The calculations based on spectral data showed better agreement with real devices than the results calculated

from molecular orbital energy levels. Values of j_{SC} are very poorly predictable without determination of loses during charge carrier transport. The study of transport phenomenon was outside the scope of this work. The values of V_{OC} may be estimated relatively accurately from the energies of CT emission. It emphasizes the importance of research of CT states.

4.1.5 Conclusion of Optical Studies

Studies of fluorescence quenching in solution and thin films of π-conjugated polymers by fullerenes were presented. Results of the studies of electron processes in solutions showed significant contribution of resonance energy transfer from polymer to fullerenes in comparison with charge transfer driven by exciton diffusion. In addition the studies of fluorescence quenching based on the modelling by Stern-Volmer and Perrin model enable to delineate these processes in thin layers.

Another goal of optical studies was focused on detection of CT states by analysis of fluorescence emission. Based on this analysis, the energy of maximum of emission peak originating from relaxation of excited CT states were determined.

Finally parameters of photovoltaic devices prepared from studied blends were estimated from optical spectra and molecular energy levels of materials.

4.2 Detection and Study of Charge Transfer States by Optoelectrical Methods

The studied polymer:fullerenes blends described in previous sections were used for preparation of organic photovoltaic devices based on bulk heterojunction. The current-voltage characteristic and spectrally resolved photocurrents measurements were evaluated with respect to the parameters describing efficiency of photovoltaic conversion. Subsequently, optoelectrical experiments focused on detection of CT states based on spectrally resolved photocurrent and electroluminescence measurements were realized. Finally,

these results were evaluated in order to determine the influence of CT states on photovoltaic parameters.

4.2.1 Photovoltaic Efficiency

Prepared photovoltaic devices were characterized by current voltage measurement under illumination by solar simulator and photovoltaic conversion efficiency was evaluated. Examples of current-voltage characteristics are plotted on *Fig. 42*.

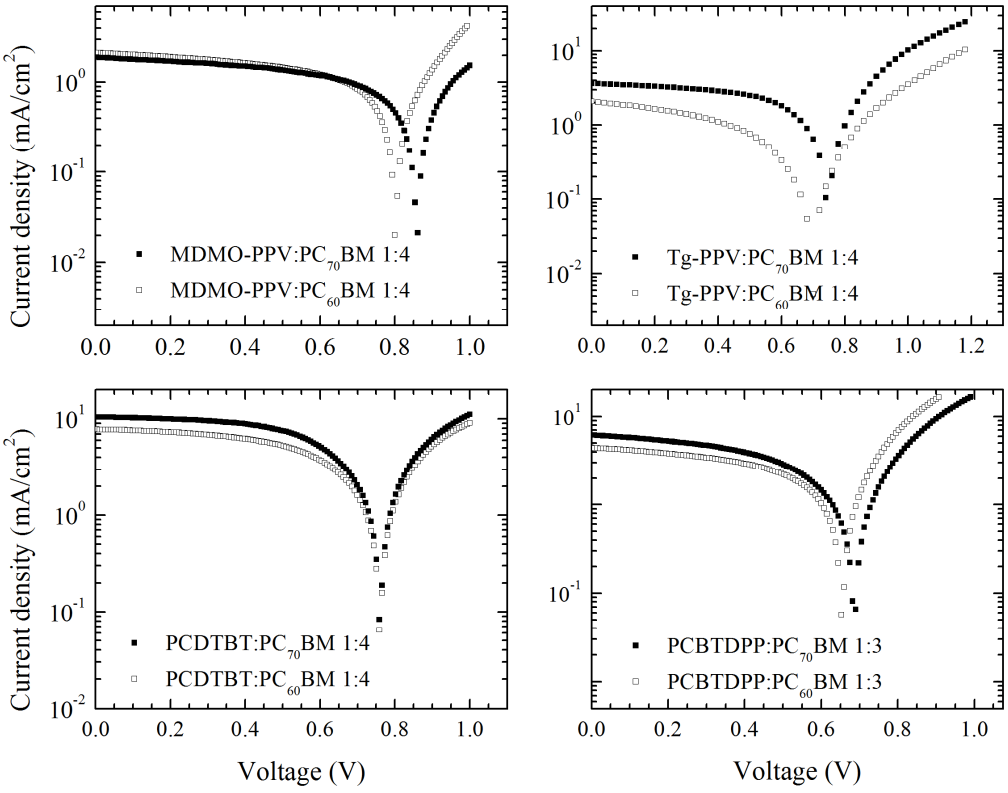

Fig. 42: Examples of current-voltage characteristic measured under light irradiation of π-conjugated polymers:fullerenes devices.

The photovoltaic conversion efficiency η of prepared devices was evaluated by standard procedure from measured characteristics according to scheme on *Fig. 43*. Values of short current density j_{SC} was evaluated as values of current density at zero voltage and values of open circuit voltage V_{OC} as values of voltage at zero current density, respectively. The maximum

electrical power P_{max} was deducted from electrical power-voltage characteristic which was derived from current-voltage characteristic by application of term:

$$P = jV\,. \tag{51}$$

The calculated values of maximum power P_{max} were compared with theoretical maximum power $P_{max\ ideal}$ which is defined as the product of j_{SC} and V_{OC}. The comparison was realized trough fill factor *FF*:

$$FF = \frac{P_{max}}{j_{SC}V_{OC}}100\,\%, \tag{52}$$

The fill factor of ideal solar cell without loses is equal to 100 % [65].

The photovoltaic conversion efficiency η was calculated according to term:

$$\eta = \frac{P_{max}}{I}100\,\%, \tag{53}$$

where I is the intensity of incident light [65]. The light intensity of solar simulator was 100 mWcm^{-2}.

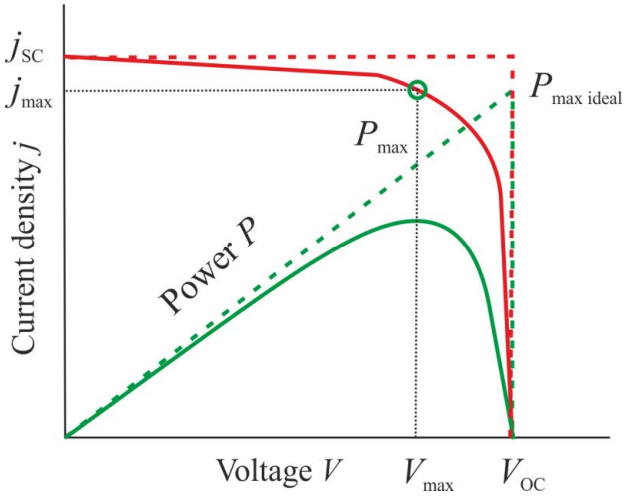

Fig. 43: Current-voltage characteristic and power-voltage characteristic of photovoltaic devices under illumination.

The achieved photovoltaic conversion efficiencies of devices are summarized in *Table 16*, together with appropriate values of short current density j_{SC}, open circuit voltage V_{OC} and fill factor *FF*.

Table 16 includes also the photovoltaic parameters of devices prepared from pristine polymers and pristine fullerenes. Photovoltaic conversion efficiencies of these devices from pristine materials are poor. It is in agreement with generally accepted model of efficient organic photovoltaic device which require charge transfer process from donor to acceptor for achievement of efficient photogeneration of charge carriers [30]. However, the parameters of pristine devices are necessary for evaluation of subsequent optoelectrical experiments and therefore were included in *Table 16.*

Table 16: The achieved photovoltaic parameters of prepared devices and thickness (d) of their active layers.

Device	***d* (nm)**	***j*SC (mA/cm²)**	***V*OC (V)**	***FF* (%)**	***η* (%)**
MDMO-PPV	94 ± 5	$(8 \pm 2)\cdot10^{-3}$	1.03 ± 0.02	26 ± 1	$(4 \pm 1)\cdot10^{-3}$
MDMO-PPV:$PC_{60}BM$ 1:4	130 ± 20	2.04 ± 0.08	0.76 ± 0.03	42 ± 2	0.65 ± 0.07
MDMO-PPV:$PC_{70}BM$ 1:4	260 ± 10	1.81 ± 0.09	0.85 ± 0.01	40 ± 4	0.65 0.07
Tg-PPV	420 ± 5	$(3.1 \pm 0.1)\cdot10^{-4}$	1.05 ± 0.05	29 ± 1	$(1.1 \pm 0.5)\cdot10^{-4}$
Tg-PPV:$PC_{60}BM$ 1:4	140 ± 20	2.2 ± 0.1	0.68 ± 0.06	30 ± 2	0.46 0.09
Tg-PPV:$PC_{70}BM$ 1:4	123 ± 5	3.9 ± 0.2	0.74 ± 0.02	44 ± 2	1.3 ± 0.1
PCDTBT	63 ± 5	$(31 \pm 2)\cdot10^{-3}$	0.92 ± 0.03	24.7 ± 0.3	$(7 \pm 1)\cdot10^{-3}$
PCDTBT:$PC_{60}BM$ 1:4	53 ± 5	7.8 ± 0.2	0.75 ± 0.01	45 ± 2	2.6 ± 0.1
PCDTBT:$PC_{70}BM$ 1:4	52 ± 5	11.0 ± 0.5	0.74 ± 0.01	46 ± 1	3.7 ± 0.1
PCBTDPP	40 ± 10	$(70 \pm 1)\cdot10^{-3}$	0.82 ± 0.01	26 ± 1	0.02 ± 0.01
PCBTDPP:$PC_{60}BM$ 1:3	62 ± 5	4.4 ± 0.4	0.71 ± 0.02	37 ± 1	1.2 ± 0.1
PCBTDPP:$PC_{70}BM$ 1:3	86 ± 5	6.1 ± 0.2	0.67 ± 0.02	37 ± 1	1.53 ± 0.06
$PC_{60}BM$	30 ± 10	0.02 ± 0.01	0.13 ± 0.01	32 ± 1	$(0.9 \pm 0.2)\cdot10^{-4}$
$PC_{70}BM$	40 ± 10	0.26 ± 0.01	0.59 ± 0.01	36 ± 2	0.05 ± 0.02

According to parameters in *Table 16*, the best performance solar cells were prepared from the PCDTBT:$PC_{70}BM$ blend. This finding is consistent with the data presented in *Table 1*, which summarizes the photovoltaic parameters of the devices published by other authors. Also the observation of higher photogeneration efficiency in case of devices containing $PC_{70}BM$ in comparison with devices containing fullerene $PC_{60}BM$ are in good agreement with previously published data as follows from *Table 16 and Table 1*.

Overall, the prepared devices had smaller photovoltaic conversion efficiency than published devices summarized in *Table 1*. In the most cases prepared devices had reduced values of short current density and fill factor in comparison with published devices. It indicates higher contact barrier of prepared devices as the solar cells were prepared only with aluminium top contact without other transport layers, which are applied to reduce the contact barriers (for example most used interlayer is LiF) [123]. However, the optimization of the OSC structure (with respect to the aditional layers) is not a part of this thesis.

Moreover, the thickness of active layer can also limit the photogenerated current. The active layer thickness was determined by means of mechanical profilometer and values are also summarized in *Table 16*. The active layer thickness of PPV's devices was found in many cases bigger than 100 nm, which is generally considered to be ineffective for efficient charge carrier transport in organic thin films [123].

4.2.2 External Quantum Efficiency Spectra

In order to investigate spectral response of photovoltaic devices, all prepared solar cells were characterized by measurements of the photocurrent spectra at zero voltage. Obtained photocurrent spectra were recalculated in temrs of external quantum efficiency (EQE), which is defined as ratio between number of generated charges N_e and number of incident photons N_{ph}:

$$\mathrm{EQE} = \int \frac{N_e(\lambda)}{N_{ph}(\lambda)} \mathrm{d}\lambda . \tag{54}$$

Values of N_e were calculated from measured photocurrent and N_{ph} from light intensity. Equation for calculation of EQE can be overwritten as:

$$\mathrm{EQE} = \int \frac{hc}{q} \frac{I_{ph}(\lambda)}{\lambda P(\lambda)} \mathrm{d}\lambda , \tag{55}$$

where h is the Planck constant, c is speed of light; q is the elemental charge

and λ the light wavelength. EQE can be expressed in percentage when values are multiplied by 100.

EQE spectra are represented by plots on *Fig. 44–Fig. 48*. There are unambiguous differences between EQE quantity of pristine materials and of polymer:fullerene blends used in photovoltaic devices. Whereas the best EQE of pristine materials reaches units of percent, the blends exhibit significantly

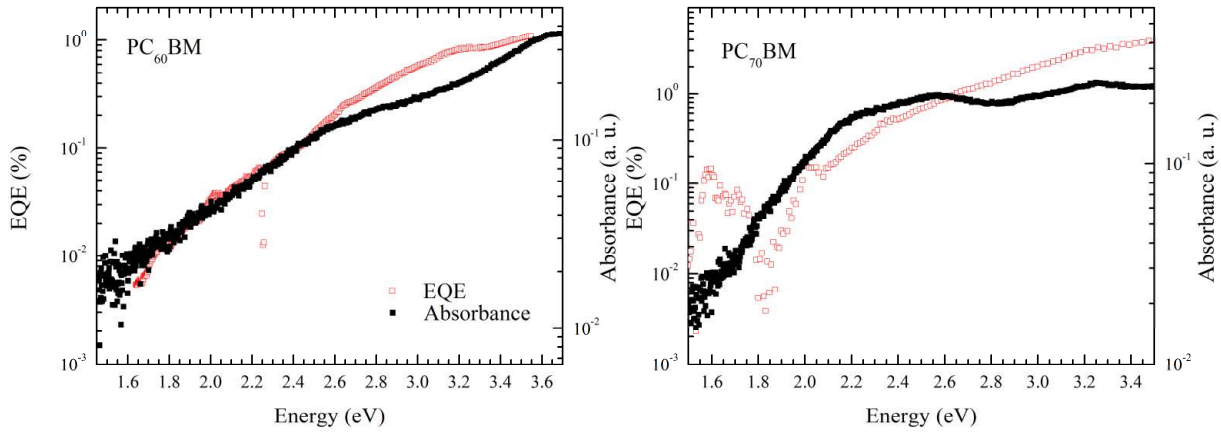

Fig. 44: EQE spectra and absorption spectra of fullerenes.

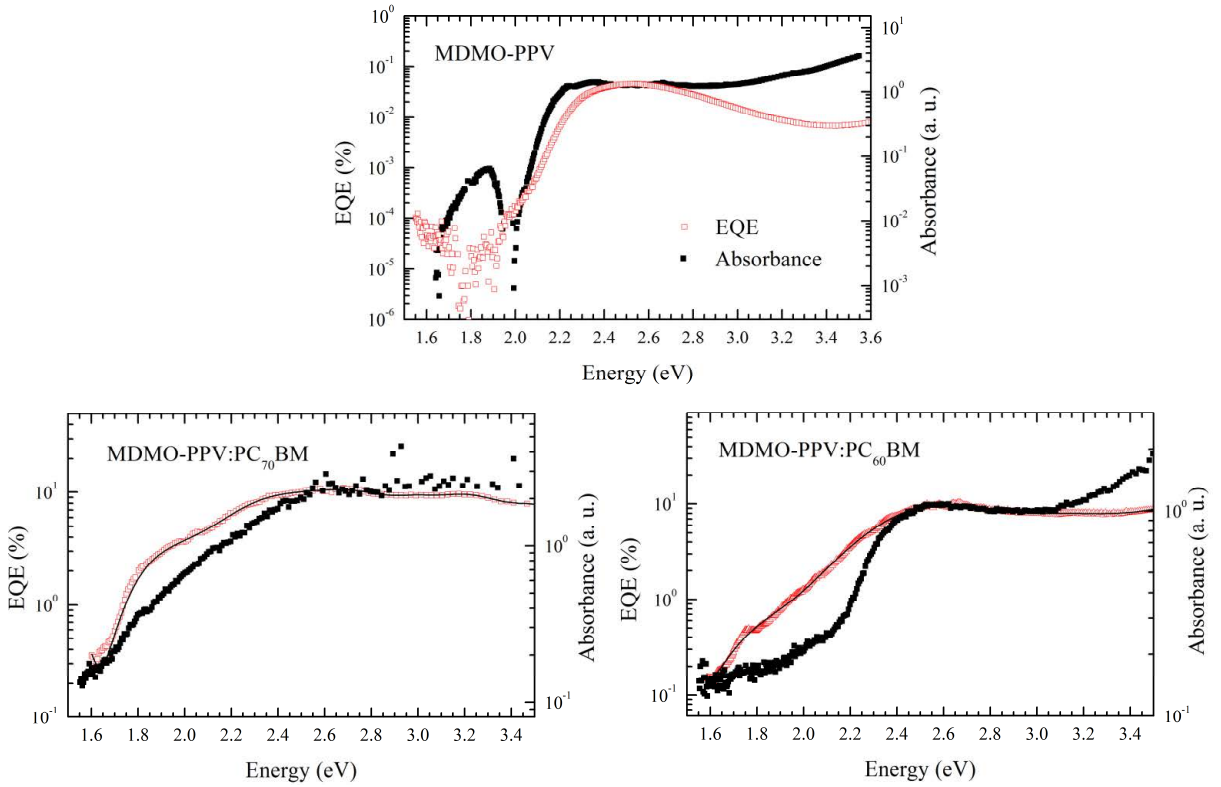

Fig. 45: EQE spectra and absorption spectra of MDMO-PPV and then of photovoltaic devices MDMO-PPV:PC_{60}BM 1:4 and MDMO-PPV:PC_{70}BM 1:4.

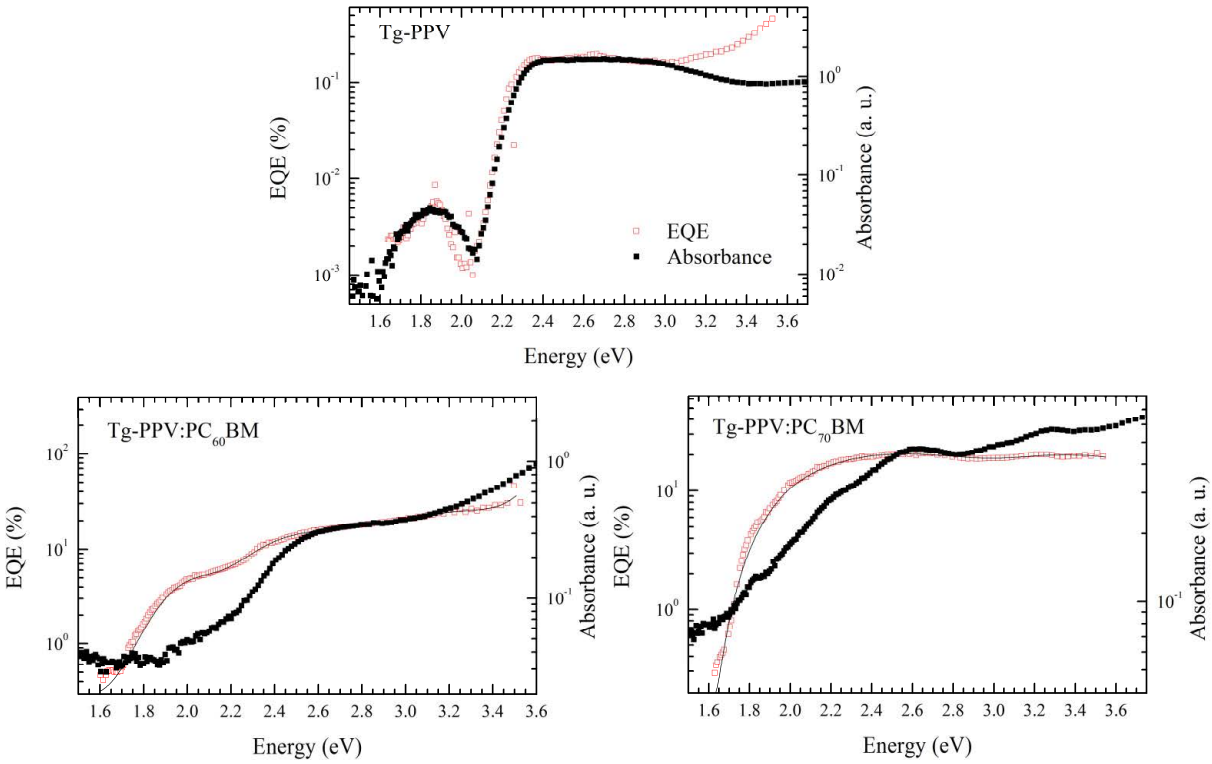

Fig. 46: EQE spectra and absorption spectra of Tg-PPV and then of photovoltaic devices Tg-PPV:PC_{60}BM 1:4 and Tg-PPV:PC_{70}BM 1:4.

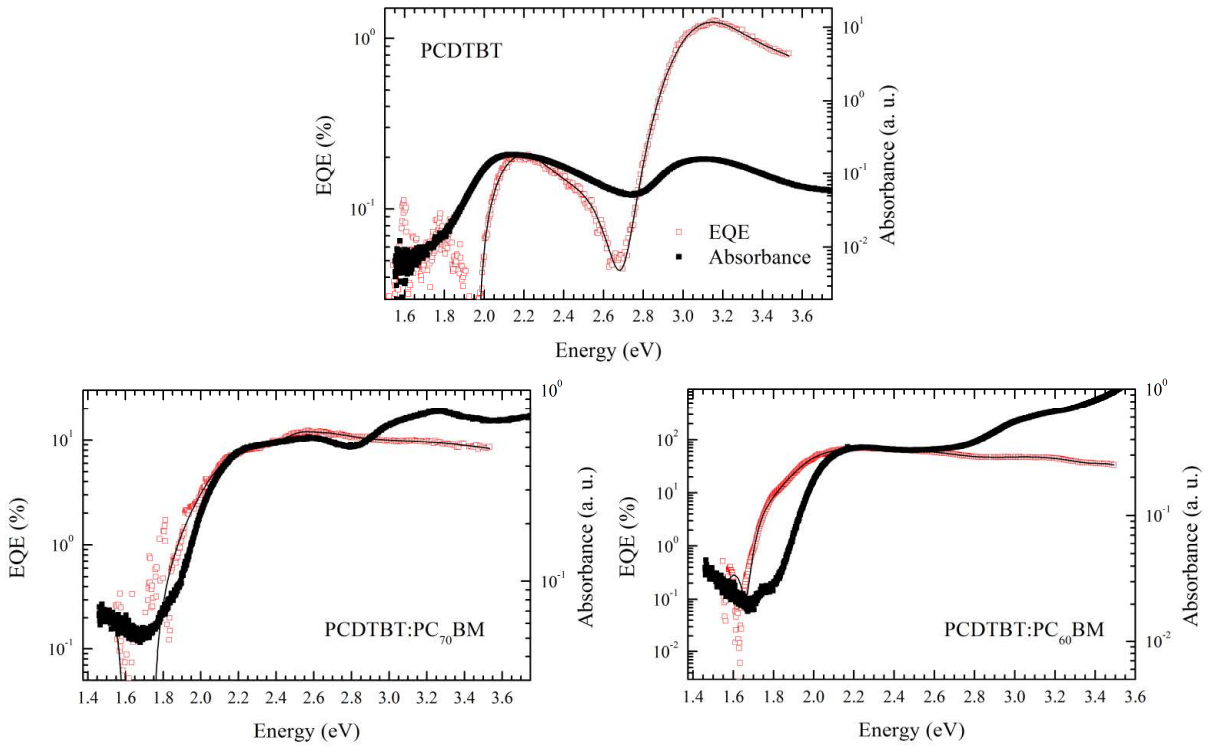

Fig. 47: EQE spectra and absorption spectra of PCDTBT and then of photovoltaic devices PCDTBT:PC_{60}BM 1:4 and PCDTBT:PC_{70}BM 1:4.

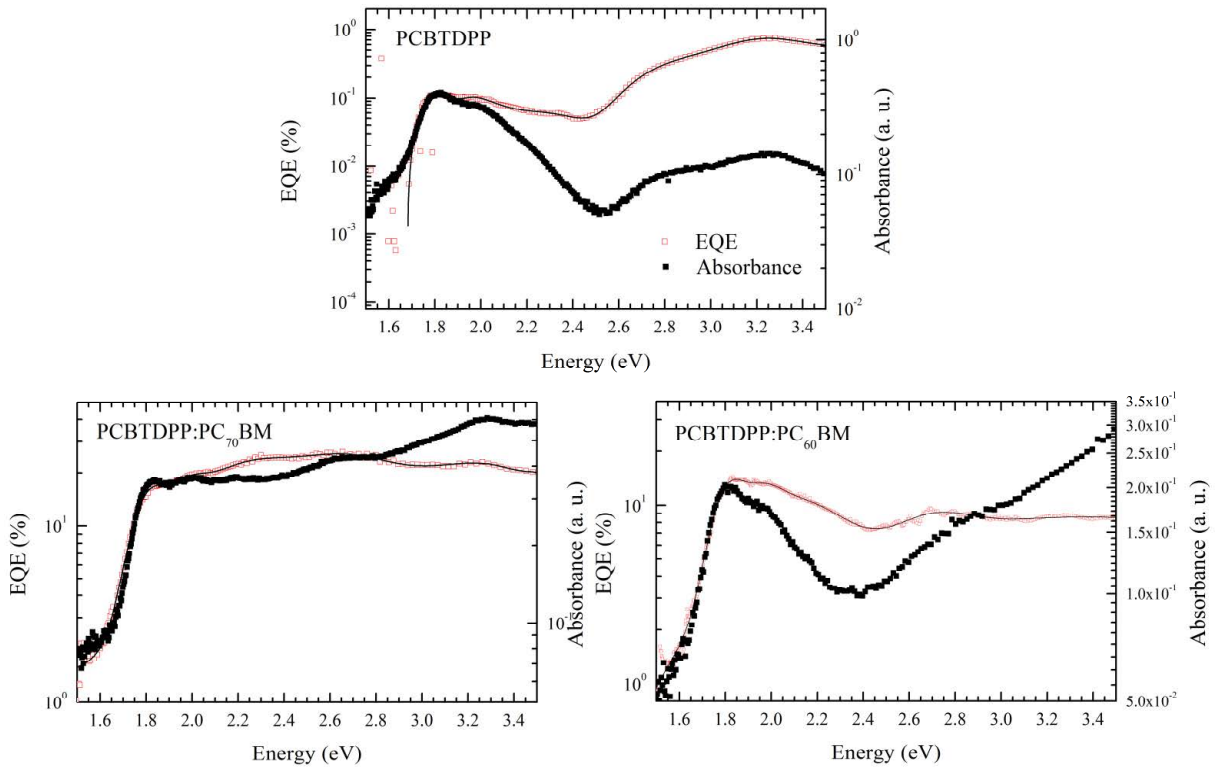

Fig. 48: EQE spectra and absorption spectra of PCBTDPP and then of photovoltaic devices PCBTDPP:PC_{60}BM 1:3 and PCBTDPP:PC_{70}BM 1:3.

higher EQE in order of tens percent. This result is in accordance with values of j_{SC} (see *Table 5*), since the integral of measured photocurrent spectra is equal to the value of short current I_{SC}.

The comparison of EQE spectra with absorption spectra should contribute to deeper insight into studied photogeneration phenomena as they can provide the additional information about conversion of absorbed light to generated photocurrent. Absorption spectra are included in *Fig. 44–Fig. 48*. The shape of EQE spectra in all cases are not accurately followed by absorption spectra. There are similarities of peak positions, but peaks amplitudes vary. First explanation of these differences can be explained by light interference caused by the back reflection from aluminium electrode. The sharp minima in EQE spectra (PC_{70}BM approximately at 1.8 eV, MDMO-PPV at 1.8 eV, Tg-PPV at 2 eV, PCDTBT at 2 eV and 2.7 eV, PCDTBT:PC_{60}BM at 1.6 eV) indicate the presence of the interference. Thus EQE spectra allowed

assessing of photogeneration losses due to inappropriate tuning of layer thicknesses.

EQE spectra also showed that in photovoltaic devices both components of active layer: electron donor (π-conjugated polymer in our case) and electron acceptor (fullerene) materials are contributing to the photogeneration by absorption of light. This is an important proof, that the usually presented description of photogeneration processes (light absorption by donor, exciton diffusion, electron transfer to acceptor, electron-hole pair separation and charges transport to electrodes) in organic photovoltaic devices are not the only contributing mechanisms to photogeneration efficiency.

Fig. 44 shows EQE spectra of pristine fullerenes. The EQE values are the same order of magnitude as EQE values of pristine polymers. In fullerene:polymere blends light absoption by fullerenes caused increase of EQE values by one or more orders of magnitude. This is evidence that pristine electron acceptor provides non-efficient photovoltaic devices as pristine polymers. Nevertheless after addition of hole acceptor (electron donating polymer in this case), which allows charge transfer (directly or by means of energy transfer) contribution of photons absorbed by fullerenes to photogeneration efficiency is significant.

Simultaneously comparison of EQE and absorption spectra confirm that estimation of j_{SC} parameter from absorption spectra of blends is appropriate approximation as described in *section 4.1.4*.

The utilization of spectrally resolved photocurrent measurement to detection of CT states absorption bands was referred in *section 2.2.3.1*. However, the detection limits of our apparatus used for spectrally resolved photocurrent experiments didn't allows observation of these CT bands. For further information about the apparatus see the *Appendix No 6.*

4.2.3 Studies of Electroluminescence of Photovoltaic Devices

In order to detect the bimolecular recombination, the intensity of electroluminescence was measured simultaneously with current voltage characterization of photovoltaic devices in dark. Results are summarized in plots on *Fig. 49*. Measured current was re-calculated on current density (the value of current was divided by the area of the electrodes - 0.06 cm^2) and the applied voltage was recalculated on electric field (applied voltage was divided by the active layer thickness, see *Table 16*) to achieve the characteristics independent to sample dimensions. It was found that the radiative bimolecular recombination took place in photovoltaic devices (polymer:fullerenes blends) as well as in pristine materials.

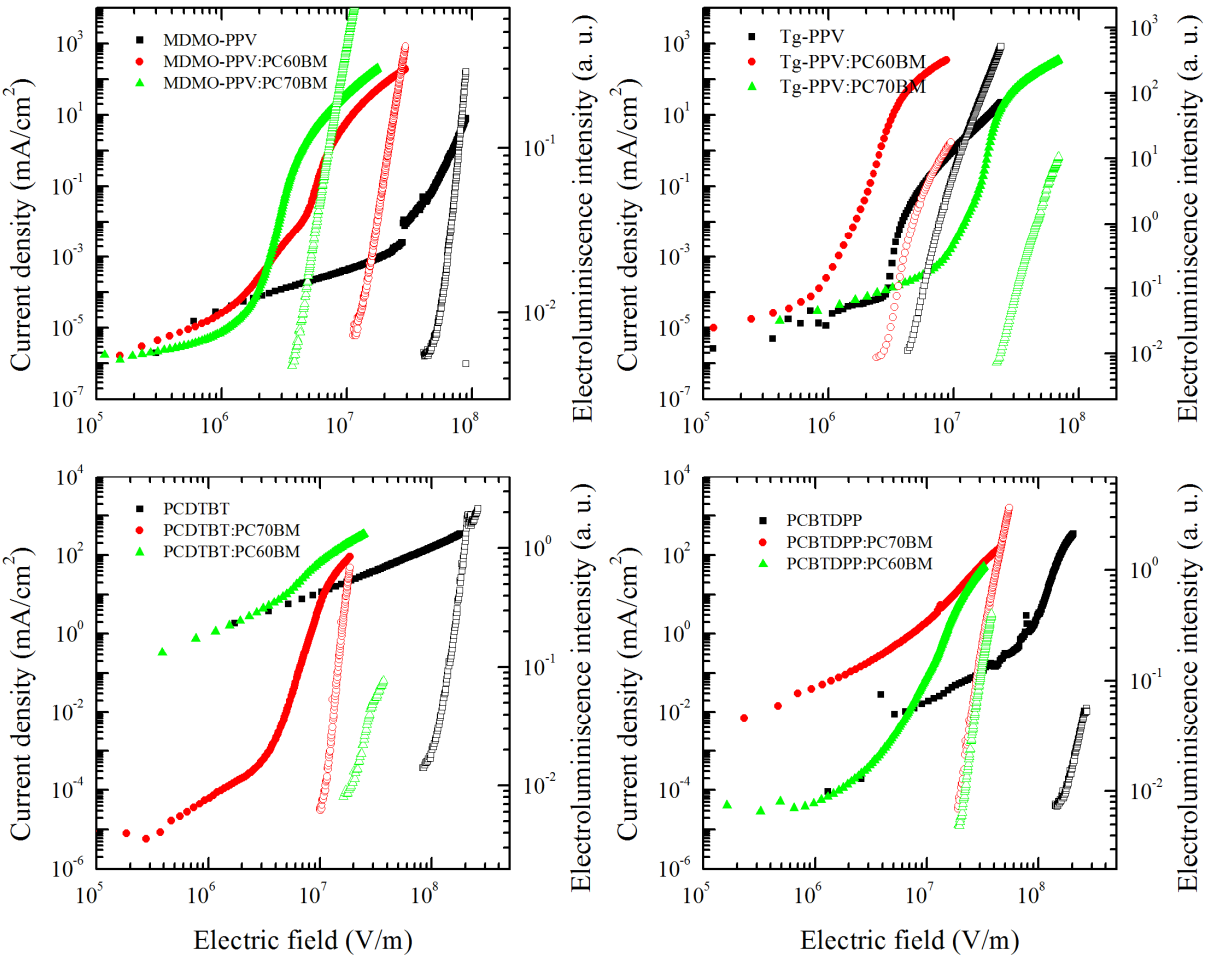

Fig. 49: Dark current voltage characteristics (filled symbols) compared with detected integral electroluminescence intensity (empty symbols).

Therefore electroluminescence spectra were measured to identify of recombination centres. *Fig. 50* plots electroluminescence spectra of pristine materials and their blends. These spectra were compared with photoluminescence spectra. It was found that shape and position of electroluminescence spectra of pristine materials are similar to fluorescence spectra. Only in case of PCBTDPP, this comparison was impossible, since PCBTDPP did not show any fluorescence in thin film as it was described in *section 4.1.1.2.*

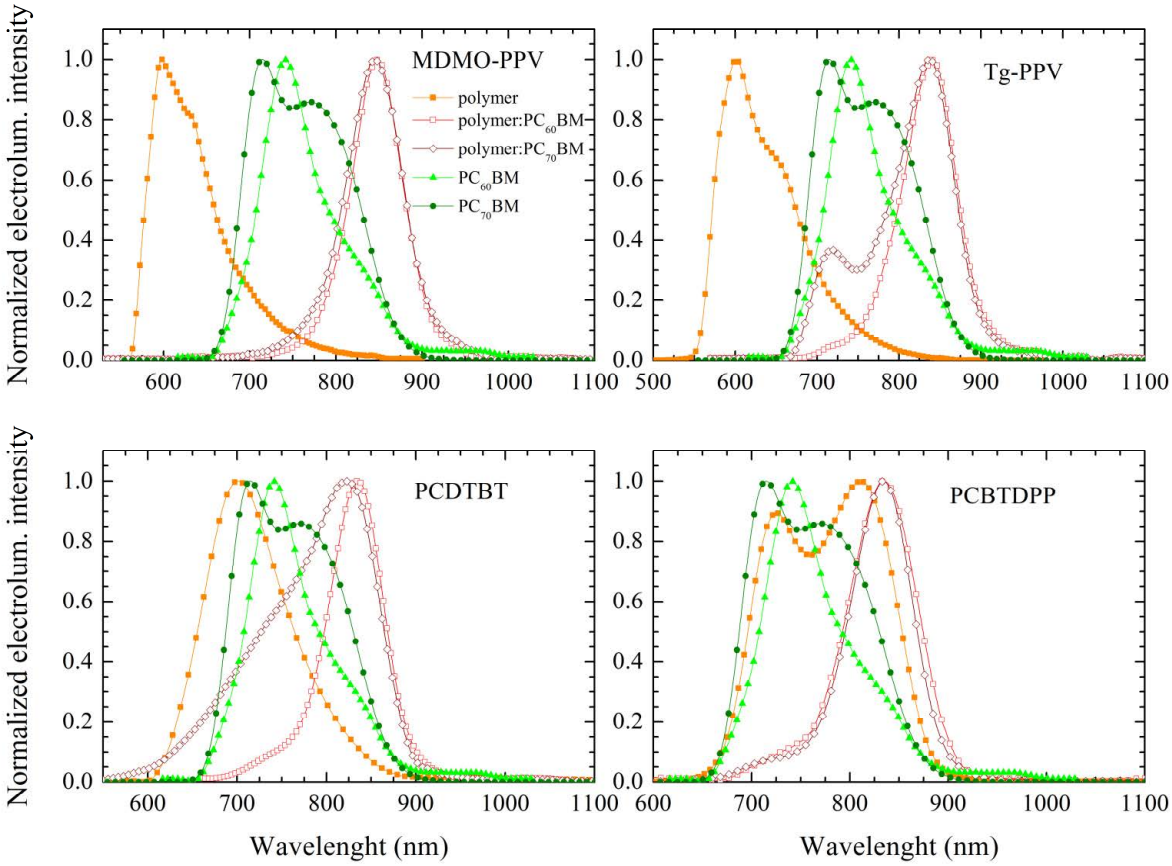

Fig. 50: Smoothed electroluminescence spectra of pristine materials and their blends (orange curves – polymers, green curves – fullerenes, red curves – blends).

All of the blends presented a electroluminescence peak maximum at 1.48 ± 0.02 eV (e.g. about 850 nm), independently on used polymers or fullerenes. This result is not consisting with fluorescence spectra, where new emission bands were observed in the range from 1.26 to 1.36 eV (e.g. about 912 – 985 nm). There is also disagreement of measured electroluminescence

spectra of MDMO-PPV:$PC_{60}BM$ device and published spectra. Tvingstedt et al. [105] presented electroluminescence spectrum with position of emission maxima at 1.27 eV (980 nm).

Explanation can be found in emission from fullerenes triplet states, which showed peak maxima at about 1.5 eV [99]. Emission from triplet states is preferred over emission from CT, if the energy level of triplet state is lower lying than the energy level of CT [99]. In case of PCBTDPP blends calculated E_{CT} values are similar to the value of 1.5 eV, see *Table 14*. E_{CT} values of PPV and PCDTBT blends do not fulfilled the condition because values are smaller than 1.5 eV.

However, the morphology of active layer can influence electroluminescence spectrum. The spectra of Tg-PPV:$PC_{70}BM$ and PCDTBT:$PC_{70}BM$ are conclusively composed from peaks originating from pristine materials. This observation is in contrast with observations reported by Tvingstedt et al. [105]. This slight discrepancy may be caused by imperfections of layers morphology and can be supported by the explanation of electroluminescence spectra by emission from fullerenes triplet states.

Electroluminescence measurements were used for calculation of electroluminescence external quantum efficiency EQE_{EL}.

$$EQE_{EL} = \int \frac{N_{ph}(\lambda)}{N_{inj}} d\lambda \,, \tag{56}$$

where N_{ph} is the number of emitted photons and N_{inj} is the number of charges injected into the devices. These data were used for further calculation described in following *section 4.2.4* and are also presented in *Appendix No* 7.

In summary, electroluminescence of photovoltaic devices was studied in details. Electroluminescence spectra of pristine materials were in good agreement with fluorescence spectra, while spectra of blends showed unanimously maximum emission at 1.48 eV independently on used donor

and acceptor material. It was decided that electroluminescence rather came from triplet states of fullerenes although this result was unexpected with regard to previous published results by other authors [104, 105]. This suggests that there are more conditions driving the origin of electroluminescence in photovoltaic devices, for example the layer morphology. Investigation of influence of bulk heterojunction morphology of active layer on energy levels of CT states is beyond the aims of this thesis; however interesting topic for further work.

4.2.4 Reciprocity between External Quantum Efficiency and Electroluminescence Spectra

The ground CT states according to literature [104] can affect photogeneration efficiency. The aim of this chapter is to identify the CT absorption band by computional procedure based on recalculation of emission spectra. For verification of this fact, CT absorption bands were calculated from electroluminescence spectra according to equation [175]:

$$EQE(E) = \frac{EL(E)}{\phi_{bb}(E)} \frac{1}{\exp\left(\frac{qV_{bi}}{kT}\right) - 1}, \tag{57}$$

where ϕ_{bb} is spectral photon density of black body and V_{bi} stands for built-in voltage determined from difference of LUMO energy level of acceptor and HOMO energy level of donor [176].

EQE spectra were also calculated by substitution of electroluminescence spectral data $EL(E)$ by optical fluorescence spectral data $PL(E)$ in equation (56), because electroluminescence spectra of polymer:fullerene blends differ from the photoluminescence spectra in IR. It was claimed [100] that the electroluminescence originates more presumably from fullerene triplet states. Examples of calculated EQE spectra are shown on *Fig. 51*. EQE spectra obtained from spectrally resolved photocurrent measurements were used also for calculation of emission spectra, by means of *Eq.* (53). Plots on *Fig. 51* show that calculated spectra of pristine materials fit relatively well

edge of experimental spectra. In the case of blends, some novel absorption bands were modelled from the emission spectra. Because of the difference of the fluorescence and electroluminescence spectra, both of them were used for the model calculations.

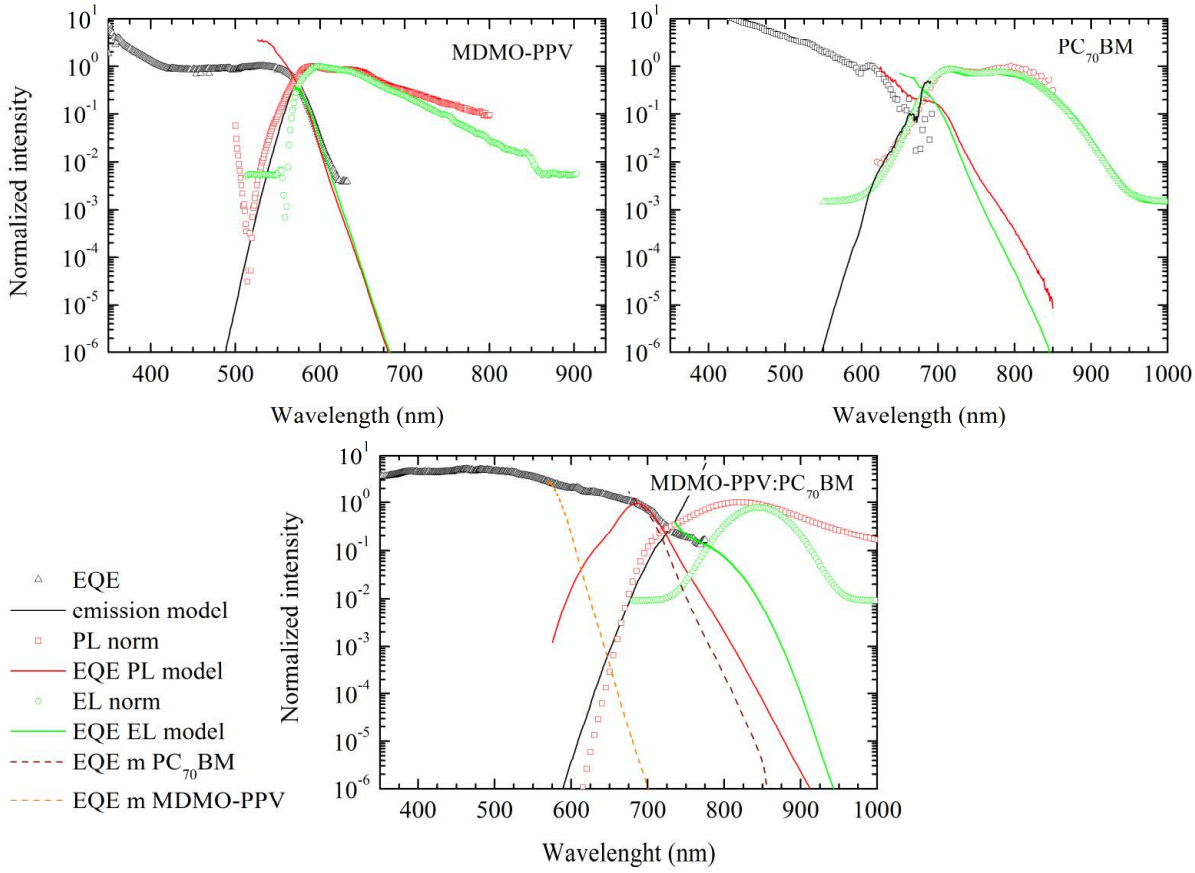

Fig. 51: Normalized EQE, fluorescence and electroluminescence spectra with calculated edges according to equation (53) for the reciprocity of EQE and electroluminescence spectra.

The contribution of light absorption in near IR region was verified through calculation of j_{SCrad} and V_{OCrad} from these extended EQE spectra.

Values of short current density j_{SCrad} were obtained by integration of EQE spectra and solar emission intensity spectra (where the AM 1.5 spectrum with integral intensity 1000 W/m^2 was used):

$$j_{SCrad} = q\int EQE(E)\phi_{Sun}(E)dE \tag{58}$$

Open circuit voltage V_{OCrad} were determined according to following term:

$$V_{\mathrm{OC\,rad}} = \frac{kT}{q}\ln\left(\frac{j_{\mathrm{SC}}}{j_{\mathrm{rad0}}}+1\right), \tag{59}$$

where j_{rad0} is the saturation current density for radiative recombination of the devices and can be obtained from EQE spectra:

$$j_{rad\,0} = q\int EQE(E)\phi_{bb}(E)dE\,. \tag{60}$$

j_{SC} value required in *Eq.* (58) was obtained from current voltage characteristics [175, 179].

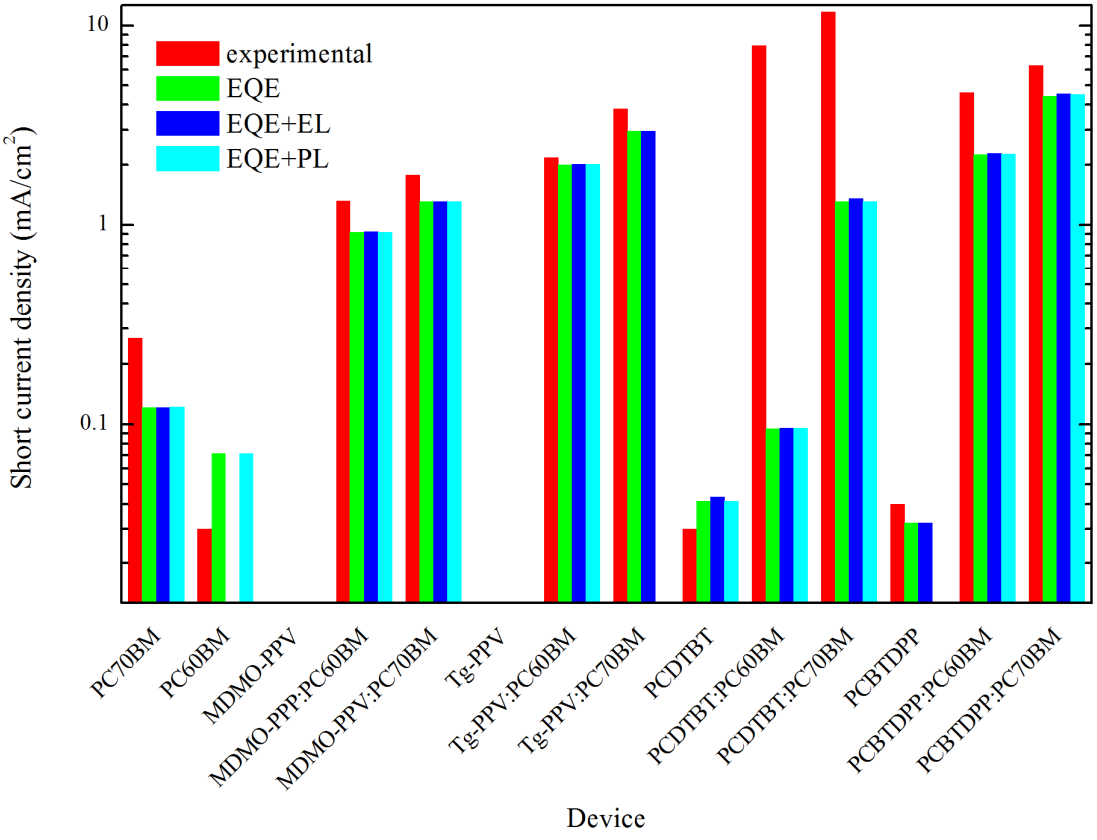

Fig. 52: The comparison of short current density j_{SC} values obtained from current voltage characteristics (red), by integration of EQE spectra (green) and EQE spectra with IR tail calculated from electroluminescence data (dark blue) and from photoluminescence data (light blue).

j_{SCrad} and V_{OCrad} were calculated from experimentally obtained EQE spectra as well as from EQE spectra with near infrared absorption tail calculated from either electroluminescence (parameters marked V_{OCrad}EL, j_{SCrad}EL) or

from photoluminescence (parameters marked V_{OCrad}PL, j_{SCrad}PL) experiments. The results are presented on *Fig. 52*, *Fig. 53* and the values are appended in *Appendix No 8.*, where the values of j_{rad0} are also summarized. The calculated parameters are compared with parameters calculated from current voltage measurements.

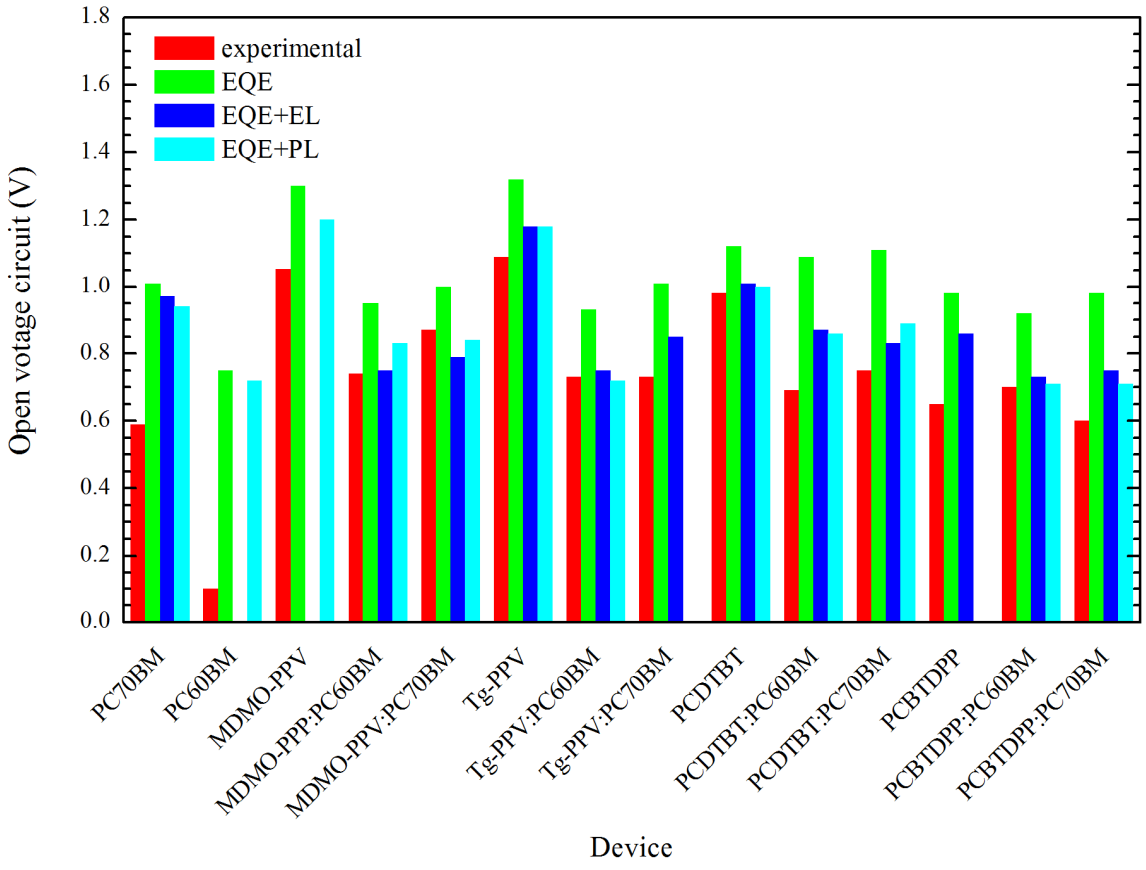

Fig. 53: The comparison of open circuit voltage V_{OC} values obtained from current voltage characteristics (red), by calculation from EQE spectra obtained from photocurrent spectra measurements (green), from EQE spectra with IR tail calculated from electroluminescence data (blue) and from EQE spectra with IR tail calculated from photoluminescence data (cyan).

The contribution of IR absorption to short current density is conclusively negligible, as was expected according to reported small absorption coefficients [99]. The integrated values are in many cases smaller than values obtained from current-voltage measurements. This disproportion can be induced by different light intensity of light sources used during measurements of current voltage characteristic and spectrally resolved

photocurrent (solar simulator with integral intensity 100 mW/cm^2 vs. monochromatic light with intensity smaller than 0.1 mW/cm^2, and with integral intensity 1 mW/cm^2), when dependence of photogeneration efficiency on light intensity was described [180]. Finally, degradation of the devices has to be taken into account, because samples were exposed to considerable stress due to large amount of performed optoelectrical characteristics.

Values of open circuit voltage V_{OCrad} obtained by calculation from measured EQE spectra are up to 0.3 V bigger than values calculated from EQE spectra extended by absorption edge calculated from emission spectra, see *Fig. 53*. Simultaneously values of V_{OCrad} calculated from extended EQE spectra are in better agreement with experimental values of V_{OC} than values of V_{OCrad} calculated from only measured EQE spectra. It confirms that low energy states, despite the fact that these states showed only small contribution to EQE, significantly reduce values of V_{OC}.

Plot on *Fig. 53* is also comparing usage of the electroluminescence or photoluminescence spectra to calculation of edge of EQE spectra. Values of V_{OCrad} are only slightly affected by choice between these two types of luminescence spectra.

The calculations showed that emission spectra can be used for completion of missing parts of EQE spectra, which are experimentally inaccessible due to detection limits (see *Appendix 6*). Simultaneously, significant influence of CT states on the photogeneration efficiency was confirmed, when it was shown that low band gap of CT states reduces the V_{OC} value of photovoltaic devices.

4.2.5 The Comparison of Open Circuit Voltage Determined from Optical and Optoelectrical Characteristics

The demonstrated optical and optoelectrical experiments were focused on the detection of CT states and on contribution of these states to the parameters of photovoltaic devices. It was turned out that CT states

influence the V_{OC} more than the j_{SC}. Simultaneously, V_{OC} values are connected with CT states band gap by the empiric relation of (48). Therefore, V_{OC} values determined from energy level of materials, from optical spectra and from optoelectrical spectra are compared with the experimental values in this paragraph.

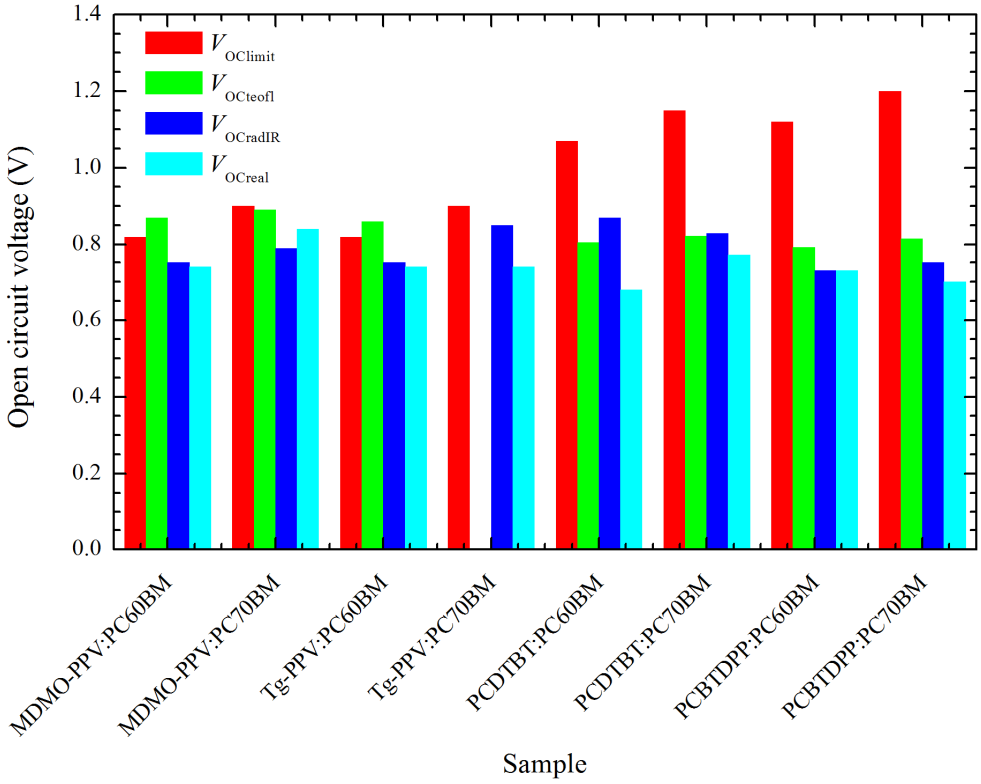

Fig. 54: Diagram comparing the values of open circuit voltage V_{OC} determined by different ways.

Table 17: Open circuit values determined by different ways.

Sample	$V_{OClimit}$ (V)	$V_{OCteofl}$ (V)	$V_{OCradIR}$(V)	V_{OCreal} (V)
MDMO-PPV:PC_{60}BM	0.82	≈ 0.87	0.75	0.74
MDMO-PPV:PC_{70}BM	0.90	≈ 0.89	0.79	0.84
Tg-PPV:PC_{60}BM	0.82	0.86	0.75	0.74
Tg-PPV:PC_{70}BM	0.90		0.85	0.74
PCDTBT:PC_{60}BM	1.07	0.81	0.87	0.68
PCDTBT:PC_{70}BM	1.15	0.82	0.83	0.77
PCBTDPP:PC_{60}BM	1.12	0.79	0.73	0.73
PCBTDPP:PC_{70}BM	1.20	0.81	0.75	0.70

Determined values of open circuit voltage are summarized in *Table 17* and compared in diagram on *Fig. 54*. There is a good agreement between V_{OCreal} and $V_{OCteofl}$ as well as between V_{OCreal} and $V_{OCradIR}$. Values of $V_{OClimit}$ are absolutely inconsistent with V_{OCreal} for photovoltaic devices prepared from low band gap polymers. These results reveal the importance of direct CT states detection in the solar cell's active layer for the estimation of the V_{OC} parameters.

4.2.6 Conclusion

The contribution of CT states to photogeneration processes in polymer solar cells were studied by optoelectrical methods.

Significant contribution of light absorption of fullerenes to photogeneration efficiency was found by EQE spectra study. These spectra also showed photogeneration loses caused by light interferences in active layer.

Subsequently, energies of bimolecular recombination centres were determined from electroluminescence spectra of prepared devices. It was concluded that value of energies rather correspond to energy level of fullerenes triplet states than CT states.

In order to identify of absorption CT states band, reciprocal relation between EQE spectra and electroluminescence spectra were studied. Electroluminescence spectra were substituted by photoluminescence spectra, which enable to determine the emission from CT states. Extended EQE spectra were used for estimation of open circuit voltage and calculation of short current density of prepared devices, which was in good agreement with parameters obtained by standard procedure from current voltage measurements.

Finally values of open circuit voltage determined from molecular energy levels, fluorescence spectra of CT states, extended EQE spectra were compared with values obtained from current voltage measurements and it

was confirmed direct relation between energy of CT states and value of open circuit voltage.

4.3 Textile Organic Solar Cells

In the Introduction the advanced features of organic electronic devices were described. One of them is mechanical flexibility. It is the reason why part of work was paid to development of textile-based solar cell. The development was a part of solution of European project DEPHOTEX realized in our working group.

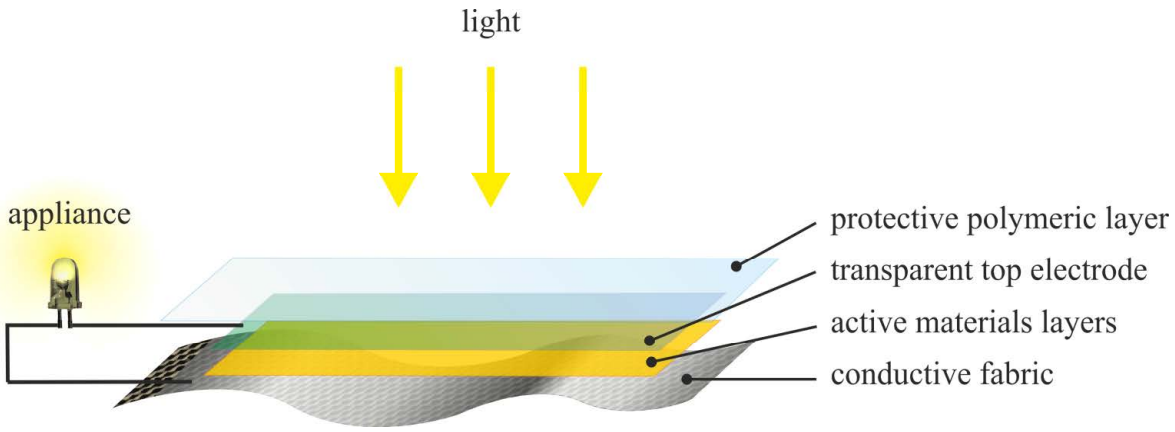

Fig. 55: General structure of textile solar cell is consisting of conductive fabric layer, active layer, transparent top electrode and protective polymer layer.

The goal of the project was the development of textile based OSC, which general structure is shown on *Fig. 55.* Devices consist of conductive fabric, active layer, top transparent electrode and protective transparent polymer layer. The conductive fabric were supplied by partners of project DEPHOTEX, see *Table 9* in *section 3.2.3*. Active layer was created by Tg-PPV:$PC_{60}BM$ blend. Efficient hole transport was provided by transport layer from PEDOT:PSS.

The development of textile photovoltaic devices required solution of wide range of tasks. Our effort was focused especially on the development of deposition methods for multi-layered OSC structure and optimization of

preparation conditions, which will be discussed in details in following subsections.

4.3.1 Development of Deposition Methods for Multilayered Organic Solar Cells Structure

Two possible approaches of textile photovoltaic device preparation was proposed:

1. Solar cells preparation is started by deposition of OSC structure on PET foil with transparent ITO electrode and textile is connected finally on top electrode.

2. Solar cells preparation is started by deposition of OSC structure on textile substrate with electrode and final structure is encapsulated by protective foil.

Both approaches were tested and the second one was found to be more suitable. It was due to final step, when connection of textile to OSC structure on PET foil by silver or carbon paste caused usually OSC structure destruction.

The main attention was paid to study of deposition methods. Spin-coating is suitable mainly for laboratory thin layers deposition with only a few cm^2 small area, therefore inkjet print and electrophoretic deposition methods were developed and tested as alternatives which allow preparation of large area devices.

Tg-PPV layers prepared by spin-coating and inkjet printed on silica slides are shown on *Fig. 56*, where also the electrophoretically deposed Tg-PPV thin film onto the ITO/glass (the electrophoretic deposition can be processed only on the substrate with electrode) is pictured. Prepared thin films showed distinguishable qualities at first sight. Spin-coated and electrophoretically deposed layers are clearly transparent and homogenous, while the inkjet layers are textured with ink drops which created lines and made the layers

opaque. This observation was confirmed by measurement on mechanical profilometer, see *Appendix No. 9*.

Fig. 56: Photography of Tg-PPV layers; left to right: spin-coated, inkjet printed and electrophoretically deposed layer.

Optoelectrical properties of layer were characterized by current voltage measurement under 1 mW/cm^2 light illumination. Examples of characterization of prepared Tg-PPV diodes are shown in the *Fig. 57*.

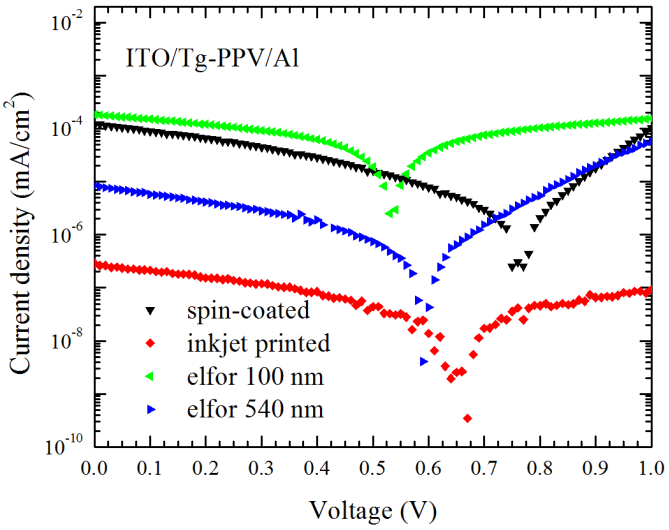

Fig. 57: Comparison of current voltage characteristics of Tg-PPV and Tg-PPV: PCBM 1:4 solar cells prepared utilizing the inkjet printing, electrophoretical deposition and by means of spin-coating.

Averaged values of j_{SC} (short current density), V_{OC} (open circuit voltage), FF (fill factor) and η_{rel} (relative efficiency of photogeneration related to the spin-coated sample) of analyzed Tg-PPV diodes are summarized in *Table 18*.

Table 18: Parameters of ITO/Tg-PPV/Al diodes prepared by different deposition methods.

Deposition method	RSWOS	Layer thickness (nm)	j_{SC} (mA/cm²)	V_{OC} (V)	*FF* (%)	η (%)
spin-coated	24%	120 ± 20	$(1.2 \pm 0.7)\cdot10^{-4}$	0.60 ±0.2	22 ± 8	$(1.8 \pm 0.3)\cdot10^{-3}$
inkjet printed	50%	480 ± 50	$(3.7 \pm 0.4)\cdot10^{-7}$	0.45 ± 0.07	21 ± 1	$3\cdot10^{-6}$
electro-phoretic	13%	100 ± 20	$1.75\cdot10^{-4}$	0.52	22	$2.0\cdot10^{-3}$
electro-phoretic 2	63%	290 ± 80	$(1.8 \pm 0.6)\cdot10^{-4}$	0.57 ± 0.05	26 ± 3	$(2.7 \pm 0.9)\cdot10^{-3}$
electro-phoretic 3	13%	540 ± 80	$9\cdot10^{-6}$	0.59	21	$1.1\cdot10^{-4}$

Inkjet prepared Tg-PPV layers showed lower efficiency of photogeneration than the spin-coated and electrophoretically deposed samples. On the other hand, thickness of layers needed to be assessed also, since it directly influences the layer conductivity. Therefore, only the layers of similar thicknesses can be directly compared. Under these conditions, electrophoretically deposed Tg-PPV layer with thickness of 100 nm showed similar efficiency of photogeneration as the spin-coated layer (see *Table* 18). The ink-jet printed layer was found to be 480 nm thick and this is reasons why the j_{SC} value is low and the final values of photogeneration efficiency as well. All samples showed reduction of V_{OC} value, the expected value is about 1 V.

However results showed that after optimization of deposition processes, all studied methods provides polymeric thin films with comparable optoelectrical properties.

To quantify the reproducibility, an empirical parameter Reproducibility of the Structures Within one Sample RSWOS (the ratio of electrodes actually photogenerating current to a total number of electrodes prepared on one sample) was assessed. Inkjet printed layers usually performed an RSWOS higher than 50 % while layers prepared by other methods in a few cases exceed 30 %. So, the inkjet layers were the most reproducible in terms of optoelectrical characteristics, see *Table* 18. It is the reason, why this deposition method was chosen for textile solar cells preparation. Other

reason was that inkjet print showed to be the friendliest to textile substrates, which interacted with solvents.

The textile solar cells were prepared in standard laboratory conditions, as one of the aims of the project was the development of the deposition methods which does not require the inert atmosphere and clean rooms. It is the reason why achieved photovoltaic efficiency of these devices was low. Influence of controlled conditions provided by glovebox can be demonstrated on devices glass/ITO/PEDOT:PSS/PCDTBT:$PC_{60}BM$/Al. One device was prepared under standard laboratory conditions and second in controlled conditions of glovebox. Both devices were deposed from the same solutions by means of spin-coating.

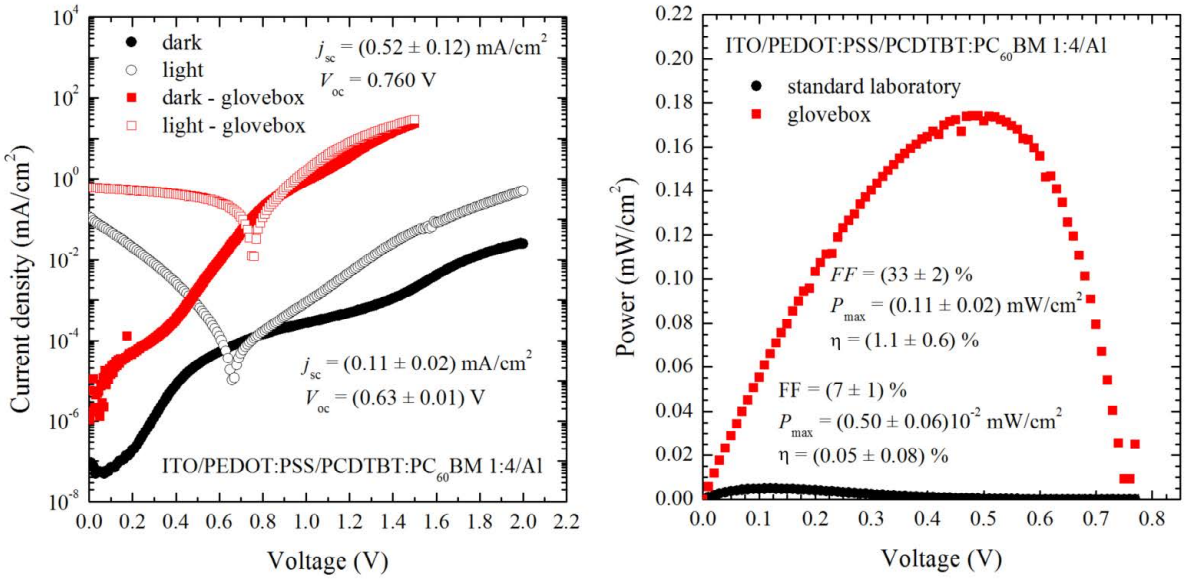

Fig. 58: Plot comparing current voltage characteristics and photovoltaic power characteristics of photovoltaic device ITO/PEDOT:PSS/PCDTBT:$PC_{60}BM$/Al prepared at ambient condition in ordinary lab and prepared in glovebox in clean lab.

Devices were characterized at 1 mWcm^2 illumination of xenon lamp or solar simulator. Example of current voltage characteristics for both PCDTBT:$PC_{60}BM$ device are shown on *Fig. 58*. Sample of PCDTBT:$PC_{60}BM$ prepared in glovebox achieved 22 times bigger maximal photogeneration efficiency than sample prepared in ordinary laboratory at ambient atmosphere. Such improvement of efficiency is distinguishable mainly as the

enhanced values of measured photocurrents and calculated value of fill factor – increased from 7 % to 33 %. All the parameters are summarized in *Fig. 58.*

4.3.2 Characterization of Prepared Samples

Example of current-voltage characteristic of successfully inkjet printed textile solar cell with structure textile/Al/Tg-PPV:PCBM 1:4/PEDOT/Au is showed on *Fig. 59.* Figure shows the current-voltage curves measured in the dark and under light irradiation of 1 mW·cm^{-2} intensity.

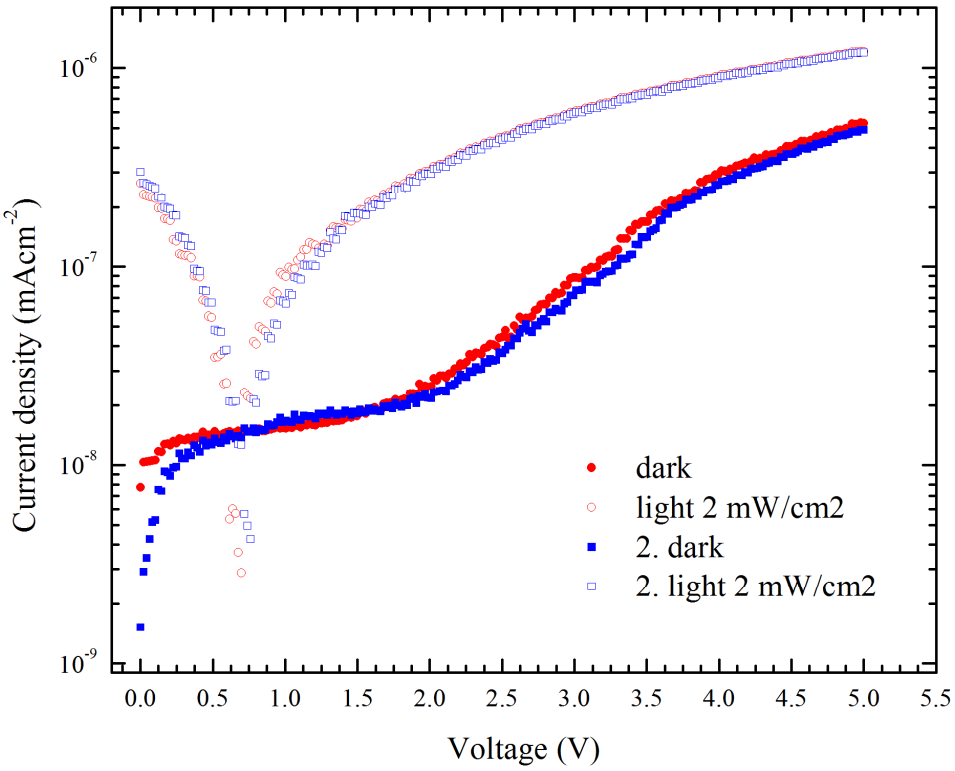

Fig. 59: Current voltage characteristics of one of the solar cells prepared on textile with the structure: textile/Al/Tg-PPV:PCBM 1:4/PEDOT H. C. Starck/Au. In the first run (red dots), the solar cell was measured in dark and next under light for evaluation of photovoltaic conversion efficiency. In the second run (blue squares), repeatability of measurements was reviewed.

Table 19: Electrical parameters of solar cells prepared by inkjet printing or spin-coating on glass, PET foil, or textile substrate.

Sample	Substrate	Layer structure	Deposition method	RSWOS (%)	I (mW/cm²)	j_{SC} (mA/cm²)	V_{OC} (V)	FF	η_{rel}
1	glass/ITO	PEDOT/Tg-PPV:PCBM 1:4/Al	spin-coated	24%	1	$4 \cdot 10^{-4}$	0.85	0.18	1
2	glass/ITO	Tg-PPV:PCBM 1:4 (12 lay.)/Al	inkjet printed	81%	2	$(3.4 \pm 0.4) \cdot 10^{-5}$	0.50 ± 0.02	0.15 ± 0.01	0.04
3	PET foil/ITO	PEDOT/Tg-PPV:PCBM 1:4/Al	spin-coated	13%	1	$4.2 \cdot 10^{-6}$	0.24	0.28	0.009
4	PET foil/ITO	PEDOT/Tg-PPV:PCBM(1:4) /Al/Ag-PES PU textile	spin-coated	-	1	$(9 \pm 3) \cdot 10^{-6}$	0.3 ± 0.2	0.26 ± 0.07	0.02
5	textile/Al	Tg-PPV:PCBM 1:4 (12 lay.)/Au	inkjet printed	38%	2	$(2.6 \pm 0.6) \cdot 10^{-7}$	0.75 ± 0.11	0.23 ± 0.09	0.001
6	textile/Al	Tg-PPV:PCBM 1:4 (12 lay.)/PEDOT/Au	inkjet printed	38%	2	$(3.3 \pm 0.2) \cdot 10^{-5}$	0.21 ± 0.05	0.26 ± 0.08	0.003

Achieved efficiencies are shown in the *Table 19* and graphically processed in charts on the *Fig. 60,* where are compared with similar structures prepared by spin-coating and/or other substrates (glass, PET foil). Results summarized in this table and chart are considered as important, since they showed that achieved photogeneration efficiency of textile solar cells were near to the inkjet printed solar cells prepared on rigid substrates.

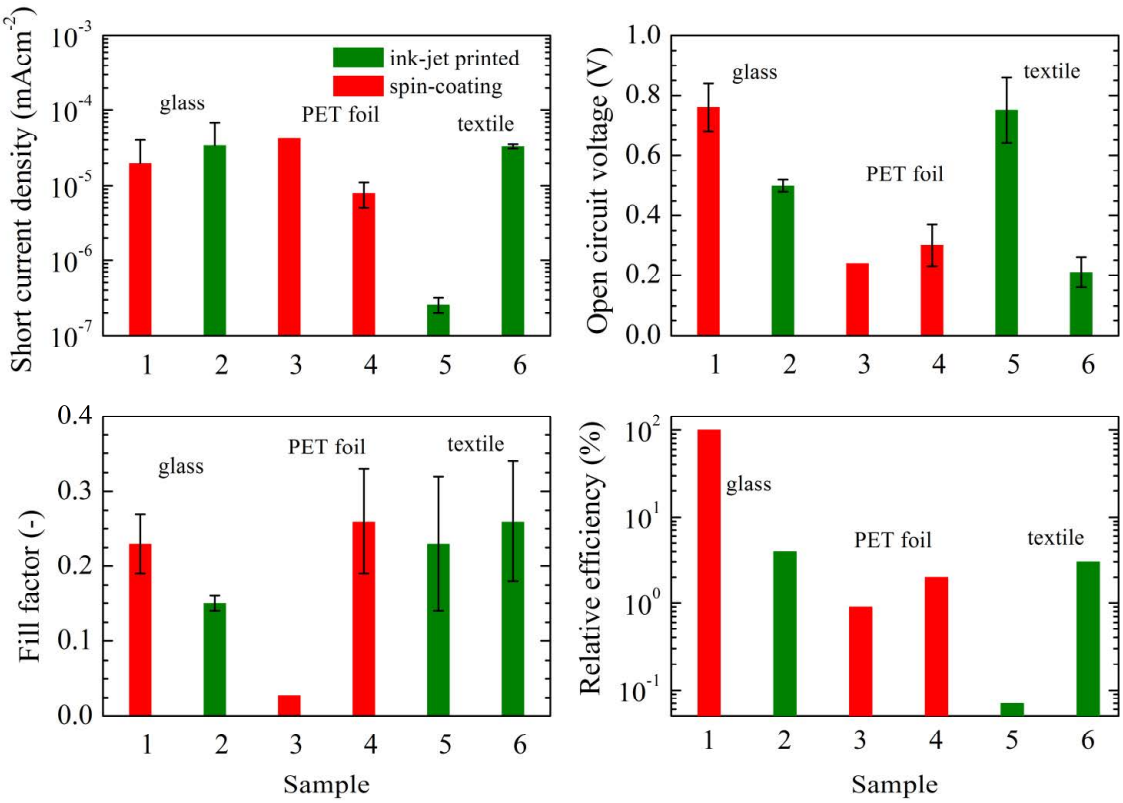

Fig. 60: Statistics of parameters of solar cells calculated from current voltage characteristics. From upper left: Short current density, open circuit voltage, fill factor and relative photogeneration efficiency at the maximal power. Numbers of samples present: 1 - glass/ITO/PEDOT/Tg-PPV:PCBM 1:4/Al, 2 - glass/ITO/ Tg-PPV:PCBM 1:4 (12 lay.)/Al, 3 – PET foil/ITO/ PEDOT/Tg-PPV:PCBM 1:4/Al, 4 – PET foil/ITO/ PEDOT/Tg-PPV:PCBM 1:4/Al/Ag-PES PU textile, 5 – textile/Al/ Tg-PPV:PCBM 1:4 (12 lay.)/Au, 6 – textile/Al/ Tg-PPV:PCBM 1:4 (12 lay.)/PEDOT/Au

Inkjet print provides simple up-scale of photovoltaic device area and for this reason, textile solar cells with active area to 7.5 cm^2 were prepared as *Fig. 61* shows. The largest properly working solar cells were of 1 cm^2 large.

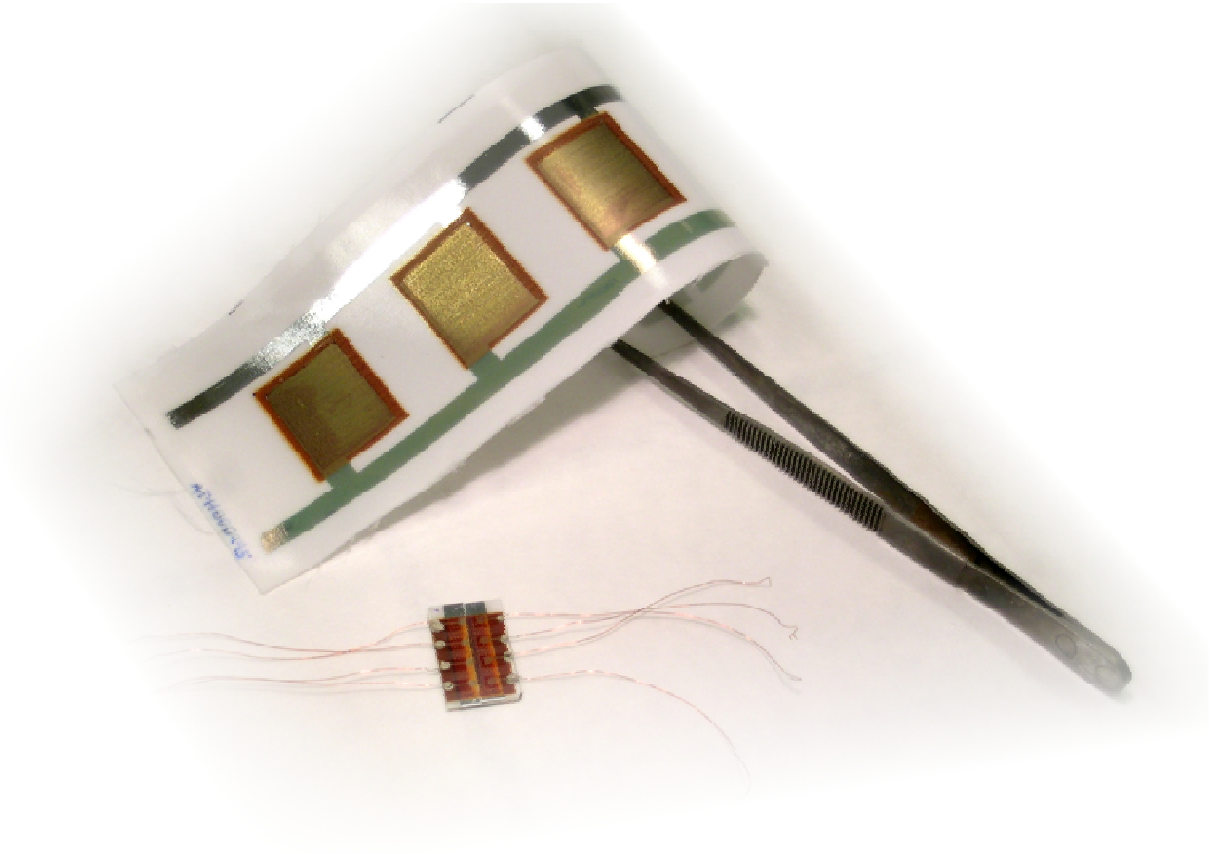

Fig. 61: The flexible module of four solar cells with 7.5 cm^2 active area prepared by inkjet printing on textile substrate. Standard sample (2.5 × 1.5) cm^2 with eight small electrodes (area 0.03 cm^2) is depicted for comparison too.

These experiments showed that preparation of OSC devices on textile by ink-jet printing is possible, however a significant effort must be paid to reach the parameters suitable for practical applications.

5 SUMMARY

The photogeneration processes especially charge transfer and resonance energy transfer in polymeric solar cells were studied by optical and optoelectrical methods. Four electron donating π-conjugated polymer MDMO-PPV, Tg-PPV, PCDTBT and PCBTDPP and two electron accepting fullerenes $PC_{60}BM$ and $PC_{70}BM$ were used in experiments.

The research of electronic interaction between electron donating and electron accepting materials by optical methods were realized by fluorescence quenching experiments in solution and thin films. Results of the studies in solutions showed significant contribution of resonance energy transfer from polymer to fullerenes in comparison with charge transfer driven by exciton diffusion. In addition the studies of fluorescence quenching based on the modelling by Stern-Volmer and Perrin model enable to delineate these processes in thin layers.

Another goal of optical studies was focused on detection of CT states by analysis of fluorescence emission. Based on this analysis, the energy of maximum of emission peak originating from relaxation of excited CT states were determined.

Futhermore parameters of photovoltaic devices prepared from studied blends were estimated from optical spectra and molecular energy levels of materials.

Subsequently, the charge transfer states were studied by optoelectrical methods including the analysis of spectrally resolved external quantum efficiency and electroluminescence.

Significant contribution of light absorption of fullerenes to photogeneration efficiency was found by EQE spectra study. These spectra also showed photogeneration loses caused by light interferences in active layer.

Analysis of electroluminescence spectra allowed determination of energies of bimolecular recombination centres. It was concluded that value of energies rather correspond to energy level of fullerenes triplet states than CT states.

In order to identify of absorption CT states band, reciprocal relation between EQE spectra and electroluminescence spectra were studied. Electroluminescence spectra were substituted by photoluminescence spectra, which enable to determine the emission from CT states. Extended EQE spectra were used for estimation of open circuit voltage and calculation of short current density of prepared devices, which was in good agreement with parameters obtained by standard procedure from current voltage measurements.
Finally values of open circuit voltage determined from molecular energy levels, fluorescence spectra of CT states, extended EQE spectra were compared with values obtained from current voltage measurements and it was confirmed direct relation between energy of CT states and value of open circuit voltage.

In last part of the thesis results of textile organic solar cells development were demonstrated. The successful samples of photovoltaic devices prepared by inkjet print on textile substrates were presented.

6 REFERENCES

[1] KREBS, F. C., BIANCARDO, M., WINTHER-JENSEN, B., SPANGGARD, H. and ALSTRUP, J.: Strategies for Incorporation of Polymer Photovoltaics into Garments and Textiles; *Solar Energy Materials and Solar Cells* 90 (2006), 1058–1067. DOI: 10.1016/j.solmat.2005.06.003.

[2] In Focus: BASF Technology in the smart forvision Concept Car; *Daimler Magazine for Innovation, Technology, Mobility* (2011), 1–4.

[3] GREEN, M. A.; EMERY, K.; HISHIKAWA, Y.; WARTA; W. and DUNLOP, E. D.: Solar Cell Efficiency Tables (version 42), *Progress in Photovoltaic: Research Applications* (2013), 21, 827–837. DOI: 10.1002/pip.2404.

[4] NIELSEN, T. D.; CRUICKSHANK, C.; FOGED, S.; THORSEN, J. and KREBS, F. C.: Businness, Market and Intellectual Property Analysis of Polymer Solar Cells. *Solar Energy Materials and Solar Cells* 94 (2010), 1553–1571. DOI: 10.1016/j.solmat.2010.04.074.

[5] *PVTECH information server*; URL <www.pv-tech.org>, [cit. 2014-03-10].

[6] *Plus Plastic Electronics*. Information server URL <http://www.plusplasticelectronics.com>, [cit. 2014-03-10].

[7] XI, D., SHI, CH., YAO, Y., YANG, Y., PEI, Q.: Nanostructured Polymer Solar Cells; IEEE CFP08RPS-CDR *46th Annual International Reliability Physics Symposium*, Phoenix, 2008.

[8] YUN, J.-M., YEO, J.-S., KIM, J. et al.: Solution-Processable Reduced Graphene Oxide as a Novel Alternative to PEDOT:PSS Hole Transport Layers for Highly Efficient and Stable Polymer Solar Cells; *Advanced Materials* (2011), 23, 4923–4928. DOI: 10.1002/adma.201102207.

[9] BERRY, J. J., WIDJONARKO, N. E., BAILEY, B. A., SIGDEL, A. K., GINLEY, D. S. and OLSON, D. C.: Surface Treatment of NiO Hole Transport Layers for Organic Solar Cells; IEEE *Journal Of Selected*

Topics In Quantum Electronics 16 (2010), 6, 1649–1655. DOI: 10.1109/JSTQE.2010.2049347.

[10] ZILBERBERG, K., TROST, S., SCHMIDT, H. and RIEDL, T.: Solution Processed Vanadium Pentoxide as Charge Extraction Layer for Organic Solar Cells; *Advanced Energy Materials* 1 (2011), 3, 377–381. DOI:10.1002/aenm.201100076.

[11] SCHMIDT, H., FLÜGGE, H., WINKLER, T., BÜLOW, T., RIEDL, T., and KOWALSKY, W.: Efficient Semitransparent Inverted Organic Solar Cells with Indium Tin Oxide Top Electrode; *Applied Physics Letters* 94 (2009), 243302. DOI:10.1063/1.3154556.

[12] WALDAUF, C., MORANA, M., DENK, P., SCHILINSKY, P., COAKLEY, K., CHOULIS, S. A., and BRABEC, C. J.: Highly Efficient Inverted Organic Photovoltaics Using Solution Based Titanium Oxide as Electron Selective Contact; *Applied Physics Letters* 89 (2006), 233517. DOI: 10.1063/1.2402890.

[13] OLSON, D.C., LEE, Y.-J., WHITE, M. S., KOPIDAKIS, N., et al.: Effect of ZnO Processing on the Photovoltage of ZnO/poly(3-hexylthiophene) Solar Cells; *Journal of Physical Chemistry C* 112 (2008), 26, 9544–9547. DOI: 10.1021/jp802626u.

[14] STEIM, R., KOGLER, F.R. and BRABEC, CH. J.: Interface Materials for Organic Solar Cells; *Journal of Materials Chemistry* (2010), 20, 2499–2512. DOI: 10.1039/B921624C.

[15] MURDOCH, G. B., HINDS, S., SARGENT, E. H., TSANG, S. W., MORDOUKHOVSKI, L., and LU, Z. H.: Aluminium Doped Zinc Oxide for Organic Photovoltaics; *Applied Physics Letters* 94 (2009), 213301. DOI: 10.1063/1.3142423.

[16] PANG, S., HERNANDEZ, Y., FENG, X. and MÜLLEN, K.: Graphene as Transparent Electrode Material for Organic Electronics; *Advanced Materials* 23 (2011), 25, 2779–2795. DOI: 10.1002/adma.201100304.

[17] CHOE, M., LEE, B. H., JO, G., PARK, J., PARK, W., LEE, S., HONG, W.-K., SEONG, M.-J., JAHNY, Y. H., LEE, K. and LEE, T.: Efficient Bulk-heterojunction Photovoltaic Cells with Transparent Multi-layer Graphene Electrodes; *Organic Electronics* 11 (2010), 1864–1869. DOI: 10.1016/j.orgel.2010.08.018.

[18] LEE, W.H., CHUANG, S.Y., CHEN, H.L., SU, W.F. and LIN, C.H.: Exploiting Optical Properties of P3HT:PCBM Films for Organic Solar Cells with Semitransparent Anode, *Thin Solid Films* 518 (2010), 7450–7454. DOI: 10.1016/j.tsf.2010.05.021.

[19] SHROTRIYA, V., WU, E. H.-E, LI, G., YAO, Y., and YANG, Y.: Efficient Light Harvesting in Multiple-device Stacked Structure for Polymer Solar Cells, *Applied Physics Letters* 88 (2006), 064104. DOI: 10.1063/1.2172741.

[20] MEISSA, J., RIEDE, M. K., and LEO, K.: Towards Efficient Tin-doped Indium Oxide (ITO)-free Inverted Organic Solar Cells Using Metal Cathodes, *Applied Physics Letters* 94 (2009), 013303. DOI: 10.1063/1.3059552.

[21] TVINGSTEDT, K. and INGANÄS, O.: Electrode Grids for ITO-free Organic Photovoltaic Devices, *Advanced Materials* 19 (2007), 2893–2897. DOI: 10.1002/adma.200602561.

[22] YOOA, J. E., LEEB, K. S., GARCIAC, A. et al.: Directly Patternable, Highly Conducting Polymers for Broad Applications in Organic Electronics, *PNAS* 13 (2010) 107, 5712–5717. DOI: 10.1073/pnas.0913879107.

[23] PRICE, S. C., STUART, A. C., YANG, L., ZHOU, H., and YOU, W.: Fluorine Substituted Conjugated Polymer of Medium Band Gap Yields 7% Efficiency in Polymer–Fullerene Solar Cells; *Journal of the American Chemical Society* 133, (2011), 12 4625–4631. DOI: 10.1021/ja1112595.

[24] NA, S.-I., KIM, S.-S., JO, J., and KIM, D.-Y.: Efficient and Flexible ITO-Free Organic Solar Cells Using Highly Conductive Polymer Anodes, *Advanced Materials* 20 (2008), 4061–4067. DOI: 10.1002/adma.200800338.

[25] DONG, Q., ZHOU, Y., PEI, J., LIU, Z., LI, Y., YAO, S., ZHANG, J.,and TIAN, W.: All-spin-coating Vacuum-free Processed Semi-transparent Inverted Polymer Solar Cells with PEDOT:PSS Anode and PAH-D Interfacial Layer, *Organic Electronics* 11 (2010), 1327–1331. DOI: 10.1016/j.orgel.2010.04.012.

[26] WINTHER-JENSEN, B. and KREBS, F. C.: High-conductivity Large-area Semi-transparent Electrodes for Polymer Photovoltaics by Silk Screen Printing and Vapour-phase Deposition, *Solar Energy Materials & Solar Cells* 90 (2006), 123–132. DOI: 10.1016/j.solmat.2005.02.004.

[27] HAU, S. K., YIP, H.-L., ZOU, J. AND JEN, A. K.-Y.: Indium Tin Oxide-free semi-transparent Inverted Polymer Solar Cells Using Conducting Polymer as Both Bottom and Top Electrodes, *Organic Electronics* 10 (2009), 1401–1407. DOI: 10.1016/j.solmat.2005.02.004.

[28] ZHOU, Y., ZHANG, F., TVINGSTEDT, K., BARRAU, S., LI, F., TIAN, W., and INGANÄS, O.: Investigation on Polymer Anode Design for Flexible Polymer Solar Cells, *Applied Physics Letters* 92 (2008), 233308. DOI: 10.1063/1.2945796.

[29] BRÉDAS, J. L., Norton, J. E., Cornil; J. and Coropceanu, V.: Molecular Understanding of Organic Solar Cells: The Challenges; *Accounts of Chemical Research* 42, (2009), 11, 1691–1699. DOI: 10.1021/ar900099h.

[30] CLARKE, T. M. AND DURRANT J. R.: Charge Photogeneration in Organic Solar Cells; *Chemical Reviews* (2010), 110, 6736–6767. DOI: 10.1021/cr900271s.

[31] MORTEANI, A. C., SREEARUNOTHAI, P., HERZ, L. M., FRIEND, R. H. AND SILVA, C.: Ultrafast Charge Photogeneration and Exciton Regeneration at Polymeric Semiconductor Heterojunctions *Physical Review Letters* 92 (2004), 247402.

[32] BÄSSLER, H.: Excitons in Conjugated Polymers; *Primary Photoexcitations In Conjugated Polymers: Molecular Exciton Versus Semiconductor Band Model*. Edited by Sariciftci, N. S. World scientific, Singapur 1997, ISBN 9810228805.

[33] ZADE, S. S., ZAMOSHCHIK, N., AND M. BENDIKOV: From Short Conjugated Oligomers to Conjugated Polymers. Lessons from Studies on Long Conjugated Oligomers; *Accounts of Chemical Research* 1 (2011), 44, 14–24. DOI: 10.1021/ar1000555.

[34] GIERSCHNER, J., CORNIL, J. AND EGELHAAF H.-J.: Optical Bandgaps of π-Conjugated Organic Materials at the Polymer Limit: Experiment and Theory; *Advanced Materials* (2007), 19, 173–191. DOI: 10.1002/adma.200600277.

[35] MEIER, H., STALMACH, U., KOLSHORN, H.: Effective Conjugation Length and UV/vis Spectra of Oligomers; *Acta Polymerica* 48 (1997), 9, 379–384. DOI: 10.1002/actp.1997.010480905.

[36] TRAIPHOL, R., CHAROENTHAI, N.: Effects of Conformational Change and Segmental Aggregation on Photoemission of Illuminophores in Conjugated Polymer MEH-PPV: Blue Shift Versus Red Shift; *Synthetic Metals* 158 (2008), 135–142. DOI: 10.1016/j.synthmet.2007.12.014.

[37] RASSAMESARD, A., HUANG, Y.-F., LEE, H.-Y. et al.: Environmental Effect on the Fluorescence Lifetime and Quantum Yield of Single

Extended Luminescent Conjugated Polymers. *Journal of Physical Chemistry C* (2009), 113, 18681–18688. DOI: 10.1021/jp905996p.

[38] SNEDDEN, E. W., CURY, L. A., BOURDAKOS, K. N., AND MONKNAM, A. P.: High Photoluminescence Quantum Yield due to Intramolecular Energy Transfer in the Super Yellow Conjugated Copolymer; *Chemical Physicals Letters* 490 (2010), 76–79. DOI: 10.1016/j.cplett.2010.03.030.

[39] ALSALHI, M. S., IBNAOUF, K. H., MASILAMANI, V. AND YASSIN, O. A.: Excimer state of a conjugate polymer (MEH-PPV) in liquid solutions; *Laser Physics* 17 (2007), 12, 1361–1366. DOI: 10.1134/S1054660X07120043.

[40] RUNCALI, J.: Synthetic Principles for Bandgap Control in Linear π-Conjugated; *Chemical Reviews* 97 (1997), 173. DOI: 10.1021/cr950257t.

[41] HOPPE, H. and SARICIFTCI, N. S.: Polymer Solar Cells; *Adv. Polym. Sci.* 12 (2007), 121. DOI:10.1007/12_2007_121.

[42] LAQUAI, F., PARK Y.-S., KIM J.-J. and BASCHÉ, T.: Excitation Energy Transfer in Organic Materials: From Fundamentals to Optoelectronic Devices; *Macromolecular Rapid Communications* (2009). 30, 1203–1231. DOI: 10.1002/marc.200900309.

[43] THOMPSON, B. C. and FRÉCHET, J. M. J.: Polymer-Fullerene Composite Solar Cells; *Angew. Chem. Int. Ed.* (2008), 47, 58–77. DOI: 10.1002/anie.200702506.

[44] BUNDGARD, E. and KREBS, F. C.: Low Band Gap Polymers for Organic Photovoltaics; *Solar Energy Materials & Solar Cells* 91 (2007), 954–985. DOI: 10.1016/j.solmat.2007.01.015.

[45] KIM, J. Y., LEE, K. et al.: Efficient Tandem Polymer Solar Cells Fabricated by All-Solution Processing; *Science* 317 (2007), 222–225. DOI: 10.1126/science.1141711.

[46] DENNLER, G., SCHARBER, M. C. and BRABEC, CH. J.: Polymer-Fullerene Bulk-Heterojunction Solar Cells; *Advanced Materials* 21 (2009), 1323–1338. DOI: 10.1002/adma.200801283.

[47] GILOT, J., WIENK, M. M., and JANSSEN R. A. J.: Optimizing Polymer Tandem Solar Cells; *Advanced Materials* 22 (2010), E67–E71. DOI:10.1002/adma.200902398.

[48] DEIBEL, C. and DYAKONOV, V.: Polymer–fullerene Bulk Heterojunction Solar Cells; *Reports on Progress in Physics* 73 (2010), 096401. DOI: 10.1088/0034-4885/73/9/096401.

[49] SANTBERGEN, R.: *Optical Absorption Factor of Solar Cells for PVT Systems*. Dissertations thesis on Technische Universiteit Eindhoven (2008), promoted by prof.dr.ir. R. J. Ch. van Zolingen and prof.dr.ir. A. A. van Steenhoven. ISBN: 978–90–386–1467–0.

[50] DENNLER, G., FORBERICH, K. et al: Angle Dependence of External and Internal quantum Efficiencies in Bulk-heterojunction Organic Solar Cells; *Journal of Applied Physics* 102, (2007), 054516. DOI: 10.1063/1.2777724.

[51] NAM, Y. M., HUH, J. and JO, W. H.: Optimization of Thickness and Morphology of Active Layer for High Performance of Bulk-heterojunction Organic Solar Cells; *Solar Energy Materials & Solar Cells* 94 (2010), 1118–1124. DOI: 10.1016/j.solmat.2010.02.041.

[52] SLOOFF, L. H., VEENSTRA, S. C. et al.: Determining the internal quantum efficiency of highly efficient polymer solar cells through optical modelling; *Applied Physics Letters* 90 (2007), 143506. DOI:10.1063/1.2718488.

[53] KIM, J. Y., KIM, S. H., LEE, H. H., LEE, K., MA, W., GONG, X., and HEEGER, A. J.: New Architecture for High-efficiency Polymer Photovoltaic Cells Using Solution-based Titanium Oxide as an Optical

Spacer; *Advanced Materials* (2006),18, 572–576. DOI: 10.1002/adma.200501825.

[54] LEE, K. et al.: *Architecture for High Efficiency Polymer Photovoltaic Cells Using an Optical Spacer.*1. September 2011, United States Application US20110209759.

[55] ANDERSSON, B. V., HUANG, D. M., MOULÉ, A. J. and INGANÄS, O.: An optical spacer is no panacea for light collection in organic solar cells; *Applied Physics Letters* 94 (2009), 043302. DOI: 10.1063/1.3073710.

[56] GILOT J., BARBU I. WIENK, M. M. AND JANSSEN, R. A. J.: The Use of ZnO as Optical Spacer in Polymer Solar Cells: Theoretical and Experimental Study; *Applied Physics Letters* 91(2007), 113520. DOI:10.1063/1.2784961.

[57] DATTA, D., IYER, S. S. K. et al: Role of Exciton Blocking Layers as Optical Spacer in Cupc/C60 Based Organic Solar Cells, *Photovoltaic Specialists Conference* (2010), ISBN: 978-1-4244-5890-5.

[58] TVINGSTEDT, K., ZILIO, S. D., INGANÄS, O. and TORMEN, M.: Trapping Light with Micro Lenses in Thin Film Organic Photovoltaic Cells; *Optics Express* 16 (2008), 26, 21609. DOI: 10.1364/OE.16.021608.

[59] NALWA, K. S. and CHAUDHARY, S.: Design of Light-Trapping Microscale-Textured Surfaces for Efficient Organic Solar Cells; *Optics Express* 5 (2010), 18, 5168–5178. DOI: 10.1364/OE.18.005168.

[60] ATWATER, H. A. and POLMAN, A.: Plasmonics for Improved Photovoltaic Devices; *Nature Materials* 9 (2010), 205–213. DOI 10.1038 /nmat2629.

[61] RIM, S.-B. ZHAO, S.; SCULLY, S. R.; McGEHEE, M. D. and PEUMANS, P.: An Effective Light Trapping Configuration for Thin-Film Solar Cells; *Applied Physics Letters* 91 (2007), 243501. DOI: 10.1063/1.2789677.

[62] KOTLARKI, J. D. and BLOM, P. W. M.: Impact of Unbalanced Charge Transport on the Efficiency of Normal and Inverted Solar Cells; *Applied Physics Letters* 100 (2012), 013306. DOI: 10.1063/1.3663860.

[63] SCHEBLYKIN, I. G., YARTSEV, A., PULLERITS, T., GULBINAS, V., and SUNDSTROM, V.: Excited State and Charge Photogeneration Dynamics in Conjugated Polymers. *Journal of Physical Chemistry B*, 111 (2007), 23, 6303–6321. DOI: 10.1021/jp068864f.

[64] KNUPFER, M., FINK, J., ZOJER, E., LEISING, G. and FICHOU, D.: Universal Exciton Size Scaling in π-conjugated Systems; *Chemical Physics Letters* 318 (2000), 585–589. DOI: 10.1016/S0009-2614(00)00033-6.

[65] KAO, K. CH.: *Dielectric phenomena in solids*. Elsevier in United States of America 2004, ISBN: 0-12-396561-6.

[66] OSTERBACKA, R., AN, C. P., JIANG, X. M. and VARDENY, Z. V.: Two-Dimensional Electronic Excitations in Self-assembled Conjugated Polymer Nanocrystals; *Science* 287 (2000), 839. DOI: 10.1126/science.287.5454.839.

[67] ARKHIPOV, V. I. and BÄSSLER, H.: Exciton Dissociation and Charge Photogeneration in Pristine and Doped Conjugated Polymers; *Phys. Status Solid A* 201 (2004), 1152–1187. DOI: 10.1002/pssa.200404339.

[68] KNUPFER, M.: Exciton Binding Energies in Organic Semiconductors; *Journal of Applied Physics A* 77 (2003), 623–626. DOI: 10.1007/s00339-003-2182-9.

[69] MARKOV, D. E, AMSTERDAM, E. et al.: Accurate Measurement of the Exciton Diffusion Length in a Conjugated Polymer Using a Heterostructure with a Side-Chain Cross-Linked Fullerene Layer. *Journal of Physical Chemistry* A (2005), 109, 5266–5274. DOI: 10.1021/jp0509663.

[70] HALLERMANN, M., et al.: Charge Transfer Excitons in Polymer/Fullerene Blends; The Role of Morphology and Polymer Chain Conformation; *Advanced Functional Materials* (2009), 19, 3662–3668. DOI: 10.1002/adfm.200901398.

[71] COWAN, S. R., LEONG, W. L. et al.: Identifying a Threshold Impurity Level for Organic Solar Cells: Enhanced First-Order Recombination via Welldefined $PC_{84}BM$ Traps in Organic Bulk Heterojunction Solar Cells; *Advanced Functional Materials* (2011) 20, 1–20. DOI: 10.1002/adfm.201100514.

[72] WANG, J. et al.: Photoluminescence of Water-Soluble Conjugated Polymers: Origin of Enhanced Quenching by Charge Transfer; *Macromolecules* (2000), 33, 5153–5158. DOI: 10.1021/ma000081j.

[73] WANG, J. et al.: Dynamic Quenching of 5-(2'-ethyl-hexyloxy)-*p*-phenylene vinylene (MEH-PPV) by Charge Transfer to a C_{60} Derivative in Solution; *Journal of Applied Polymer Science* (2001), 82, 2553–2557. DOI: 10.1002/app.2106.

[74] ZHENG M., et al.: The Interaction between Conjugated Polymer and Fullerenes; *Journal of Appllied Polymer Science* (1998), 70, 599–603. DOI: 10.1002/(SICI)1097-4628(19981017)70:3<599::AID-APP22>3.0.CO;2-V.

[75] LUNT et al: Exciton diffusion lengths of organic semiconductor thin films measured by spectrally resolved photoluminescence quenching; *Journal of Applied Physics* 105 (2009), 053711. DOI: 10.1063/1.3079797.

[76] SCHWEITZER, B. et al.: Geminate Pair Recombination in a Conjugated Polymer; *Chemical Physics Letters* 313 (1999), 57–62. DOI: 10.1016/S0009-2614(99)01014-3.

[77] LAKOWICZ, J. R.: *Principles of Fluorescence Spectroscopy*, third edition. Spring (2006). ISBN-13: 978-0387-31278-1.

[78] VALEUR B.: *Molecular Fluorescence Principles and Applications*, Wiley-VCH Verlag GmbH (2001), ISBN 3-527-60024-8.

[79] KOHLER, A. AND BELJONNE, D.: The Singlet-Triplet Exchange Energy in Conjugated Polymers; *Advanced Functional Materials* 14 (2004) 11. DOI: 10.1002/adfm.200305032.

[80] LIU, X. Y., SUMMERS, M. A., SCULLY, S. R. and MCGEHEE, M. D.: Resonance energy transfer from organic chromophores to fullerene molecules; *Journal of Applied Physics* 99 (2006) 093521. DOI: 10.1063/1.2195890.

[81] LAQUAI, F., PARK, Y.-S., KIM J.-J. and BASCHÉ, T.: Excitation Energy Transfer in Organic Materials: From Fundamentals to Optoelectronic Devices; *Macromolecular Rapid Communications* (2009), 30, 1203–1231. DOI: 10.1002/marc.200900309.

[82] HWANG, I. and SCHOLES, G. D.: Electronic Energy Transfer and Quantum-Coherence in p-Conjugated Polymers. *Chemistry of Materials* 23 (2011), 610-620. DOI: 10.1021/cm102360x.

[83] WARD, A. J.; RUSECKAS, A. and SAMUEL, I. D. W.: A Shift from Diffusion Assisted to Energy Transfer Controlled Fluorescence Quenching in Polymer-Fullerene Photovoltaic Blends, *The Journal of Physical Chemistry C* (2012), 116, 23931–23937. DOI: 10.1021/jp307538y.

[84] ENGMANN, S.; TURKOVIC, V.; DENNER, P.; HOPPE, H. and GOBSCH, G.: Optical Order of the Polymer Phase within Polymer/Fullerene Blend Films. Journal of Polymer Science (2012), 50, 1363–1373. DOI: 10.1002/polb.23131.

[85] COFFEY, D. C., FERGUSON, A. J., KOPIDAS, N. and RUMBLES, G.: Photovoltaic Charge Generation in Organic Semiconductors Based on Long-Range Energy Transfer. *ACS Nano 4* (2010), 9, 5437–5445. DOI: 10.1021/nn101106b.

[86] GERHARD, A. and BÄSSLER, H.: Delayed Fluorescence of a Poly(*p*-phenylenevinylene) Derivative: Triplet-triplet Annihilation versus Geminate Pair Recombination; *Journal of Chemical Physics* 117 (2002), 15. DOI: 10.1063/1.1507107.

[87] LEWIS. A. J. et al.: Singlet Exciton Diffusion in MEH-PPV Films Studied by Exciton-Exciton Annihilation; *Organic Electronics* 7 (2006), 452–456. DOI: 10.1016/j.orgel.2006.05.009.

[88] MARCUS, A. R.: Electron Transfer Reactions in Chemistry: Theory and Experiment. Nobel Lecture, 8. 12. 1992, California Institute of Technology, USA.

[89] COOK, S., KATOH, R. and FURUBE, A.: Ultrafast Studies of Charge Generation in PCBM:P3HT Blend Films following Excitation of the Fullerene PCBM, *Journal of Physical Chemistry C* 113 (2009), 6, 2547–2552. DOI: 10.1021/jp8050774.

[90] GÜNES, S., NEUGEBAUER, H., and SARICIFTCI, N. S.: Conjugated Polymer–Based Organic Solar Cells; *Chemical Reviews* 107 (2007), 4, 1324–1338. DOI: 10.1021/cr050149z.

[91] BAKULIN, A. A., HUMMELEN, J. C., PSHENICHNIKOV, M. S. and VAN LOOSDRECHT P. H. M.: Ultrafast Hole-Transfer Dynamics in Polymer/PCBM Bulk Heterojunctions. *Advanced Functional Materials* 20 (2010), 1653–1660. DOI: 10.1002/adfm.200902099.

[92] BRÉDAS, J.-L. et al: Charge-Transfer and Energy-Transfer Processes in π-Conjugated Oligomers and Polymers: A Molecular Picture. *Chem. Rev.* (2004), 104, 4971–5003. DOI: 10.1021/cr040084k.

[93] SCHWENN, P. E. et al.: Kinetics of charge transfer processes in organic solar cells: Implications for the design of acceptor molecules. Organic Electronics 13 (2012), 2538–2545. DOI: 10.1016/j.orgel.2012.07.008.

[94] GODOVSKY, D.: Modeling the Ultimate Efficiency of Polymer Solar Cell using Marcus Theory of Electron Transfer; *Organic Electronic* 12 (2010), 190–194. DOI: 10.1016/j.orgel.2010.10.015.

[95] TOKMAKOFF A.: Fermi's Golden Rule, MIT *Department of Chemistry* (2007). URL < http://ocw.mit.edu/courses/> [cit. 2012-03-15].

[96] GAO, K. et al.: Study on Charge-transfer State in a Donor-Acceptor Polymer Heterojunction; *Organic Electronics* 12 (2011), 1010–1016. DOI: 10.1016/j.orgel.2011.03.024.

[97] MIHAILETCHI, V. D. et al.: Photocurrent Generation in Polymer-Fullerene Bulk Heterojunctions; *Physical Review Letters* 93 (2004), 21. DOI: 10.1103/PhysRevLett.93.216601.

[98] DEIBEL, C., STROBEL, T. and DYAKONOV, V.: Role of the Charge Transfer State in Organic Donor-Acceptor Solar Cells; *Advanced Materials* (2010), 22, 4097–4111. DOI: 10.1002/adma.201000376.

[99] VANDEWAL, K., GADISA, A., et al.: The Relation Between Open-Circuit Voltage and the Onset of Photocurrent Generation by Charge-Transfer Absorption in Polymer : Fullerene Bulk Heterojunction Solar Cells; *Advanced Functional Materials* (2008), 18, 2064–2070. DOI: 10.1002/adfm.200800056.

[100] VELDMAN, D., MESKERS, S. C. J. and JANSSEN, R. A. J. The Energy of Charge-Transfer States in Electron Donor-Acceptor Blends: Insight into the Energy Losses in Organic Solar Cells; *Advanced Functional Materials* 19 (2009), 1939. DOI: 10.1002/adfm.200900090.

[101] ZHU, Z., MÜHLBACHER, D., MORANA, M., KOPPE, M., SCHARBER, M.C., WALLER, D., DENNLER, G., and BRABEC, C. J.: Design Rules for Efficient Organic Solar Cells, High-Efficient Low-Cost Photovoltaics, *Springer Series in Optical Sciences* 140. Springer Berlin Heidelberg (2009), 195. ISBN 978-3-540-79358–8.

[102] YAMANARI, T., TAIMA, T., SAKAI, J. and SAITO, K.: Origin of the open-circuit voltage of organic thin-film solar cells based on conjugated polymers, *Solar Energy Materials & Solar Cells* 93 (2009), 759–761. DOI: 10.1016/j.solmat.2008.09.022.

[103] ZHANG, M., WANG, H., and TANG, C. W.: Effect of the highest occupied molecular orbital energy level offset on organic heterojunction photovoltaic cells; *Applied Physics Letters* 97, (2010), 143503. DOI: 10.1063/1.3491214.

[104] LOI, M. A., TOFFANIN, S., MUCCINI, M., FORSTER, M., SCHERF, U. and SCHARBER, M.: Charge Transfer Excitons in Bulk Heterojunctions of a Polyfluorene Copolymer and a Fullerene Derivative; *Advanced Functional Materials* (2007), 17, 2111–2116. DOI: 10.1002/adfm.200601098.

[105] TVINGSTEDT, K.; VANDEWAL, K.; GADISA, A.; ZHANG, F.; MANCA J.; AND INGANÄS, O.: Electroluminescence from charge transfer states in polymer solar cells; *Journal of the American Chemical Society* (2009), 131, 11819–11824. DOI: 10.1021/ja903100p.

[106] PARASHCHUK, O. D.; SOSOREV, A. YU.; BRUEVICH, V. V. AND PARASCHUK, D. YU: Threshold Formation of an Intermolecular Charge Transfer Complex of a Semiconducting Polymer; *Jetp letters* 91 (2010), 7. DOI:10.1134/S0021364010070064.

[107] BENSON-SMITH, J. J., GORIS, L., VANDEWAL, K., HAENEN, K., MANCA, J. V., VANDERZANDE, D., BRADLEY, D. D. C. and NELSON, J.: Formation of a Ground-State Charge-Transfer Complex in

Polyfluorene/[6,6]-phenyl-C61 Butyric Acid Methyl Ester (PCBM) Blend Films and its Role in the Function of Polymer/PCBM Solar Cells; *Advanced Functional Materials* 17 (2007), 451. DOI: 10.1002/adfm.200600484.

[108] GORIS, L., HAENEN, K., NESLÁDEK, M.: Absorption Phenomena in Organic Thin Films for Solar Cell Applications Investigated by Photothermal Deflection Spectrometry; *Journal Of Materials Science* 40 (2005) 1413–1418. DOI: 10.1007/s10853-005-0576-0.

[109] BRUEVICH, V. V., MAKHMUTOV, T. SH., ELIZAROV, S. G., NECHVOLODOVA, E. M., and PARASCHUK, D. YU.: Raman Spectrometry of Intermolecular Charge Transfer Complex between a Conjugated Polymer and an Organic Acceptor Molecule; *Journal of Chemical Physics* 127, (2007), 104905. DOI: 10.1063/1.2767266.

[110] BAKULIN, A. A., MARTYANOV, S. et al: Ultrafast Charge Photogeneration Dynamics in Ground-State Charge-Transfer Complexes Based on Conjugated Polymers. *Journal of Physichal Chemistry B* 112 (2008), 13730–13737. DOI: 10.1021/jp8048839.

[111] LENES, M., KOOISTRA, F. B. et al.: Charge Dissociation in Polymer:Fullerene Bulk Heterojunction Solar Cells with Enhanced Permittivity; *Journal of Applied Physics* 104, 114517 (2008). DOI 10.1063/1.3039191.

[112] ONSAGER, L.: The Motion of Ions: Principles and Concepts, *Nobel Lecture*, December 11, 1968.

[113] BRAUN, C, L,: Electric Field Assisted Dissociation of Charge Transfer States as a Mechanism of Photocarrier Production; *Journal of Chemical Physics* 80 (1984), 4157. DOI: 10.1063/1.447243.

[114] WOJCIK, M. and TACHIYA, M.: Accuracies of the Empirical Theories of the Escape Probability Based on Eigen Model and Braun Model

Compared with the exact extension of Onsager Theory; *Journal of Chemical Physics* 130 (2009), 104107. DOI: 10.1063/1.3082005.

[115] DEIBEL, C., STROBEL, T. and DYAKONOV, V.: Origin of the Efficient Polaron Pair Dissociation in Polymer–Fullerene Blends; *Physical Review Letters* 103 (2009), 036402. DOI: 10.1103/PhysRevLett.103.036402.

[116] ARKHIPOV, V. I., HEREMANS, P. and BASSLER, H.: Why is Exciton Dissociation so Efficient at the Interface between a Conjugated Polymer and an Electron Acceptor? *Applied Physics Letters* 82 (2003), 4605–4607. DOI: 10.1063/1.1586456.

[117] SPANGGAARD, H. and KREBS, F. C.: A brief history of development of organic and polymeric photovoltaic, *Solar Energy Materials and Solar Cells* 83 (2004), 2–3, 125–146. DOI: 10.1016/j.solmat.2004.02.021.

[118] JANSSEN, R. A. J.: Photoexcitation in conjugated oligomers. *Primary Photoexcitations In Conjugated Polymers: Molecular Exciton Versus Semiconductor Band Model*. Edited by Sariciftci, N. S. World scientific, Singapur 1997, ISBN 9810228805.

[119] GIERSHNER, J., CORNIL. J., Egelhaaf, H.-J.: Optical Bandgaps of p-Conjugated Organic Materials at the Polymer Limits: Experiment and Theory. *Advanced Materials* 19 (2007), 173–191. DOI: 10.1002/adma.200600277.

[120] PEREPICHKA, D. F., PEREPICHKA, I. F. MENG, H. and WUDL, F.: Light emitting polymers, UCLA. On-line document URL http://voh.chem.ucla.edu/vohtar/fall04/classes/285/ [cit 2014-02-10].

[121] HEEGER, A. J.: Semiconducting and Metallic Polymers: The Fourth Generation of Polymeric Materials, *Nobel Lecture* Weinheim: WILEY-VCH Verlag GmbH, (2001).

[122] CHOCHOS, C. L. and CHOULIS, S. A.: How the Structural Deviations on the Backbone of Conjugated Polymers Influence their Optoelectronic Properties and Photovoltaic Performance. *Progress in Polymer Science* 36 (2011), 1326–1414. DOI: 10.1016/j.progpolymsci.2011.04.003.

[123] TROSHIN, P. A., LYUBOVSKAYA, R. N. AND RAZUMOV, V. F.: Organic Solar Cells: Structure, Materials. Critical Characteristics and Outlook. *Nanotechnologies in Russia* (2008), 3, 242–271. DOI: 10.1134/S1995078008050029.

[124] TREAT, N. D., VAROTTO, A., TAKACS, Ch. J., et al.: Polymer-Fullerene Miscibility: A Metric for Screening New Materials for High-Performance Organic Solar Cells. Journal of the American Chemical Society 134, (2012), 15869–15879. dx.doi.org/10.1021/ja305875u.

[125] SAVENIJE, T. J., KROEZE, J. E., et al.: Mobility and Decay Kinetics of Charge Carriers in Photoexcited PCBM/PPV blends. Physical Review B 69 (2004), 155205. DOI 10.1103/PhysRevB.69.155205.

[126] LIU, F. et al: On the Morphology of Polymer-Based Photovoltaics. *Journal of Polymer science* (2012), 50, 1018–1044. DOI: 10.1002/polb.23063.

[127] ZHOU, H.; YANG, L.; STUART, A. C.; PRICE, S. C.; LIU S. and YOU W.: Development of Fluorinated Benzothiadiazole as a Structural Unit for a Polymer Solar Cell of 7 % Efficiency, *Angewandte Chemie International Edition*, 50 (2011), p. 2995 DOI: 10.1002/anie.201005451.

[128] JUNG, E. H., JO, W. H.: n-Extended Low Bandgap Polymer Based on Isoindigo and Thienylvinylene for High Performance Polymer Solar Cells. *Energy and Enviromental Science* (2014), 7, 650–654. DOI:10.1039/C3EE42297F.

[129] HUO, L.; ZHANG, S.; GUO, X.; XU, F.; LI, Y. and HOU, J.: Replacing Alkoxy Groups with Alkylthienyl Groups: A Feasible Approach To

Improve the Properties of Photovoltaic Polymers, *Angewandte Chemie,* 41 (2011), 9871–9876. DOI: 10.1002/ange.201103313.

[130] HE, Z., ZHONG, Ch., SU, S., XU, M., WU, H. and CAO, Y.: Enhanced Power-Conversion Efficiency in Polymer Solar Cells Using an Inverted Device Structure. *Nature Photonics 6* (2012). DOI:10.1038/nphoton.2012.190.

[131] HENDRIKS, K. H.; HEINTGES, G. H. L.; GEVAERTS, V. S.; WIENK M. M. and JANSSEN, R. A. J.: High-Molecular-Weight Regular Alternating Diketopyrrolopyrrole-based Terpolymers for Efficient Organic Solar Cells, *Angewandte Chemie International Edition* (2013), 52, 8341–8344 DOI: 10.1002/anie.201302319.

[132] GUO, X., ZHOU, N. LOU, S. J., SMITH, J., TICE, D. B., HENNEK, J. W., et al.: Polymer Solar Cells with Enhanced Fill Factor. *Nature Photonics* (2013) DOI: 10.1038/nphoton.2013.207.

[133] SHOAEE, s., ENG, M. P., DSPILDORA, E., DELGADO, J. L., CAMPO, B., MARTIN, N., VANDERZANDE, D. and DURRANT, J. R.: Influence of Nanoscale Phase Separation on Geminate versus Bimolecular Recombination in P3HT:fullerene Blend Films. *Energy and Enviromental Science 7* (2010), 971–976. DOI:10.1039/C003394D.

[134] LIU, T. and TROISI, A.: What Makes Fullerenes Acceptors Special as Electron Acceptors in Organic Solar Cells and How to Replace Them. Advenced 25 (2013), 1038–1041. DOI: 10.1002/adma.201203486.

[135] JANSSEN, R. A. J and NELSON, J.: Factors Limiting Device Efficiency in Organic Photovoltaic. *Advenced Materials* 25 (2013), 1847–1858. DOI: 10.1002/adma.201202873.

[136] MAKAROVA, T. L.: Electrical and Optical Properties of Pristine and Polymerized Fullerenes. *Semiconductors* 35 (2001), 3, 243–278. DOI: 10.1134/1.1356145.

[137] SONG, Q. L., GONG, Ch., et al.: Photocurrent generation in plain [6,6]-phenyl C61 butyric acid methyl ester. *Solar Energy Materials and Solar Cells* 94 (2010) 2422–2425. DOI: 10.1016/j.solmat.2010.09.001.

[138] AHMED, E. et al: Design of New Electron Acceptor Materials for Organic Photovoltaics: Synthesis, Electron Transport, Photophysics, and Photovoltaic Properties of Oligothiophene-Functionalized Naphthalene Diimides. *Chemistry of Materials* 23 (2011), 4563–4577. DOI: 10.1021/cm2010668.

[139] WALKER, B., HAN, X. et al: Solution-Processed Organic Solar Cells from Dye Molecules: An Investigation of Diketopyrrolopyrrole:Vinazene Heterojunctions. *Applied materials and interfaces* 4 (2011), 244–250. DOI: 10.1021/am201304e.

[140] WIEMER, M., NENASHEV, A. V., JENSSON, F and BARANOVSKII, S. D.: On the Efficiency of Exciton Dissociation at the Interface between a Conjugated Polymer and an Electron Acceptor. *Applied Physics Letters* 99 (2011), 013302. DOI: 10.1063/1.3607481.

[141] LEE, J: et al.: Charge Transfer State Versus Hot Exciton Dissociation in Polymer-Fullerene Blended Solar Cells; *Journal of the American Chemical Society* (2010), 132, 11878–11880.

[142] SCHWENNA, P. E., GUIB, K., ZHANGB, Y. et al: Kinetics of charge transfer processes in organic solar cells: Implications for the design of acceptor molecules. *Organic Electronics* 13, (2012), 11, 2538–2545. DOI: 10.1016/j.orgel.2012.07.008.

[143] BERTHO, S., HAELDERMANS, I. et al.: How Stable are polymer:PCBM bulk heterojunction solar cell? *Spie-Int Society Optical Engineering* (2006) DOI: 10.1117/12.663256.

[144] BERTHO, S., JANSSEN, G., CLEIJ, T. J. et al.: Effect of Temperature on the Morphological and Photovoltaic Stability of Bulk Heterojunction

Polymer:fullerene Solar Cells; *Solar Energy Materials & Solar Cells* 92 (2008), 753–760. DOI: 10.1016/j.solmat.2008.01.006.

[145] *Innovative Materials for Next Generation Electronics*, Merck. Electronical document URL <http://www.merck-chemicals.com/showBrochure/201004.144.ProNet.pdf> [cit. 2012-03-02].

[146] WIENK, M. M.; KROON, J. M.; VERHEES, W. J. H.; KNOL, J.; HUMMELEN, J. C.; VAN HAL, P. A.; JANSSEN, R. A. J.: Efficient Methano[70]fullerene/MDMO-PPV Bulk Heterojunction Photovoltaic Cells. *Angewandte Chemie International Edition* (2003), *42*, 3371–3375. DOI: 10.1002/anie.2000351647.

[147] BLOUIN, N.; MICHAUD, A.; LECLERC, M.: A Low-Bandgap Poly(2,7-Carbazole) Derivative for Use in High-Performance Solar Cells. *Adv. Mater.* (2007) 19, 2295. DOI: 10.1002/adma.200602496.

[148] Ossila Ltd, Kroto Innovation Centre: *Ossila enabling organic electronics*, website URL <http://www.ossila.com>, [cit. 2014-02-10].

[149] PARK, S. H., ROY, A.; BEAUPRÉ, S., CHO, Sh., COATES, N., MOON, J., S., MOSES, D., LECLERC, M., LEE, K., HEEGER, A. J.: Bulk Heterojunction Solar Cells with Internal Quantum Efficiency Approaching 100%. *Nature Photonics* (2009), 3, 297–302. DOI: 10.1038/nphoton.2009.69.

[150] AÏCH, R. B., ZOU, Y., LECLERC, M., TAO, Y.: Solvent Effect and Device Optimization of Diketopyrrolopyrrole and Carbazole Copolymer Based Solar Cells. Organic Electronics 11 (2011), 1053–1058. DOI: 10.1016/j.orgel.2010.03.004.

[151] JO, J.; GENDRON, D.; NAJARI, A.; MOON, J. S.; CHO, Sh.; LECLERC, M.; HEEGER, A. J.: Bulk Heterojunction Solar Cells Based on a Low-

Bandgap Carbazole-Diketopyrrolopyrrole Copolymer. *Appl. Phys. Lett.* (2010), *97*, 203303. DOI: 10.1063/1.3508951.

[152] HUO, L.; HOU, J.; CHEN, H.-Y.; ZHANG, Sh.; JIANG, Y.; CHEN, T. L.; YANG, Y.: Bandgap and Molecular Level Control of the Low-Bandgap Polymers Based on 3,6-Dithiophen-2-yl-2,5-dihydropyrrolo[3,4-c]pyrrole-1,4-dione toward Highly Efficient Polymer Solar Cells. *Macromolecules* (2009), 42, 6564–6571. DOI: 10.1021/ma9012972.

[153] SHAHEEN, S. E., BRABEC, Ch. J., SARICIFTCI, N. S., PADINGER, F., FROMHERZ, T., HUMMELEN, J. C.: 2.5% Efficient Organic Plastic Solar cells. *Appl. Phys. Lett.* 6 (2001), 78, 841–843. DOI: 10.1063/1.1345834.

[154] PORRÈS, L.; HOLLAND, A.; PÅLSSON, L.-O.; MONKMAN, A. P.; KEMP, CH. and BEEBY, A: Absolute Measurements of Photoluminescence Quantum Yields of Solutions Using an Integration Sphere, *Journal of Fluorescence*, 16 (2006), 2. DOI: 10.1007/s10895-005-0054-8.

[155] PETERS, C. H., SACHS-QUINTANA, I. T., KASTROP, J. P., DEAUPRÉ, S., LECLERC, M. and McGEHEE, M. D.: High Efficiency Polymer Solar Cells with Long Operating Lifetimes. Advanced Energy Materials 1 (2011), 491–494. DOI: 10.1002/aenm.2011000138.

[156] BELJONNE, D., CORNIL, J., DOS SANTOS, D.A., SHUAI, Z. and BRÉDAS, J.L.: Excited States in Poly(paraphenylenevinylene) and Related Oligomers: Theoretical Investigation of Their Relation to Electrical and Optical Properties N.S. Sariciftci (Ed.), *Primary Photoexcitations in Conjugated Polymers: Molecular Exciton versus Semiconductor Band Model*, World Scientific Publishing Company, Incorporated (1997), 559–585 (Chapter 19). ISBN: 978-981-4518-21-5.

[157] GIESEKING, B., JAECK, B., PREIS, E., JUNG, S., FORSTER, M., SCHERF, U., DEIBEL, C. and DYAKONOV, V.: Excitation Dynamics in Low Band Gap Donor-Acceptor Copolymers and Blends. *Adv. Energy Mater.*, 2 (2012), 1477. DOI: 10.1002/aenm.201200304.

[158] HEINRICHOVÁ, P.; DZIK, P.; ZHIVKOV, I.; MLADENOVA, D.; WEITER, M.: Development of Organic Solar Cells Based on Conjugated Polymers. *Chemické listy* (2011); s895. Contribution on conference: 5th Chemistry and life, Brno, Czech Republic. 14-16. 9. 2011.

[159] POPE, M. and SWENBERG, C. E.: *Electronic Processes in Organic Crystals and Polymers*, vol. 2, Oxford University Press, New York (1982). ISBN: 978-0195129632.

[160] ISO 9845-1; *Solar energy – Reference solar spectral irradiance at the ground at different receiving conditions – Part 1: Direct normal and hemispherical solar irradiance for air mass 1.5.* 1992.

[161] Reference Cells, *ReRa Solutions* (2013). Website URL <http://www.rera.nl/index.php/reference-cells/> [cit. 2013-03-15]

[162] *Photomultiplier tube R3896, Hamamatsu*. Document online: URL <https://www.hamamatsu.com/resources/pdf/etd/R3896_TPMS101E04.pdf> [cit. 2013-03-15].

[163] HEINRICHOVA, P; VALA, M.; WEITER, M: Energy versus charge transfer in π-conjugated polymer:fullerene blends, *Chemical Physics Letters 592* (2014), 314–319. DOI: 10.1016/j.cplett.3013.12.050

[164] SHEKA, E. F., RAZBIRIN, B. S., STARUKHIN, A. N., NELSON, D. K., DEGUNOV, M. Y., LYUBOVSKAYA, R. N. and TROSHIN, P. A.: The Nature of Enhanced Linear and Nonlinear Optical Effects in Fullerene Solutions. *Journal of Experimental and Theoretical Physics* 5 (2009), 108, 738–750. DOI: 10.1134/S1063776109050021.

[165] SCHMIEDOVÁ, V., ZMEŠKAL, O., HEINRICHOVÁ, P., WEITER, M.: Optical Characterization of Polymeric Thin Films for Photovoltaic Applications by Ellipsometry, *8th Workshop Ellipsometry*, Dresden, Germany. 10–12. 4. 2014.

[166] COOK, S., OHKITA, H., KIM, Y., BENSON-SMITH, J. J., BRADLEY, D. D. C. and DURRANT, J. R.: A Photphysical study of PCBM thin films. *Chemical Physics Letters* 445 (2007), 276–280. DOI:10.1016/j.cplett.2007.08.005.

[167] ENGMANN, S., TURKOVIC, V., DENNER, P., HOPPE, H., GOBSCH, G.: Optical Order of the Polymer Phase within Polymer/Fullerene Blend Films, *Journal Of Polymer Science Part B: Polymer Physics* (2012), 50, 1363–1373. DOI: 10.1002/polb.23131.

[168] SCULLY, S. R. and McGEHEE, M. D.: Effects of Optical Interference and Energy Transfer on Exciton Diffusion Length Measurements in Organic Semiconductors. *J. Appl. Phys.* 100 (2006), 034907. DOI: 10.1063/1.2226687.

[169] HOPPE, H.; GLATZEL, T.; NIGGEMANN, M.; SCHWINGER, W.; SCHAEFFLER, F.; HINSCH, A.; LUX-STEINER, M. CH. and SARICIFCI, N. S.: Efficiency Limiting Morphological Factors of MDMO-PPV:PCBM Plastic Solar Cells. *Thin Solid Films*, 511–512 (2006), 587–592. DOI: 10.1016/j.tsf.2005.12.071.

[170] VANDEWAL, K., TVINGSTEDT, K., GADISA, A., INGANÄS, O. and MANCA, J. V.: Relating the Open-Circuit Voltage to Interface Molecular Properties of Donor:Acceptor Bulk Heterojunction Solar Cells. *Physical Review B* 81 (2010), 125204. DOI: 10.1103/PhysRevB81.125204

[171] KRONHOLM, D. F. and HUMMELEN, J. C.: Fullerene-Based Acceptor Materials, *Organic Photovoltaics*, Wiley-VCH Verlag (2009). ISBN 97-83527623198.

[172] SCHARBER, M. C., MÜHLBACHER, D., KOPPE, M., DENK, P., WALDAUF, C., HEEGER, A. J., BRABEC, C. J.: Design Rules for Donors in Bulk-Heterojunction Solar Cells – Towards 10% Energy-Conversion Efficiency; *Advanced Materials* (2006), 18, 789–794. DOI: 10.1002/adma.200501717.

[173] SHOCKLEY, W. and QUEISSER, J.: Detailed Balance Limit of Efficiency of p-n Junction Solar Cells. *Journal of Applied Physics* 32 (1961), 510. DOI: 10.1063/1.1736034.

[174] KIRCHARTZ, T.: *Generalized Detailed Balance Theory of Solar Cells*. Jülich Forschungszentrum (2009). Vol. 38. ISBN 978-3-89 336-573-9

[175] RAU, U.: Reciprocity Relation Between Photovoltaic Quantum Efficiency and Electroluminescent Emission of Solar Cells. *Physical Review B* 76 (2007) 085303. DOI: 10.1103/PhysRevB.76.085303.

[176] BISQUERT, J. and GARCIA-BELMONTE G: On Voltage, Photovoltage and Photocurrent in Bulk Heterojunction Organic Solar Cells. *The Journal of Physical Chemistry Letters* 2 (2011), 1950–1964. DOI: 10.1021/jz2004864.

[177] *The Ossila Scharber Calculator*, Software online URL < http://www.ossila.com/support/scharber/scharber_calculator_mobile.php> [cit 2014-02-10].

[178] BURKHARD, G. F., HOKE, E. T. and MCGEHEE, M. D.: Accounting for Interference, Scattering, and Electrode Absorption to Make Accurate Internal Quantum Efficiency Measurements in Organic and Other Thin Solar Cells. *Adv. Mater.* (2010), 22, 3293–3297. DOI: 10.1002/adma.201000883.

[179] KIRCHARTZ, T. and RAU, U.: Electroluminescence Analysis of High Efficiency Cu(In,Ga)Se2 Solar Cells. *J. Appl. Phys.* 102, 104510 (2007), DOI: 10.1063/1.2817959.

[180] RIEDEL, I., PARISI, J., DYAKOV, V., LUTSEN, L., VANDERZANDE, D. and HUMMELEN, J. C.: Effect of Temperature and Illumination on the Electrical Characteristics of Polymer-Fullerene Bulk – Heterojunction Solar Cells. *Advenced Functional Materials* 14 (2004), 1. DOI: 10.1002/adfm.200304399.

[181] ZHOU, S., SUN, J., ZHOU, Ch. and Deng, Z.: Comparison of recombination models in organic bulk heterojunction. *Physica B* 415 (2013), 28–33. DOI: 10.1016/j.physb.2013.01.030.

[182] TADA, K. and ONODA, M.: Preparation of Nanostructured Conjugated Polymer Films from Suspension-Based Technique and Their Applications; *Thin Solid Films* 499 (2006) 19–22. DOI: 10.1016/j.tsf.2005.07.006.

[183] HERAEUS: Clevios™ P Jet HC V2; *Conductive polymers.* Technical specification of material on-line. URL <http://clevios.com/en/_technik/productdetail_1034012.aspx?psMarketId=1290&psApplicationId=> [cit. 2012-03-21].

[184] 60-Second Surface Metrology - 3 Steps to Understanding Surface Texture. *Digital Metrology Solution*. URL <http://www.digitalmetrology.com/SurfaceFinishIn3Steps.htm> [cit. 2013-02-21].

[185] TULADHAR, S. M.; POPLAVSKYY, D.; CHOULIS, S. A.; DURRANT, J. R.; BRADLEY, D. D. C. AND NELSON J.: Ambipolar Charge Transport in Films of Methanofullerene and Poly(phenylenevinylene)/Methanofullerene Blends. *Adv. Funct. Mater.* 2005, 15, 1171–1182. DOI: 10.1002/adfm.200400337.

LIST OF SYMBOLS AND ABBREVIATIONS

$a(\lambda)$	absorptance
a	initial donor acceptor radius
α	absorption coefficient
A	absorbance
A	electron acceptor
A_A	electron affinity of acceptor molecule
c	velocity of light in vacuum
c (M)	molar concentration
CS	states of separated charges
CS^*	excited states of separated charges
CT	charge transfer state
CT^*	excited charge transfer state
CTC	charge transfer complex
D	electron donor
D^*	excited electron donor
D+A or D/A	donor acceptor interface
$[D^*A]$ or $^1D^*/A$	exciplex of electron donor and electron acceptor
$\left[D^{\bullet+}A^{\bullet-}\right]$ or D^+/A^-	CT state; Coulombically bounded electron hole pair
e	elementary charge
e^-	electron
ε	relative permittivity of material
ε_0	permittivity in vacuum
E	energy
E_B	binding energy
E_{bb}	electronic transition energy of the unsubstantiated planar backbone
E_{cryst}	the bathochromic shift induced by intermolecular interactions in the solid state.
E_{CT}	Charge transfer state energy
E_{dist}	the hypsochromic (blue) energy shift induced by distortion from planarity in the equilibrium geometry
E_g	band gap energy
EL	electroluminescence emission
EQE	external quantum efficiency
EQE_{EL}	external quantum efficiency of electroluminescence
E_{solv}	the bathochromic (red) solvent shift compared to the value in vacuum
E_{sub}	the energy shift induced by the positive/negative inductive or mesomeric effects of chemical substituents
$\left\|E^2\right\|$	squared optical electricfield strength
f^2	orientation factor
ϕ	angle

ϕ_{bb}	black body irradiation
ϕ_f	quantum yields of fluorescence
ϕ_{Sun}	Sun irradiation
FF	fill factor
ΔG°	Gibbs free energy
$\Delta G^\dagger$	energy activation barrier
h	Planck constant
h^+	hole
HOMO	the highest occupied molecular orbital
I	intensity od light
I_D	ionization potential of donor molecule
IQE	internal quantum efficiency
ITO	indium tin oxide
j_{SC}	short current density
j_{rad0}	saturation current density for radiative recombination
k	Boltzmann constant
k_{CT}	kinetic constant of charge transfer
k_D	is rate constant of recombination
k_{diff}	kinetic constant of diffusion
k_{ET}	kinetic constant of energy transfer
k_{eT}	kinetic constant of electron transfer
k_F	recombination rate constant of geminate pair
k_{nr}	kinetic constant of non-radiative decay of exciton
k_r	kinetic constant of radiative decay of exciton
k_R	recombination rate constant of electron hole pair
k_{SC}	kinetic constant of electron hole pair dissociation
k_{SC}^*	kinetic constant of hot electron hole pair dissociation
K_{sv}	Stern-Volmer constant
λ	reorganization energy
λ_{ex}	wavelength of incident light
λ_i	inter reorganization energy
λ_o	reorganization energy of surround
LED	light emitting diode
Lico	Licocene® B
LUMO	the lowest unoccupied molecular orbital
μ	photogeneration efficiency
M	molar weight
MDMO-PPV	poly[2-methoxy-5-(3′,7′-dimethyloctyloxy)-1,4-phenylenevinylene]
ν	frequency of incident light
N_A	Avogadro's constant
N_e	the number of electrons
N_{ph}	the number of photons
N_{inj}	the number of injected electrons
OSC	organic solar cell
OLED	organic light emitting diode

$PC_{60}BM$	phenyl-C61-Butyric-Acid-Methyl Ester
$PC_{70}BM$	phenyl-C71-Butyric-Acid-Methyl Ester
PCBTDPP	poly[N-9′-heptadecanyl-2,7-carbazole-alt - 3,6 - bis (thiophen-5-yl) - 2,5-dioctyl - 2,5-dihydropyrrolo[3,4-]pyrrole-1,4-dione]
PCDTBT	poly[N-9″-hepta-decanyl-2,7-carbazole-alt-5,5-(4′,7′-di-2-thienyl-2′,1′,3′-benzothiadiazole)
PDO-123	commercial name of Tg-PPV
PEDOT:PSS	poly(3,4-ethylenedioxythiophene):poly(styrenesulfonate)
PEN	poly(ethylene 2,6-naphthalate)
PES	poly(ester) textile
PET	poly(ethylene terephtalate)
PL	photoluminescence intensity
PL_{CT}	position of maximum of CT state photoluminescence
pu	poly(urethane)
Q	quencher
Q	reaction coordinate
[Q]	molar concentration of quencher
r, R	distance or radius
rpm	rotation per minute
R_0	Förster's radius
R_a	arithmetic average roughness
R_c	collision distance
R_{eff}	effective quenching radius
R_λ	light reflectance
sil	silicone
S_0	singlet ground state
S_1	excited singled state
S_1^*	hot excited singlet state
S_i	Huang-Rhys factor
t (s)	time
τ	exciton lifetime
T	thermodynamic temperature
T_1	excited triplet state
T_1^*	hot excited triplet state
T_g	glass transition temperature
Tg-PPV	triblock co-polymer of poly[2-methoxy-5-(3′,7′-dimethyloctyloxy)-1,4-phenylenevinylene], poly{2-[4′-(3″,7″-dimethyloctyloxy)-1′,4′-phenyl]-1,4-phenylenevinylene} and poly{2-[3′-(3″,7″-dimethyloctyloxy)-1′,4′-phenyl]-1,4-phenylenevinylene)}
T_λ	transmittance
Tubi	Tubicoat® B40 latex
V_{bi}	built-in voltage

V_{OC}	open circuit voltage
w	weight fraction
Ω	spectral overlap integral between donor and acceptor

7 LIST OF PUBLICATIONS AND ACTIVITIES

Papers published in Journals with Impact factor:

HEINRICHOVA, P; VALA, M.; WEITER, M: Energy versus charge transfer in π-conjugated polymer:fullerene blends, *Chemical Physics Letters 592* (2014), 314–319. DOI: 10.1016/j.cplett.3013.12.050

MOŽÍŠKOVÁ, P.; HEINRICHOVÁ, P.; ŠEDINA, M.; VALA, M.; DAVID, J.; WEITER M.: The influence of transport layers on the photodegradation stability of polymer solar cell structures, *Journal of. Polymer Engeneering* 2 (2014), 34 ,113–123.

SIDEROV, V.; YORDANOV, R.; YORDANOVA, I.; BOYADJIEV, S.; HEINRICHOVÁ, P.; MLADENOVA, D.; WEITER, M.; ZHIVKOV, I. Optical measurements of the electrophoretic suspension kinetics. *Bulgarian chemical communications* (2013), 45, B, 181–184.

Other Publication and Conference Contributions:

HEINRICHOVÁ, P.; MOŽÍŠKOVÁ, P.; ŠEDINA, M.; WEITER, M. The Photodegradation of Polymers and Small Molecular Materials Applied in Organic Optoelectronic Devices. *Journal of Biochemical Technology* 2, (2010), 5, S53.

VALA, M.; WEITER, M.; HEINRICHOVÁ, P.; ŠEDINA, M.; OUZZANE, I.; MOŽÍŠKOVÁ, P. Tayloring of Molecular Materials for Organic Electronics. *Journal of Biochemical Technology* 2, (2010), 5, S45.

ŠEDINA, M.; HEINRICHOVÁ, P.; WEITER, M.; VALA, M.; SALYK, O. The role of various transport layers type for construction of organic solar cells. *Journal of Biochemical Technology* 2, (2011), 5, S40-S41.

HEINRICHOVÁ, P.; MOŽÍŠKOVÁ, P.; ŠEDINA, M.; WEITER, M. The Photodegradation of Polymers and Small Molecular Materials Applied in

Organic Optoelectronic Devices. In *X. Pracovní setkání fyzikálních chemiků a elektrochemiků & IV. Letní elektrochemická škola; Sborník příspěvků 23.–25. 6. 2010.* Brno: Mendel Univerzita in Brno (2010), 81-83. ISBN: 978-80-7375-396- 2. ISSN: 0974–2328.

HEINRICHOVÁ, P.; MOŽÍŠKOVÁ, P.; ŠEDINA, M.; WEITER, M. Studium fotodegradace organických materiálů pro fotovoltaické aplikace. In *Z. Remeš, M. Vaněček, A. Poruba Optical characterization methods in the solar cell research, Conference Proceeding from 5. České fotovoltaické konference, 10.–13. 11. 2010.* Brno (2011). ISBN: 978-80-254-8906-2.

HEINRICHOVÁ, P.; DZIK, P.; ZHIVKOV, I.; MLADENOVA, D.; WEITER, M. Development of Organic Solar Cells Based on Conjugated Polymers*; Chemické listy special issued volume of 5. Chemistry and Life in Brno*. Praha: Česká společnost chemická (2011), 895–895.

VALA, M.; WEITER, M.; HEINRICHOVÁ, P.; OUZZANE, I. Optical Properties of Diketo-pyrrolo-pyrroles for Organic Electronic Applications; *Chemické listy special issued volume of 5. Chemistry and life in Brno.* Praha (2011), 886–887.

ZHIVKOV, I.; VALA, M.; WEITER, M.; OUZZANE, I.; HEINRICHOVÁ, P.; MLADENOVA, D. Electrophoretic deposition of thin organic films for solar energy conversion purpose; *Chemické listy special issued volume of 5. Chemistry and life in Brno.* Praha (2011), 884–884.

OUZZANE, I.; HEINRICHOVÁ, P.; ŠEDINA, M.; WEITER, M.; VALA, M. Optical characterisation studies of novel diketo-pyrrolo-pyrroles. Castle Třešt', Czech Republic (2011).

MLADENOVA, D.; ZHIVKOV, I.; OUZZANE, I.; VALA, M.; HEINRICHOVÁ, P.; BUDUROVA, D.; WEITER, M. Thin polyphenylene vinylene electrophoretically and spin-coated films - photoelectrical properties. *Journal of Physics: Conference Series 398* (2012), 1, 1–6.

HEINRICHOVÁ, P.; ZHIVKOV, I.; MLADENOVA, D.; DAVID, J.; VALA, M.; WEITER, M: The Study of the Influence of Deposition Method on Electrical and Optical Properties of PPV Polymer with High Glass Temperature. *Journal of Physics: Conference Series* (2012), 398, 1–6.

KRAJČOVIČ, J.; WEITER, M.; VALA, M.; HEINRICHOVÁ, P.; LUŇÁK, S.; VYŇUCHAL, J. Design and synthesis of diketo-pyrrolo- pyrroles for organic electronics. In Atlanta, US: (2012). s. 207–207.

ŠPÉROVÁ, M.; VALA, M.; WEITER, M.; HEINRICHOVÁ, P. Optical and Electrical Characterization of Diketopyrrolopyrrole- based materials for organic photovoltaics. Greece (2012).

ZVĚŘINA, L.; HONOVÁ, J.; HEINRICHOVÁ, P.; WEITER, M. Optimalizace solárních článků z materiálu DPP(TBFu) 2 přídavkem dijodoktanu. In *Studentská odborná konference Chemie je život*. Brno (2013). 216–220. ISBN: 978-80-214-4823- 0.

HONOVÁ, J.; HRABAL, M.; STŘÍTESKÝ, S.; HEINRICHOVÁ, P.; VALA, M.; WEITER, M. New diketopyrrolopyrrole derivatives for organic photovoltaics. *Studentská konference Chemie je život*. Brno (2013). s. 82–82. ISBN: 978-80-214-4822- 3.

SCHMIEDOVÁ, V.; ZMEŠKAL, O.; HEINRICHOVÁ, P.; WEITER, M. Optical Characterization of Polymeric Thin Films for Photovoltaic Applications by Ellipsometry. Dresden, Germany (2014), 132–132.

Given speeches:

HEINRICHOVÁ, P.; VALA, M.; WEITER, M. The study of pi- conjugated polymers for photovoltaic application by fluorescence quenching experiments. *ReAdMat*. Pardubice (2013).

8 APPENDICES

Appendix No 1.

Specification of used materials.

Table A: Specifications of PEDOT:PSS (poly(3,4-ethylenedioxythiophene):poly(styrenesulfonate)) materials used for hole transport layers of solar cell structures.

Supplier	Important properties
Sigma-Aldrich Co, Steinheim, Germany	water dispersion 0.5 wt. % PEDOT, 0.8 wt.% PSS, conductivity 1 Sm^{-1}
H. C. Starck GmbH, Goslar, Germany	water dispersion 0.9 wt. % solid compounds, conductivity 3 Sm^{-1}
Ossila (H. C. Starck)	PEDOT:PSS ratio 1:6, water dispersion 1.3–1.7 wt. % solid compounds, conductivity 0.02–0.2 Sm^{-1}

Appendix No 2.

The details of thin layers deposition

Table A.: Solution concentrations of materials used for spin-coating. PCBM marks both fullerene derivatives $PC_{60}BM$ and $PC_{70}BM$.

Material	Concentration
MDMO-PPV	10 mg/ml
MDMO-PPV:PCBM 1:4	10 mg/ml + 40 mg/ml
Tg-PPV	6 mg/ml
Tg-PPV:PCBM 1:4	6 mg/ml + 24 mg/ml
PCDTBT	4 mg/ml
PCDTBT:PCBM 1:4	4 mg/ml + 16 mg/ml
PCBTDPP	4 mg/ml
PCBTDPP:PCBM 1:4	4 mg/ml + 12 mg/ml
PCBM	25 mg/ml

Table B: Annealing conditions for all the materials and blends. PCBM marks both fullerene derivatives $PC_{60}BM$ and $PC_{70}BM$.

Material	Temperature	Time
MDMO-PPV	50 °C	10 min
MDMO-PPV:PCBM 1:4	50 °C	10 min
Tg-PPV	70°C	10 min
Tg-PPV:PCBM 1:4	70°C	10 min
PCDTBT	70°C	20 min
PCDTBT:PCBM 1:4	70°C	20 min
PCBTDPP	70°C	20 min
PCBTDPP:PCBM 1:4	70°C	20 min
PCBM	110°C	10 min
PEDOT:PSS	110°–150°C	5–15 min

Appendix No 3.

Reprints of publication: P. HEINRICHOVÁ, I. ZHIVKOV, D. MLADENOVA, J. DAVID, M. VALA and M. WEITER: The Study of the Influence of Deposition Method on Electrical and Optical Properties of PPV Polymer with High Glass Temperature, *Journal of Physics: Conference Series* 398 (2012) 012057

The Study of the Influence of Deposition Method on Electrical and Optical Properties of PPV Polymer with High Glass Temperature

P Heinrichová[a], I Zhivkov[a,b], D Mladenova[a,b], J David[a], M Vala[a], and M Weiter[a]

[a] Brno University of Technology, Faculty of Chemistry, Materials Research Centre, Purkynova 118, 612 00 Brno, Czech Republic
[b] Institute of Optical Materials and Technologies "Acad. J. Malinowski", Bulgarian Academy of Sciences, Acad. G. Bonchev Str. bl. 101/109, 1113 Sofia, Bulgaria

E-mail: xcheinrichova@fch.vutbr.cz

Abstract. The paper is focused on comparison of electrical and optical properties of thin layers of copolymer with high glass transition temperature Tg-PPV (poly[2-methoxy-5-(3′,7′-dimethyloctyloxy)-1,4-phenylenevinylene], poly{2-[4′-(3″,7″-dimethyloctyloxy)-1′,4′-phenyl]-1,4-phenylenevinylene} and poly{2-[3′-(3″,7″-dimethyloctyloxy)-1′,4′-phenyl]-1,4-phenylenevinylene)}) prepared by two different deposition methods: by spin-coating and by electrophoretic deposition. We found several differences in absorption and emission spectra using those two preparation techniques. On the other hand, the photoelectrical properties were similar.

1. Introduction

Study of organic electronics opens the way to develop new electronic applications, which are not achievable using classical semiconducting inorganic materials as silicon, gallium arsenide, etc. Thin layers of organic semiconductors could be easily deposited by simple "wet" techniques. Key role for the control of the film structure and properties plays the choice of the deposition method. This paper is focused on a comparison of two "wet" deposition methods of organic functional materials. One is the standard laboratory deposition method spin-coating (SC) and second method is the electrophoretic deposition (EPD).

While SC is a method for deposition from solution, EPD works with colloidal particles dispersed in poor solvents of deposed material. The suspension is prepared by precipitation of deposed material solution by adding poor solvents. During the process of particle formation they are charged due to the requirement that an electrochemical equilibrium with solvent has to be achieved. Then the charged particles are deposed on the electrode by applying electrical field. Whole mechanism of the EPD is not completely known yet due to the complexity of the process, but it is used in the industry for various applications [1].

In comparison with SC [2], [3] the properties of the EPD layers are more strongly influenced by the preparation conditions. On the other hand EPD allows controlled preparation of nanostructured layers [4], and a formation of multilayer stacks from materials soluble in the same solvent [5]. In comparison

with SC the EPD uses more effectively the deposed material, but consumes more of high quality solvents.

This work is focused on the study of thin layer preparation of polymeric materials for organic electronics. Poly(*p*-phenylenevinylene) derivatives are one group of polymeric materials with a potential application in the organic electronics. One of the well-known and described derivate is the MDMO-PPV (poly[2-methoxy-5-(3′,7′-dimethyloctyloxy)-1,4-phenylenevinylene]), which serves as model electron donor material for organic electronics. Structure of MDMO-PPV is shown on figure 1. MDMO-PPV has relatively low glass transition temperature T_g = 45 °C [6], which influences negatively the thermal stability of the active layer. Triblock copolymer of poly[2-methoxy-5-(3′,7′-dimethyloctyloxy)-1,4-phenylenevinylene], poly{2-[4′-(3″,7″-dimethyloctyloxy)-1′,4′-phenyl]-1,4-phenylenevinylene} and poly{2-[3′-(3″,7″-dimethyloctyloxy)-1′,4′-phenyl]-1,4-phenylenevinylene)}, denoted here as Tg-PPV (see figure 1) with T_g = 138 °C [6, 7] seems to be a more suitable alternative. Tg-PPV is generally synthesized for use in the organic light emitting diodes. It is distributed by Merck KGaA, Darmstadt, Germany under the commercial name PDO-123 [8].

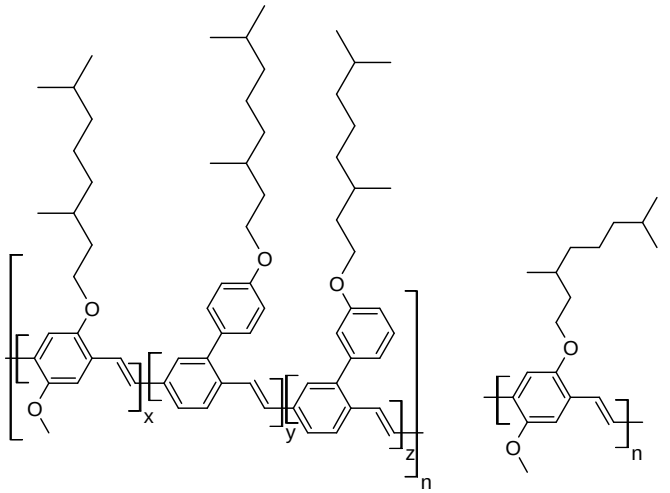

Figure 1. Structure of the used here high Tg-PPV and more studied in the literature MDMO-PPV derivate.

2. Experimental

Films of Tg-PPV were prepared on glass substrates commercially covered with ITO (indium thin oxide) electrode (Sigma–Aldrich Co., Steinheim, Germany).

SC thin layers of polymer were deposed from chlorobenzene solution of concentration 6 g/l of Tg-PPV. The deposition was performed at rotation speed of 1000 RPM for a time of 1 min on a spin-coater KW-4A (Chemat Technology, Inc., CA, U.S.A.).

EPD was carried out from Tg-PPV suspension with a concentration of $7.74 \cdot 10^{-3}$ g/l. Suspension was prepared from solution of Tg-PPV in toluene by precipitation with acetonitrile. Optimal ratio of toluene and acetonitrile of 42.5 % was determined by light absorption measurements on Varian Cary 50 double-beam spectrometer. Deposition was realized under constant current condition in the range of 0.060 to 0.150 mA. Source of electrical current was Keithley 2410 Source Meter (Keithley Instruments Inc., Cleveland, OH, U.S.A.). The value of the current controls the rate of deposition. Time of deposition varied between 30 and 60 s and influenced the final film thickness.

Optical properties for quality assurance of thin layers and for suspension optimization were studied by a measurement of UV-VIS absorption spectra on Varian Cary Probe 50 UV–VIS spectrometer and fluorescence spectra on Horiba Jobin Yvon Fluorolog (Horiba Jobin Yvon S.A.S., Chilly Mazarin,

France). Liquid samples were measured in Hellma QS 10 mm quartz cuvette (Hellma GmbH, Mühlheim, Germany).

Thicknesses of layers were characterized by optical profilometer MicroProf FRT (Fries Research & Technology GmbH).

Samples for electrical characterization with semiconductor Tg-PPV thin layers were subsequently covered with aluminium electrodes by vacuum deposition. Deposition was realized in the deposition chamber U311B Tesla (Tesla, Opočno, Czech Republic).

The samples were electrically characterized in cryostat VPF-475 (Janis Research Company Inc., Wilmington, MA, U.S.A.) at 10^{-4} Pa at laboratory temperature by picoampermeter Keithley 6478. Current voltage characteristics were measured on samples both in dark and irradiated by LSH502 LOT Oriel xenon lamp with emission spectrum similar to the sun light (LOT-Oriel Co., Darmstadt, Germany). Intensity of the incident light of 1 $mW \cdot cm^{-2}$ was controlled by irradiance meter X97 Gigahertz-Optik with radiometric detector head RW-3703-4 for UV-VIS range (Gigahertz-Optik GmbH, Türkenfeld, Germany).

3. Results and discussion

3.1. Optical study of suspension

A suspension concentration is a key parameter for optimal electrophoretic deposition. Suitable volume ratio of acetronitrile/toluene for suspension preparation was found by UV-VIS absorption spectrometry. Figure 2 A) shows absorption and emission spectra of Tg-PPV solution in toluene (0% acetonitrile) and after addition of 42 and 90 % volume ratio of acetronitrile. Noticeable bathochromic shift of absorption band from 476 nm to 494 nm with the increase of acetonitrile volume ratio was observed. The emission spectra behave similar, but they are more sensitive to acetonitrile addition. Bathochromic shift of emission maximum is from 549 nm to 590 nm. Generally the evaluation of the emission spectra is more difficult due to effects as fluorescence quenching, reabsorption of emitted light, changes in vibrational structure of spectra and others. On the other hand fluorescence spectra provide valuable additional information.

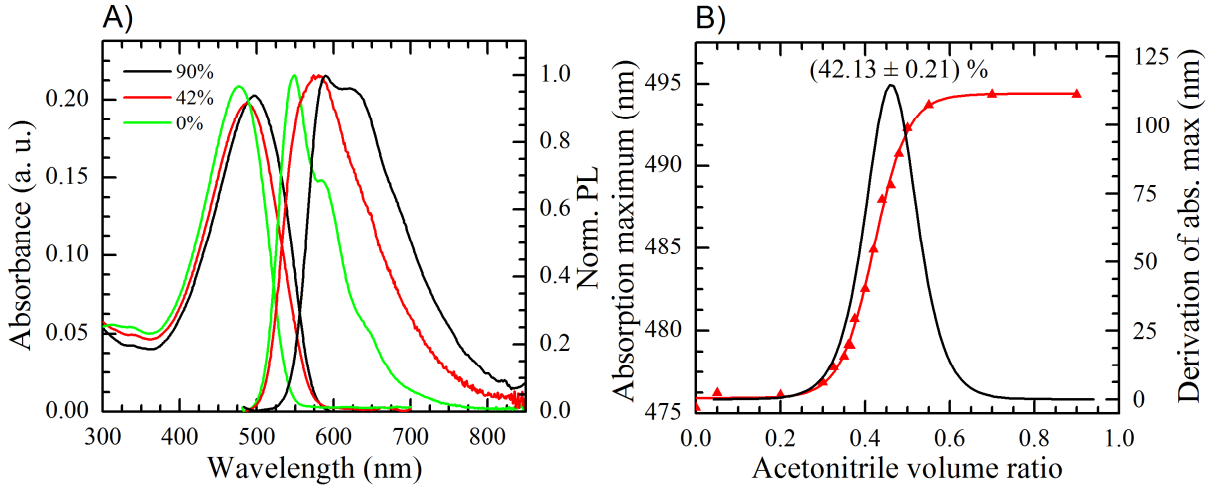

Figure 2. A) Absorption and emission spectra of toluene solution of Tg-PPV after addition of 0, 42 and 90 % volume ratio of acetonitrile. B) A dependence of absorption maxima position on the acetronitrile volume ratio *w*. Right axis is related to the first derivative of the curve. Maximum at 42.13 % of acetonitrile corresponds to the inflection point.

The position of the absorption maxima were precisely determined by taking the first derivative of the absorption spectra. The obtained values are plotted as a function of the acetonitrile volume ratio in

figure 2 B). Sigmoid curve shows range (from 30 % to 55), where acetonitrile volume ratio influences the suspension concentration. A first derivative of the sigmoid curve was also taken and inflection point at (42.13 ± 0.21) % was found. This acetonitrile volume ratio was used for EPD of thin layers.

3.2. Optical study of thin layers

Absorption and emission spectra of Tg-PPV: solution in toluene; solution in chlorobenzene; toluene/acetonitrile suspension with 90% acetonitrile; thin EPD film produced from a toluene/acetonitrile suspension with 42.5 % acetonitrile; thin SC films produced from a solution in chlorobenzene are presented in figure 3.

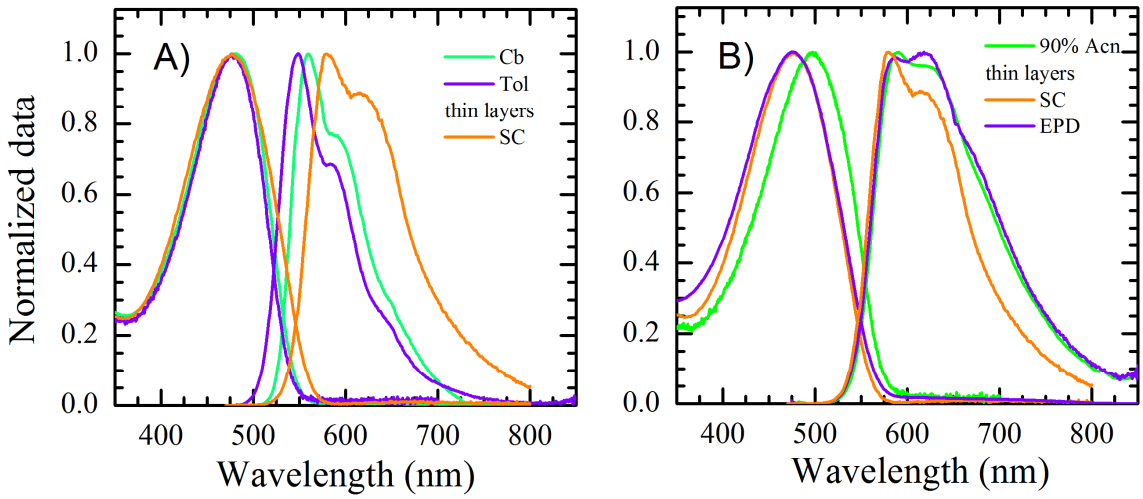

Figure 3. Comparison of absorption and emission spectra of Tg-PPV plot: A) solutions in chlorobenzene (Cb) and toluene (Tol) and thin layer prepared by SC, plot B) suspension prepared by addition of 90% volume acetronitrile (90% Acn) to a toluene solution, and thin SC and EPD layers.

Absorption spectra of chlorobenzene solution and thin film prepared by SC from chlorobenzene solution don't have resolute vibrational structure. This effect is usually related to the disordered structure of polymer [9]. Both spectra showed the same position of absorption band, only thin layer absorption edge is 20 nm red shifted. This effect is related to the closer arrangement of polymer chains in the layer due to aggregation [9]. Emission spectrum of SC layer is found fully bathochromically shifted compared to the spectrum of chlorobenzene solution [10].

More differences in spectra taken from toluene solution, acetonitrile suspension and EPD layer are seen. EPD layer performs an absorption edge at 580 nm like suspension, prepared by adding of 90% volume of acetronitrile and like SC layer, but absorption maximum lies at 476 nm like in spectra, measured from solutions and SC layer. Emission spectrum of suspension and EPD layers are overlapped, only vibrational structure of spectrum is changed. Perhaps there was particularly preserved nanostructure of suspension present and particularly spill in uniform film [11]. Strict interpretation needs more investigations to be done. However, the spectra measured don't indicate a degradation of the polymer after EPD, which may have been caused by electrical current during deposition.

3.3. Electrical study of thin layers

Several thicknesses of thin films were prepared by EPD. The aim was to prepare layers comparable to the 120 nm layer prepared by SC as a reference.

Figure 4 shows samples with best current voltages curves of SC and EPD layers. Layers were characterized in dark and under illumination with light of intensity 1 mW/cm^2. In dark, the EPD layers

were less conductive. The threshold voltage V_T, when current start strongly grow, for SC layers was around 1.1 V, whereas for SPD layers are located at much higher voltages (higher than 2 V); see figure 4. It is caused by an energy barrier for charge carries. Origin of barriers may be different: morphology of layer, bad adhesion of layers and other. Current voltage characteristics of EPD layers under illumination were on average comparable with those, taken from SC layers.

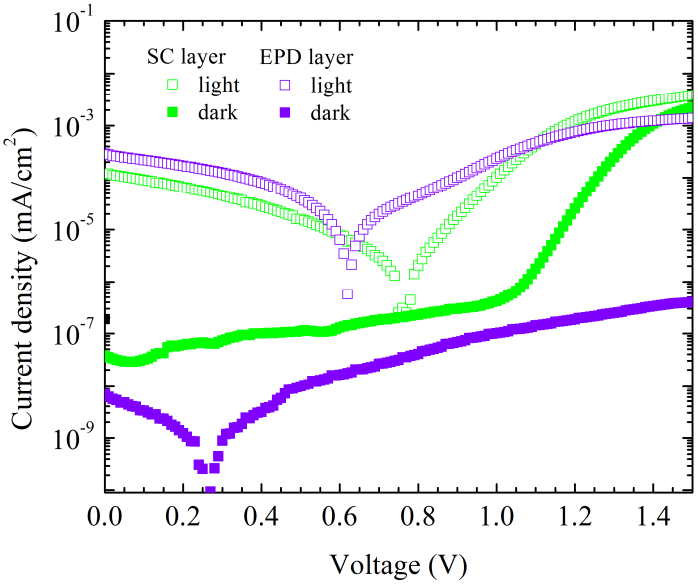

Figure 4. Comparison of current voltage characteristics measured on samples with SC and EPD layers.

Table 1. Average photovoltaic conversion parameters of three EPD layers with different thicknesses and one SC layer.

sample	**tickness (nm)**	j_{SC} **(mA/cm2)**	V_{OC} **(U)**	***FF***	μ **(%)**
SP	120 ± 20	$(1.2 \pm 0.7)\cdot 10^{-4}$	0.6 ± 0.2	0.22 ± 0.08	$(1.8 \pm 0.3)\cdot 10^{-3}$
EPD 1	≈ 100	$1.75\cdot 10^{-4}$	0.52	0.22	$2.02\cdot 10^{-3}$
EPD 2	290 ± 80	$(1.8 \pm 0.6)\cdot 10^{-4}$	0.57 ± 0.05	0.26 ± 0.03	$(2.7 \pm 0.9)\cdot 10^{-3}$
EPD 3	540 ± 80	$0.09\cdot 10^{-4}$	0.59	0.21	$0.11\cdot 10^{-3}$

Parameters as short current density j_{SC}, open circuit voltageV_{OC}, fill factor *FF* and maximal photovoltaic efficiency μ were calculated from current voltages measurements taken under light exposure. Results are compared by plotting diagrams on figure 5 and summarized in table 1. Thin EPD layers (sample EPD 1 and EPD 2) have similar parameters as SC layers within the measured uncertainty. Thick layers EPD 3 (540 nm) has a reduced value of the short current density. This is an expected result, because the conductivity of the organic layers is driven by the electric field, which depends on the distance between the electrodes [12, 13].

4. Conclusion

Electrical and optical properties of thin Tg-PPV layers prepared by SC and EPD were compared. The differences in the emission spectra could be related to a nanostructure of the EPD films, while the SC films are more structureless.

Similar photovoltaic parameters of SC and EPD layers were found, only the dark-conductivity of EPD layers is lower, due to presence of higher barrier observed in current voltage curves.

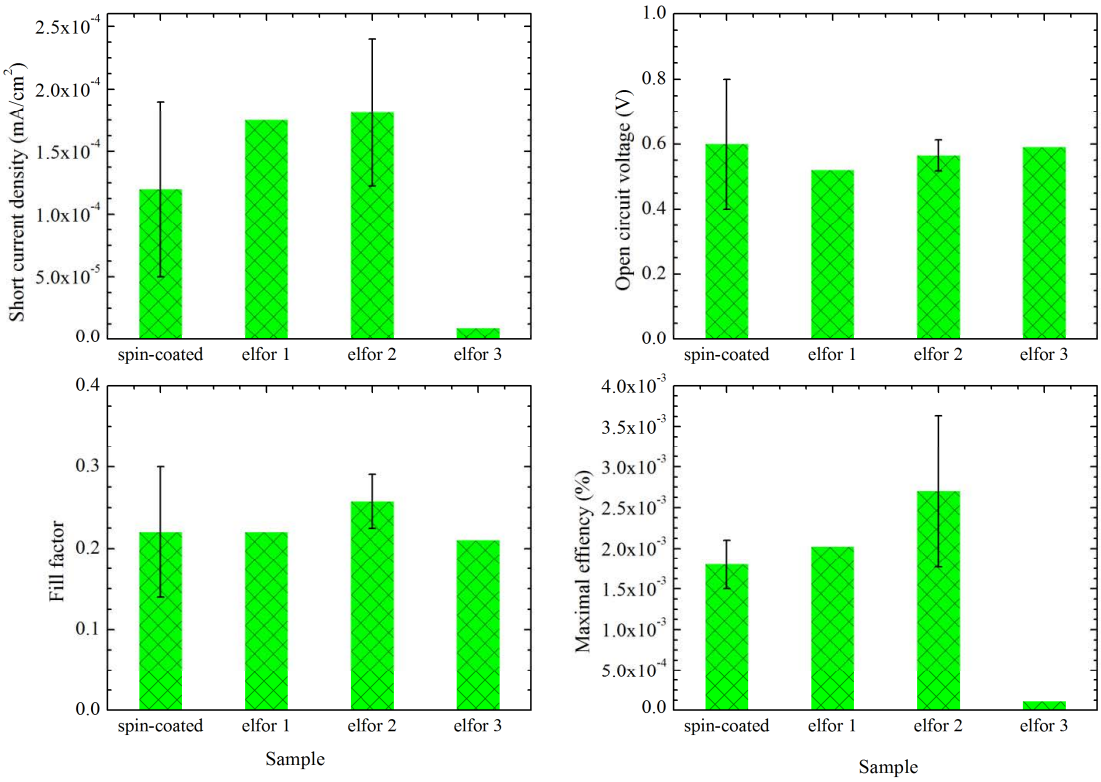

Figure 5. Diagrams of average photovoltaic conversion parameters of three EPD layers with different thicknesses (see table 1) and one SC layer.

Acknowledgement
This work was supported by the South Moravian Region and the Seventh Framework Programme for Research and Development (grant SIGA 885), Grant Agency of the Czech Republic project No. P205/10/2280, project "Centre for Materials Research at FCH BUT" No. CZ.1.05/2.1.00/01.0012 supported by ERDF and the National Fund of the Ministry of Education and Science, Bulgaria (grant DO 02-254).

References

[1] Van Tassel J J and Randall C A 2006 *Key Engineering Materials* **314** 167-174
[2] Norrman K, Ghanbari-Siahkali A and Larsen N B 2005 *Annu. Rep. Prog. Chem., Sect. C,* **101** 174–201
[3] Besra L and Liu M 2007 *Progress in Materials Science* **52** 1–61
[4] Tada K and Onoda M 2006 *Thin Solid Films* **499** 19-22
[5] Mladenova D, Sinigersky V et al. 2010 *Journal of Physics: Conference Series* **253** 012041
[6] Vandewal K, Gadisa A et al. 2008 *Advanced Functional Materials* **18** 2064–2070
[7] Bertho S, Haeldermans I et al. 2006 *Spie-Int Society Optical Engineering* DOI: 10.1117/12.663256.
[8] *Innovative Materials for Next Generation Electronics*, Merck. Electronical document URL <http://www.merck-chemicals.com/showBrochure/201004.144.ProNet.pdf> [cit. 2012-08-02].
[9] Lemmer U and Göbel E O 1997 *Primary Photoexcitations In Conjugated Polymers: Molecular Exciton Versus Semiconductor Band Model* ed Sariciftci N. S. (World scientific, Singapur) Chapter 9
[10] Traiphol R and Charoenthai N 2008 *Synthetic Metals* **158** 135–142

[11] Tada K and Onoda M 2008 *J. Phys. D: Appl. Phys*. **41** 4
[12] Blom P W M and Vissenberg M C J M 2000 *Materials Science and Engineering* **27** 53–94
[13] Deibel C, Dyakonov V 2010 *Rep. Prog. Phys*. **73** 096401

Appendix No 4.

Reprints of publication: HEINRICHOVA, P; VALA, M.; WEITER, M: Energy versus charge transfer in π-conjugated polymer:fullerene blends, *Chemical Physics Letters 592* (2014), 314–319. DOI: 10.1016/j.cplett.3013.12.050

Chemical Physics Letters 592 (2014) 314–319

Contents lists available at ScienceDirect

Chemical Physics Letters

journal homepage: www.elsevier.com/locate/cplett

Energy versus charge transfer in π-conjugated polymer:fullerene blends

Patricie Heinrichova *, Martin Vala, Martin Weiter

Materials Research Centre, Faculty of Chemistry, Brno University of Technology, Purkyňova 118, Brno 612 00, Czech Republic

ARTICLE INFO

Article history:
Received 25 October 2013
In final form 17 December 2013
Available online 24 December 2013

ABSTRACT

The article is focused on the detailed elucidation of fluorescence quenching by charge and/or energy transfer in π-conjugated polymers. The processes were studied in blends of MDMO-PPV, Tg-PPV, PCDTBT and PCBTDPP with fullerenes $PC_{60}BM$ and $PC_{70}BM$ in chlorobenzene. Fluorescence quenching was evaluated by the Perrin equation for static quenching and quenching sphere radiuses were calculated. These radiuses were found to be the same as the Förster critical distances for resonance energy transfer. It was concluded that energy transfer prevails over charge transfer under the conditions where the donor and acceptor are not in close contact.

1. Introduction

Since the discovery of the electrical conductivity of polyacetylene, π-conjugated polymers have become widely studied for their possible use in electronics, e.g. in sensors, light emitting diodes, solar cells and other components [1–4]. Among others, poly(*p*-phenylene vinylene) (PPV) and poly(3-hexyl-thiophene) (P3HT) are widely known representatives of polyaromatic polymers, the so-called second generation of π-conjugated polymers. P3HT-based solar cells exceeding 5% power conversion efficiency have been demonstrated [5]. The PPV derivatives are often used as a model π-conjugated polymer for studies of electron phenomena in organic semiconductors [6].

Currently research interest is focused on alternating aromatic copolymers containing electron donor and electron acceptor monomeric units (so called D–A copolymers), which cause the formation of a new optical band due to the presence of internal charge transfer. This third generation of π-conjugated polymers is characterized by low band gap energy, which increases their application potential because they absorb in near IR, possess high absorption coefficients, and exhibit better electrical conductivity and higher stability [7]. These properties make this polymeric generation especially suitable for photovoltaic applications.

Light absorption by π-conjugated polymers leads to the creation of excitons (Coulombically bound electrons and holes), which are delocalized along conjugated units of polymeric chains [6]. Because the polymer chains take many different conformations based on the environment and processing conditions, the length of effective conjugation is not fixed but exhibit significant distribution. Excitons can diffuse along chains as well as between chains, if their distance is favorable [8]. The decay of excitons is often accompanied by radiative recombination, i.e. fluorescence. Since the excited state is sensitive to changes in its surroundings, changes in fluorescence are used to monitor the excited state reactions.

An important excited state quenching process utilized primarily in organic photovoltaics is photoinduced charge transfer (CT) between the electron donor (D) and acceptor (A). In bulk heterojunction solar cell (BHJSC) the charge transfer occurs at the interface between the donor and acceptor. In these devices, light absorption induced charge transfer leads to the creation of a weakly bonded electron and hole located on the donor acceptor (DA) pair. These processes have been extensively studied in solution [9–12] and in thin films [13,14]. However, recently, it was shown that other quenching processes also have to be taken into account, e.g. resonance energy transfer (RET), in order to understand charge photogeneration in OSC and thus improve their efficiency.

Studies of exciton dissociation kinetics by ultrafast time resolved spectroscopy showed that exciton dissociation is a very fast process with a duration of only tens to hundreds of femtoseconds [15,16]. Therefore it was suggested and subsequently experimentally verified [17] that relatively slow exciton diffusion cannot significantly contribute to charge photogeneration. Subsequently, it was proposed that RET between the polymer exciton and electron acceptor plays a significant role in organic solar cells based on the bulk heterojunction concept with fullerenes as the acceptor [17].

However, most of the previous studies of π-conjugated polymer fluorescence quenching by fullerenes overlooked RET and generally assumed that quenching is caused by CT [9–12]. These studies focused on the question of whether the quenching is static or dynamic and, thus, whether it is limited by diffusion. Finally, static quenching was found to be dominant and the Perrin quenching sphere radius was identified in the order of tens nanometers. However, this value is ten times bigger than the expected distance for CT. Authors interpreted this discrepancy as being the result of the presence of polymeric coils with a similar diameter [11] and

* Corresponding author.
E-mail address: xcheinrichova@fch.vutbr.cz (P. Heinrichova).

0009-2614/$ - see front matter © 2013 Elsevier B.V. All rights reserved.
http://dx.doi.org/10.1016/j.cplett.2013.12.050

by exciton diffusion along the polymeric chain [12]. However, in the short time-window where CT is possible, the distance the exciton diffuses will be negligible and thus cannot contribute to the unanticipated radius of the Perrin quenching sphere.

In this Letter, we show that the size of the quenching sphere can be explained in terms of the Förster critical distance under the given experimental conditions, in contrast to previous studies. We used the four electron donating π-conjugated polymers depicted in Figure 1: MDMO-PPV (poly[2-methoxy-5-(3′,7′-dimethyloctyloxy)-1,4-phenylenevinylene]); Tg-PPV (Triblock copolymer of poly[2-methoxy-5-(3′,7′-dimethyloctyloxy)-1,4-phenylenevinylene], poly{2-[4′-(3″,7″-dimethyloctyloxy)-1′,4′-phenyl]-1,4-phenylenevinylene} and poly{2-[3′-(3″,7″-dimethyloctyloxy)-1′,4′-phenyl]-1,4-phenylenevinylene)}); PCDTBT (poly[*N*-9″-hepta-decanyl-2,7-carbazole-*alt*-5,5-(4′,7′-di-2-thienyl-2′,1′,3′-benzothiadiazole)); and PCBTDPP (poly[*N*-9′-heptadecanyl-2,7-carbazole-alt-3,6-bis (thiophen-5-yl)-2,5-dioctyl-2,5-dihydropyrrolo[3,4-]pyrrole-1,4-dione]); and two electron accepting fullerenes: $PC_{60}BM$ ([6,6]-phenyl-C_{61}-butyric acid methyl ester) and $PC_{70}BM$ ([6,6]-phenyl-C_{71}-butyric acid methyl ester). Thus, we show that the concept is rather general. In order to distinguish RET from CT, this study was performed in solution. Nevertheless, it is useful to note that the energy transfer also takes place in thin films, and therefore, can directly influence the operating principle of bulk heterojunction organic solar cells (BHJSC).

2. Experimental

Fluorescence quenching processes between polymers and fullerenes were studied in chlorobenzene (Sigma–Aldrich). MDMO-PPV, PCBTDPP and $PC_{60}BM$ were provided by Sigma Aldrich; Tg-PPV was obtained from Merck; and the rest of the chemicals from Ossila. The relevant properties of the studied polymers and fullerenes are summarized in Table 1.

The molar concentration of polymer in solutions was $0.36{\cdot}10^{-5}$ mol·dm^{-3} spectroscopic units (SPUN) [18,19] SPUNs represent the part of the polymer chain where the singlet excited state (exciton) is located [20] and, thus, determine the spectral properties of the polymer. The length of the PPV-based polymer SPUN (MDMO-PPV and Tg-PPV) was estimated from the comparison of fluorescence emission maximum $\lambda_{PL\ max}$ with published values for PPV oligomers of various length [18]. The SPUN length was estimated on seven monomeric units for both polymers. The PCDTBT SPUN was used according to the work of Gieseking et al. [19] and, for PCBTDPP, an analogous structural unit was assigned. The SPUNs in these polymers are constituted by a carbazole unit accompanied by one thienyl and one benzothiadiazol unit from each side in the case of PCDTBT, and by one thienyl and one diketopyrrolopyrrole units from each side of the carbazole unit in the case of PCBTDPP. The calculated molar weights M_{SPUN} are summarized in Table 1.

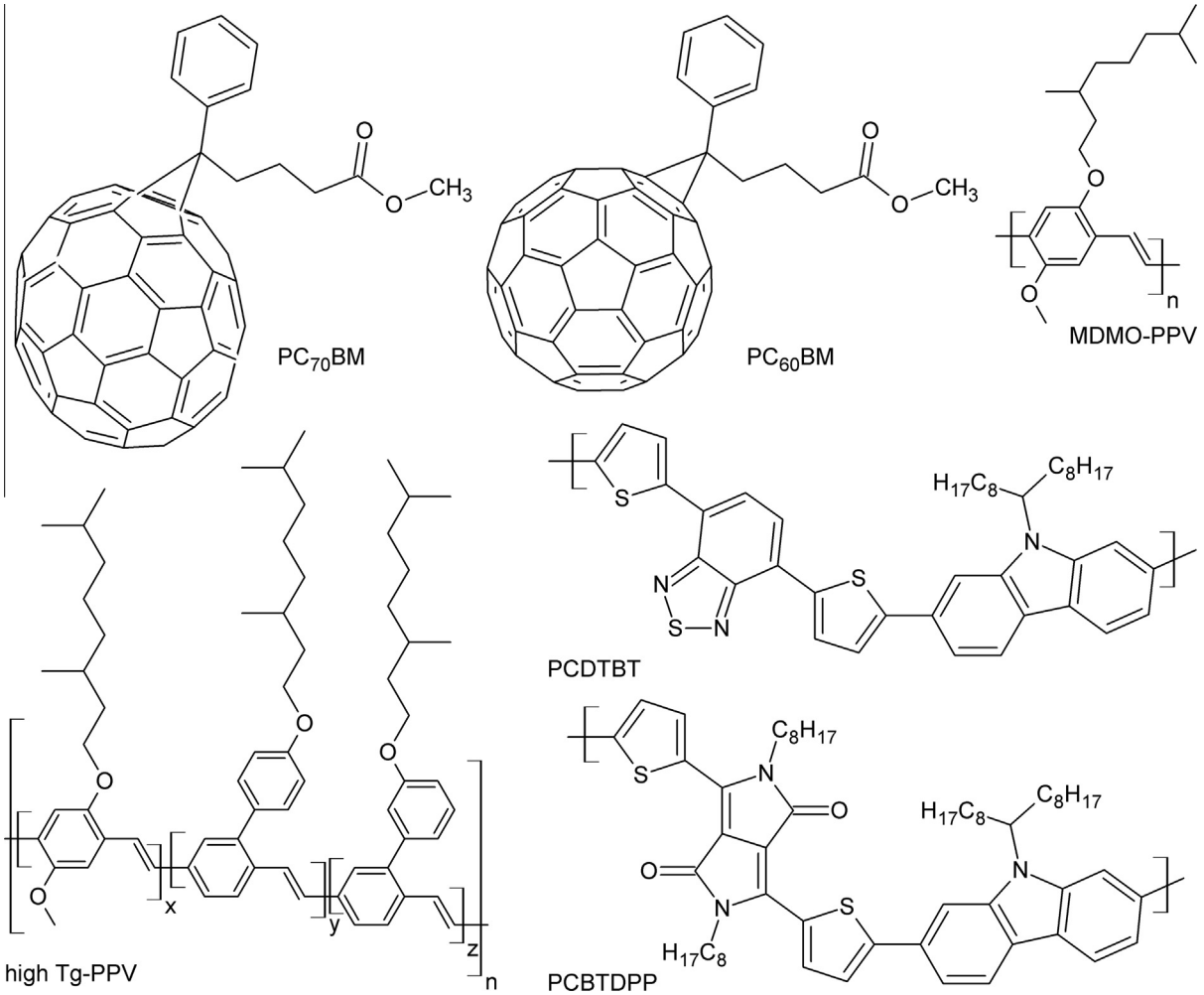

Figure 1. Molecular structures of the studied materials.

Table 1
Properties of the studied electron donating polymers and fullerenes: M_n is the molecular weight of the polymeric chain, PDI is the polydispersity index, M_u is the molecular weight of the monomer unit, M_{SPUN} is the molecular weight of the spectroscopic unit, E_g is the band gap energy calculated from E_{HOMO} and E_{LUMO}.

Material	M_n (g·mol^{-1})	PDI	M_u (g·mol^{-1})	M_{SPUN} (g·mol^{-1})	E_{HOMO} (eV)	E_{LUMO} (eV)	E_g (eV)
MDMO-PPV	23000	N/A	288.42	2018.94	−5.2 [22]	−3.1 [22]	2.1
Tg-PPV	340000	5.15	455.67	3189.69	−5.2 [b]	−2.9 [23]	2.3[a]
PCDTBT	16700	2.01	702.04	918.32	−5.5 [24]	−3.6 [24]	1.9
PCBTDPP	≈25000	N/A	926.41	1397.05	−5.4 [25]	−3.9 [25]	1.5
$PC_{60}BM$					−6.1 [22]	−4.4 [22]	1.7
$PC_{70}BM$					−6.0 [24]	−4.3 [24]	1.7

[a] Estimated from intersection of thin film absorption and emission spectra.
[b] $E_{HOMO} = E_{LUMO} - E_g$.

The absorption and fluorescence spectroscopy were carried out in the ambient environment (25 °C, atmospheric pressure). Absorption spectra of samples were measured using a Varian Cary Probe 50 UV–VIS spectrometer. Absorption coefficients were determined from the dependence of absorption on concentration $A = f(c)$ (concentration range of (1–5)·10^{-5} mol·dm^{-3} SPUN). Fluorescence spectra and fluorescence quantum yields were measured using a Horiba Jobin Yvon Fluorolog. Fluorescence emission spectra of polymer:fullerene blends were corrected on the re-absorption of fluorescence and co-absorption of the blend components according to the method published by Zheng et al. [9], see Supplementary information for details. Fluorescence quantum yields were measured by absolute methods using an integrating sphere. The polymer solution concentrations were adjusted to a level of light absorption equal to 0.1 in a 10 mm cuvette.

3. Results

3.1. Optical properties

The absorption and fluorescence spectra of pure materials dissolved in chlorobenzene are shown in Figure 2. The PPV-based polymers have similar position of maximum, around 480 nm, of the longest wavelength absorption band (π–π^* transition). The absorption of donor–acceptor type co-polymers (PCDTBT and PCBTDPP) is bathochromically shifted due to the presence of intramolecular charge transfer. The absorption maxima for PCDTBT and PCBTDPP were observed at 574 nm and 660 nm, respectively. The onset of PCBMs absorption was observed at 720 nm. Thus, the absorption of PCBM and polymers greatly overlap. Subsequently, due to the similar molar absorption coefficients of polymers and PCBM, it was necessary to perform the correction of fluorescence spectra on re-absorption and co-absorption in the case of polymer:PCBM mixtures. The determined optical parameters are summarized in Table 2.

The plot in Figure 2B shows the fluorescence spectra of the pure materials in chlorobenzene. The emission spectra of both PPV derivatives had a maximum at about 560 nm and continued up to 750 nm, whereas PCDTBT and PCBTDPP, which represents D–A copolymers with internal charge transfer, emit in the red region with a maximum at 685 nm and their spectra extend up to near IR range. Fullerenes exhibit several emission peaks in different wavelength ranges: a high energy emission in violet range around 350 nm (nor shown here), a green emission around 500 nm and the most often observed emission in red part around 700 nm. This red emission is overlapped with fluorescence emission of PCDTBT and PCBTDPP, the green emission overlaps the polymers absorption. The fluorescence intensity of fullerenes was found to be significantly smaller than the polymers.

The addition of PCBM to the polymer solution causes strong polymer fluorescence quenching, as can be seen from Figure 3. The figure shows plots of the fluorescence emission spectra of each polymer and its blends with $PC_{60}BM$ or $PC_{70}BM$ at a 1·10^{-4} mol·dm^{-3} concentration. In order to explore this effect, fluorescence quenching experiments were carried out at fullerene concentrations varying from 1·10^{-5} mol·dm^{-3} to 1·10^{-3} mol·dm^{-3}.

3.2. Fluorescence quenching

The quenching efficiency was evaluated from the dependence of the ratio between the fluorescence intensity of pure polymer and the fluorescence intensity of polymer mixed with fullerenes (PL_0/PL) on quencher (fullerene) concentration [Q]. The dependencies

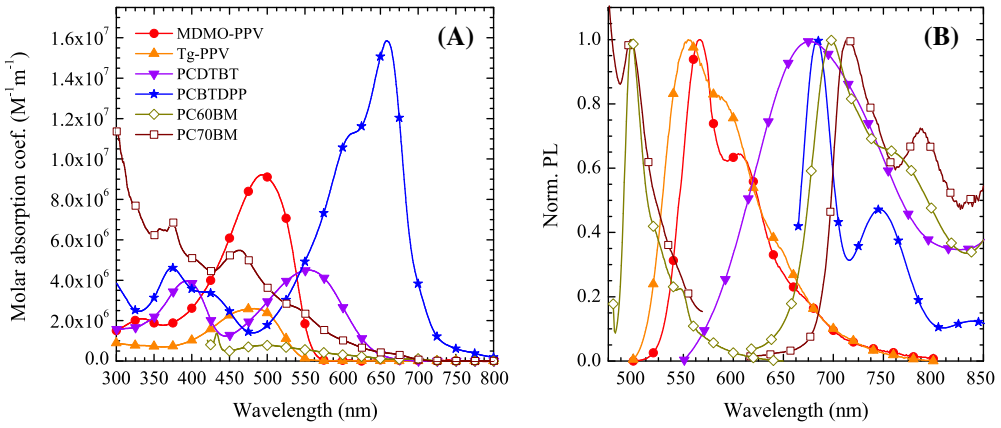

Figure 2. (A) Molar absorption coefficient spectra of the studied materials MDMO-PPV (circles), Tg-PPV (triangles), PCDTBT (rotated triangles), PCBTDPP (stars), $PC_{60}BM$ (empty rhombus) and $PC_{70}BM$ (empty squares). (B) Normalized fluorescence spectra of these materials.

Table 2
Optical parameters of polymers in chlorobenzene solution: absorption maximum $\lambda_{ABS\ max}$, molar absorption coefficient ε_{max}, fluorescence maximum $\lambda_{PL\ max}$, fluorescence lifetime τ, and quantum yield φ.

Polymer	$\lambda_{ABS\ max}$ (nm)	ε_{max} (10^7 mol^{-1} dm^3 m^{-1})	$\lambda_{PL\ max}$ (nm)	φ (%)
MDMO-PPV	495	0.92	566	41 ± 2
Tg-PPV	478	0.26	555	61 ± 6
PCDTBT	574	0.45	685	36 ± 3
PCBTDPP	660	1.58	685	40 ± 6

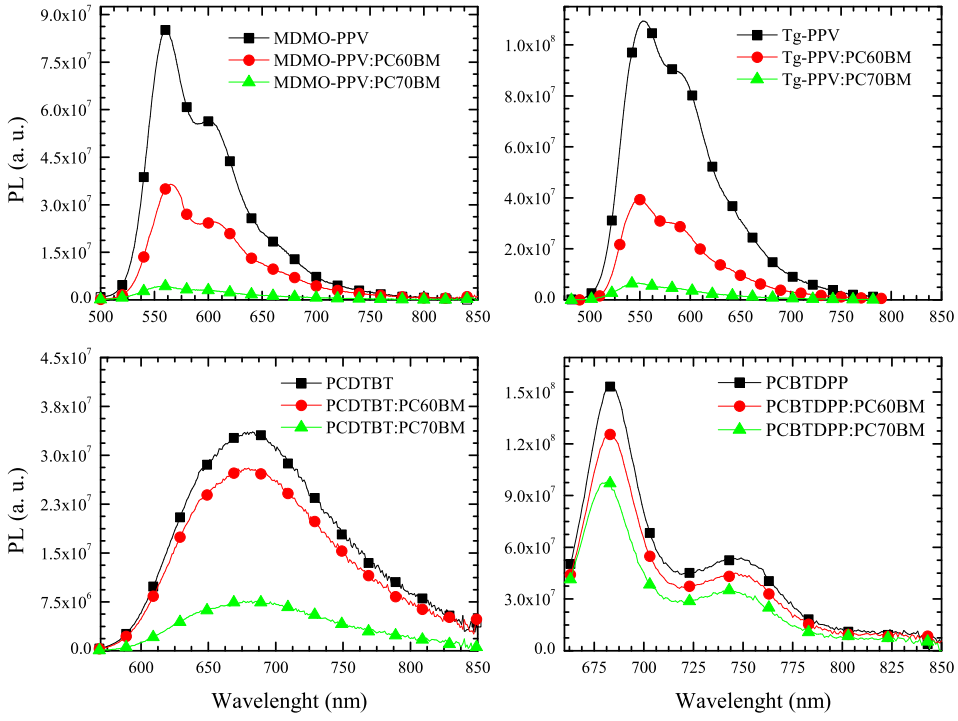

Figure 3. Emission spectra of pure polymer solutions (squares), polymer solutions with $1{\cdot}10^{-4}$ mol·dm^{-3} $PC_{60}BM$ (circles), and polymer solutions with $1{\cdot}10^{-4}$ mol·dm^{-3} $PC_{70}BM$ (triangles).

are shown in Figure 4, where fullerene concentration is depicted on a logarithmic scale, as the characterization was performed over a broad concentration range exceeding two orders of magnitude. The curve slopes were interpreted according to the Perrin equation for static quenching:

$$\frac{PL_0}{PL} = \exp(K[Q]), \tag{1}$$

where K is the equilibrium quenching constant. The Perrin model expects that quenching is possible if the distance between the exciton and quencher is smaller than radius R_{eff} [21]. This allows us to calculate the quenching sphere radius R_{eff}:

$$K = \frac{4}{3}\pi R_{eff}^3 N_A, \tag{2}$$

where N_A is Avogadro's constant. The calculated equilibrium quenching constants K are summarized in Table 3 as well as the radius of action sphere R_{eff} calculated from K. As shown in Table 3, the values of R_{eff} significantly differ according to the fullerene acceptor used ($PC_{60}BM$ vs. $PC_{70}BM$) and the type of polymer. The obtained K and R_{eff} also reveal that the fluorescence quenching of PPV polymers is more pronounced than that of copolymers PCDTBT and PCBTDPP. It was also found that the values of K noticeably correlate with the degree of polymer fluorescence and fullerene absorption overlap.

4. Discussion

It is generally accepted that fluorescence quenching in the presence of an electron acceptor (e.g. in the case of fullerenes) can take place via charge transfer (CT) or resonance energy transfer (RET). It is assumed that the thermodynamics of CT is driven by Gibbs free energy ΔG according to the Rehm–Weller equation:

$$\Delta G = I_D - E_{gap\ D} - A_A - \frac{e^2}{4\pi\varepsilon r_{AD}}, \tag{3}$$

where I_D is the ionization energy of the donor and can be approximated by the HOMO energy of the donor, A_A is the electron affinity of the acceptor and can be approximated by the LUMO energy of the acceptor, and $E_{gap\ D}$ is the bandgap of the donor; see Table 1. The last term expresses the interaction of the D–A pair with the solution, where e is the elementary charge, ε is the permittivity of the environment, and r_{AD} is the distance between the donor and the acceptor. This term can be neglected in the first approach, because its contribution is small (about 10^{-2} eV) [21]. With respect to Gibbs free energy, it is assumed that if ΔG is more negative than −0.5 eV, the quenching due to charge transfer is 100% efficient, and the small change in ΔG due to the solvent D–A pair interaction does not affect the overall charge transfer efficiency [21]. The obtained values of

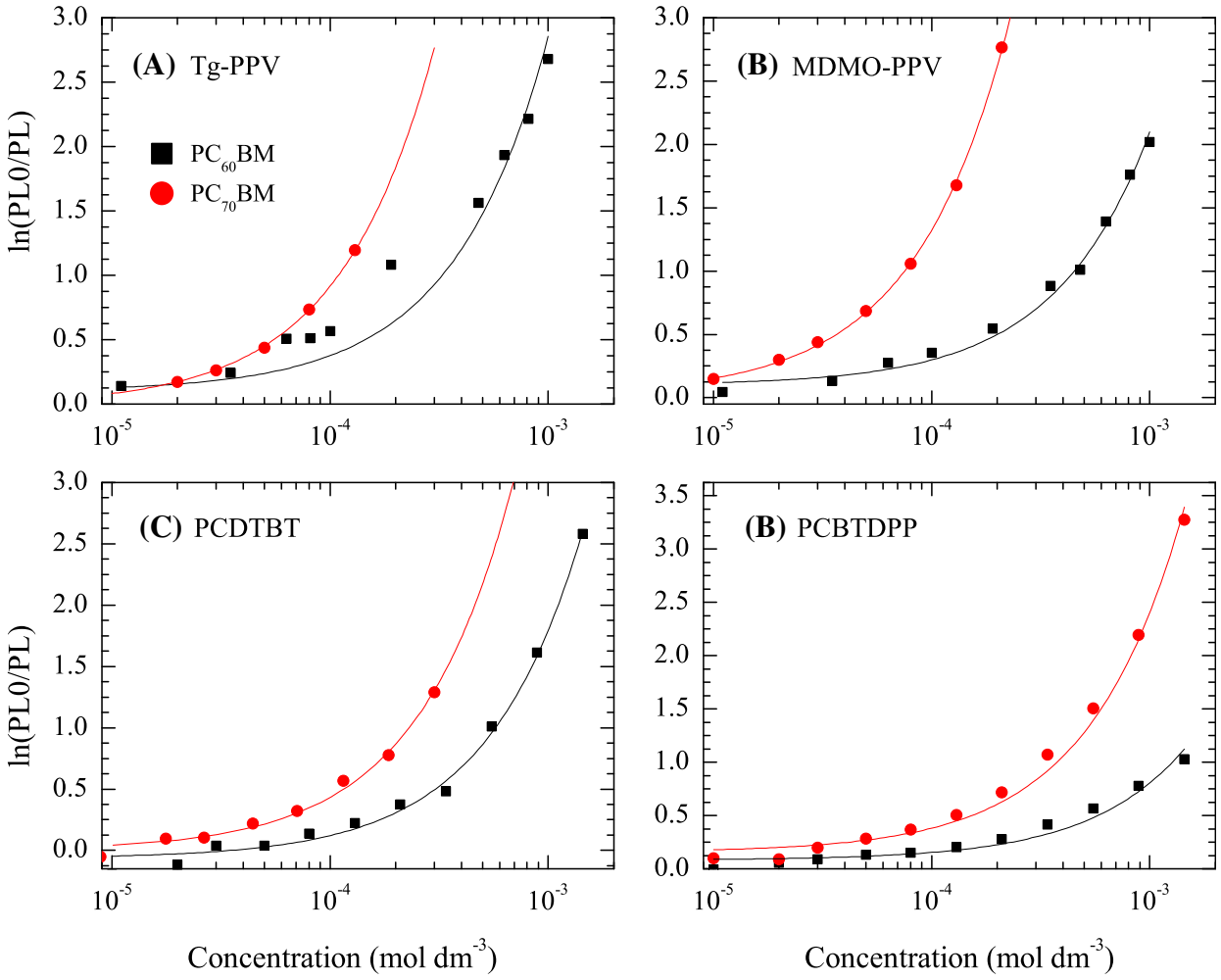

Figure 4. Perrin plots of the relative fluorescence decay of different types of polymers (A) Tg-PPV, (B) MDMO-PPV, (C) PCDTBT, and (D) PCBTDPP for concentrations of $PC_{60}BM$ (squares) and $PC_{70}BM$ (circles).

Table 3
Gibbs free energy ΔG of the charge transfer between the electron donating polymer and $PC_{60}BM$ and $PC_{70}BM$ electron acceptors, the calculated Förster critical distance R_{RET}, the experimental values of quenching equilibrium constant K calculated from the Perrin plots, and radius R_{eff} of the Perrin action sphere.

Polymer	$PC_{60}BM$					$PC_{70}BM$				
	ΔG (eV)	Ω (mol·dm^{-3} m^{-2})	R_{RET} (nm)	K (mol^{-1} dm^3)	R_{eff} (nm)	ΔG (eV)	Ω (mol·dm^{-3} m^{-2})	R_{RET} (nm)	K (mol^{-1} dm^3)	R_{eff} (nm)
MDMO-PPV	−1.28	$1.96\cdot10^{-11}$	8.5 ± 0.4	1900 ± 50	9.1 ± 0.1	−1.20	$1.55\cdot10^{-10}$	12 ± 1	6500 ± 600	13.7 ± 0.5
Tg-PPV	−1.44	$2.70\cdot10^{-11}$	10 ± 1	2380 ± 150	9.8 ± 0.2	−1.36	$2.20\cdot10^{-10}$	14 ± 1	9300 ± 500	15.4 ± 0.5
PCDTBT	−0.73	$2.49\cdot10^{-11}$	8.7 ± 0.8	1690 ± 50	8.8 ± 0.1	−0.70	$1.40\cdot10^{-10}$	12 ± 1	4300 ± 100	12.0 ± 0.1
PCBTDPP	−0.50	$0.86\cdot10^{-11}$	7 ± 1	740 ± 50	6.6 ± 0.1	−0.40	$0.42\cdot10^{-10}$	10 ± 1	2400 ± 70	9.8 ± 0.1

ΔG for each studied donor–acceptor pair are summarized in Table 3 and show that in each case the charge transfer is highly efficient.

Charge transfer, however, requires the exchange of an electron and thus the donor and acceptor have to come close together – to collide – to allow electron clouds interaction. The efficiency of CT with increasing D-A distance drops significantly and becomes negligible above 1 nm. Therefore, to observe charge transfer in our studied solutions, the concentration of the donor and acceptor had to be in the order of 10^{-1} mol·dm^{-3} to bring the molecules close enough. Close contact can also be accomplished by intermolecular interactions leading to the creation of a D–A complex. Wang et al. [10] demonstrated that water soluble PPV derivate with a highly charged backbone is strongly quenched by methyl viologen dication. This superquenching behavior was ascribed to the aggregation of the polymer and methyl viologen dication resulting from ionic interaction, which thus increased the local concentration of the quencher.

The observed large quenching constants in our study cannot be explained by this effect. Also other kinds of interaction contributing to complex formations (hydrogen bonds, cation – π-conjugated system interaction etc.) are unlikely to occur in our studied materials. It is evident that with the low concentration range used, the low frequency of donor and acceptor collisions during exciton lifetime, and the absence of D–A complexes, another quenching process efficient over a much longer distance has to occur.

One of these processes is Resonance Energy Transfer, wherein the energy is transmitted through space over a distance which can exceed more than 10 nm [21]. No collision is required and steric or electrostatic interactions play no role. The efficiency of RET can be predicted from the overlap between acceptor absorption and donor emission spectra. The spectral overlap integral Ω is given by:

$$\Omega = \int \frac{\sigma^{D}_{fluor}(\nu)\varepsilon(\nu)}{\nu^4} d\nu \quad (4)$$

where $\sigma^{D}_{fluor}(\nu)$ is the intersection of the normalized fluorescence spectrum of the donor with the normalized absorption spectrum of the acceptor, $\varepsilon(\nu)$ is the molar absorption coefficient of the acceptor ($mol \cdot dm^{-3} \cdot cm^{-1}$), and the integral is calculated over light energy expressed by wave numbers ν (cm^{-1}) [21].

The spectral overlap can be used to calculate the Förster critical distance R_{RET} at which the probability of RET is equal to 50%, according to the equation

$$R_{RET} = \left(\frac{9000 f^2 \ln 10}{128\pi^5 N_A n_0^4}\phi_D \Omega\right)^{1/6} \quad (5)$$

where f^2 is the orientational factor (for randomly orientated transition dipoles in systems [21], it is equal to 2/3), φ_D is the fluorescence yield of the donor, n_0 is the refractive index of the solvent, N_A is Avogadro's number, and Ω is the spectral overlap integral.

The calculated values of Ω and R_{RET} are listed in Table 3. There is clear evidence that the Förster critical distance R_{RET} (obtained from the spectral analysis of RET efficiency) has similar values to those obtained from the analysis of the Perrin model of static quenching R_{eff}. This proves that the observed fluorescence quenching can be fully explained by RET. Charge transfer, if present, is a minor process occurring exclusively when the polymer and PCBM collide and form a CT complex; however, such collisions will be infrequent under the conditions used here.

The molar absorption coefficient of $PC_{70}BM$ is one order of magnitude higher than of $PC_{60}BM$. As a result, the blends with $PC_{70}BM$ exhibited much higher absorption compared to the blends with $PC_{60}BM$. The fluorescence quenching experiments were therefore performed under the excitation at the maximum of the fluorescence excitation spectra of the blends in order to find the region where co-absorption by $PC_{70}BM$ is minimal. Under these conditions, R_{eff} and R_{RET} are similar and thus fluorescence quenching can be attributed to RET. MDMO-PPV did not allow such characterization and exhibited slightly higher quenching than predicted by RET.

RET as a fluorescence quenching process can also be expected in thin films, where diffusion is restricted and charge transfer can only take place at the donor–acceptor interface. Energy transfer therefore directly influences the operation of BHJ solar cells. It was suggested that the excited fullerenes (e.g. excited by the energy transfer from the polymer) undergo hole transfer to the polymer and thus contribute to the overall power conversion efficiency [17]. On the basis of the results of this work, it appears that energy transfer in BHJSC is present to a much greater extent than previously expected.

5. Conclusions

In summary, we have shown that resonance energy transfer plays a dominant role with respect to fluorescence quenching under the conditions when π-conjugated polymers and fullerenes are separated at such a distance that direct contact and electron exchange is not possible. This was concluded on the basis of the similarity between the Förster critical distance R_{RET} obtained from the spectral analysis of RET efficiency and the R_{eff} values obtained from the analysis of the Perrin model of static quenching. Resonance energy transfer is more pronounced for $PC_{70}BM$, as it has a higher absorption coefficient compared to $PC_{60}BM$.

Acknowledgement

The work was supported by the Grant Agency of the Czech Republic, project no. P205/10/2280.

Appendix A. Supplementary data

Supplementary data associated with this article can be found, in the online version, at http://dx.doi.org/10.1016/j.cplett.2013.12.050.

References

[1] T.K. Das, S. Prusty, Polym. Plast. Technol. Eng. 51 (2012) 1487.
[2] M. Ates, Mater. Sci. Eng. C 33 (2013) 1853.
[3] G. Li, R. Zhu, Y. Yang, Nat. Photon. 6 (2012) 153.
[4] N.T. Kalyani, S.J. Dhoble, Renew. Sustain. Energy Rev. 16 (2012) 2696.
[5] T. Ameri, P. Khoram, M. Min, Adv. Mater. 25 (2013) 4245.
[6] N.S. Sariciftci (Ed.), Primary Photoexcitations in Conjugated Polymers: Molecular Exciton versus Semiconductor Band Model, World Scientific Publishing Company, Incorporated, 1997.
[7] C.L. Chochos, S.A. Choulis, Prog. Polym. Sci. 36 (2011) 1326.
[8] I. Hwang, G.D. Scholes, Chem. Mater. 23 (2011) 610.
[9] M. Zheng, F. Bai, F. Li, Y. Li, D. Zhu, J. Appl. Polym. Sci. 70 (1998) 599.
[10] J. Wang, D. Wang, E.K. Miller, D. Moses, G.C. Bazan, A.J. Heeger, J. Appl. Polym. Sci. 82 (2001) 2553.
[11] J. Wang, D. Wang, D. Moses, A.J. Heeger, Macromolecules 33 (2000) 5153.
[12] H. Lin, Y. Weng, H. Huang, Q. He, M. Zheng, F. Bai, Appl. Phys. Lett. 84 (2004) 16.
[13] M. Hallermann, I. Kriegel, E. Da Como, J.M. Berger, E. von Hauff, J. Feldmann, Adv. Funct. Mater. 19 (2009) 3662.
[14] S. Engmann, V. Turkovic, P. Denner, H. Hoppe, G. Gobsch, J. Polym. Sci. Part B Polym. Phys. 50 (2012) 1363.
[15] F. Etzold, I.A. Howard, R. Mauer, M. Meister, T.-D. Kim, K.-S. Lee, N.S. Baek, F. Laquai, J. Am. Chem. Soc. 133 (2011) 9469.
[16] A.J. Ward, A. Ruseckas, I.D.W. Samuel, J. Phys. Chem. C 116 (2012) 23931.
[17] D.C. Coffey, A.J. Ferguson, N. Kopidakis, G. Rumbles, ACSnano 9 (2010) 5437.
[18] D. Beljonne, J. Cornil, D.A. dos Santos, Z. Shuai, J.L. Brédas, Excited states in poly(paraphenylenevinylene) and related oligomers: theoretical investigation of their relation to electrical and optical properties, in: N.S. Sariciftci (Ed.), Primary Photoexcitations in Conjugated Polymers: Molecular Exciton versus Semiconductor Band Model, World Scientific Publishing Company, Incorporated, 1997, pp. 559–585 (Chapter 19).
[19] B. Gieseking, B. Jaeck, E. Preis, S. Jung, M. Forster, U. Scherf, C. Deibel, V. Dyakonov, Adv. Energy Mater. 2 (2012) 1477.
[20] M. Pope, C.E. Swenberg, Electronic Processes in Organic Crystals and Polymers, vol. 2, Oxford University Press, New York, 1982.
[21] J.R. Lakowicz, Principles of Fluorescence Spectroscopy, vol. 3, Spring, 2006.
[22] D. Veldman, S.C.J. Meskers, R.A.J. Janssen, Adv. Funct. Mater. 19 (2009) 1939.
[23] K. Vandewal, A. Gadisa, W.D. Oosterbaan, S. Bertho, F. Banishoeib, I.V. Severen, Adv. Funct. Mater. 18 (2008) 2064.
[24] S.H. Park, A. Roy, S. Beaupre, S. Cho, N. Coates, J.S. Moon, D. Moses, M. Leclerc, K. Lee, A.J. Heeger, Nat. Photon. 3 (2009) 297.
[25] R. Badrou-Aich, Y. Zou, M. Leclerc, Y. Tao, Org. Electron. 11 (2010) 1053.

Appendix No 5.

Calculation of Förster critical distances in thin layers

Förster critical distances R_0 were calculated according to term:

$$R_0 = \left(\frac{9 f^2}{128 N_A \pi^5} \phi_D \int \frac{\sigma^D_{fluor}(\nu) k(\nu)}{\nu^4 n(\nu)_0^4} d\nu \right)^{1/6}$$

which is modified against to equation (24) by including the index of reflection $n(\nu)$ in spectral overlap integral due to its significant dependence on wavenumber.

$k(\nu)$ is the absorption coefficient of fullerene (in cm^{-1}). Values of $k(\nu)$ and $n(\nu)$were determined employing ellipsometry [165]. Index of reflection of Tg-PPV:$PC_{60}BM$ was substituted with data for MDMO-PPV:$PC_{60}BM$, because only negligible difference are expected. For values k and n see the following *Fig.* A and B.

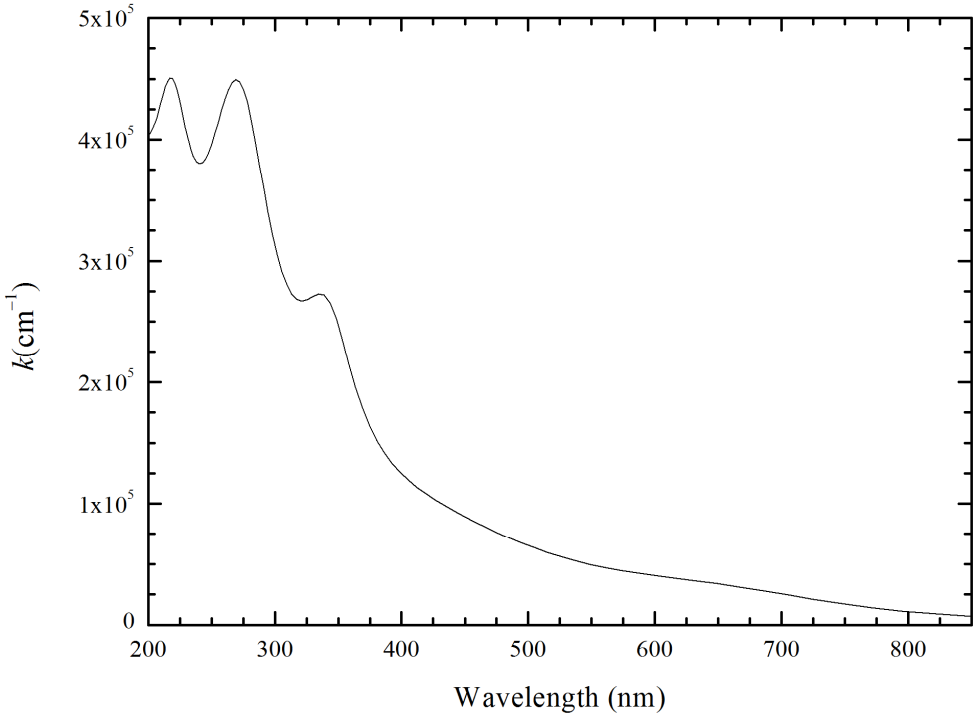

Fig. A) Extinction coefficients k of $PC_{60}BM$

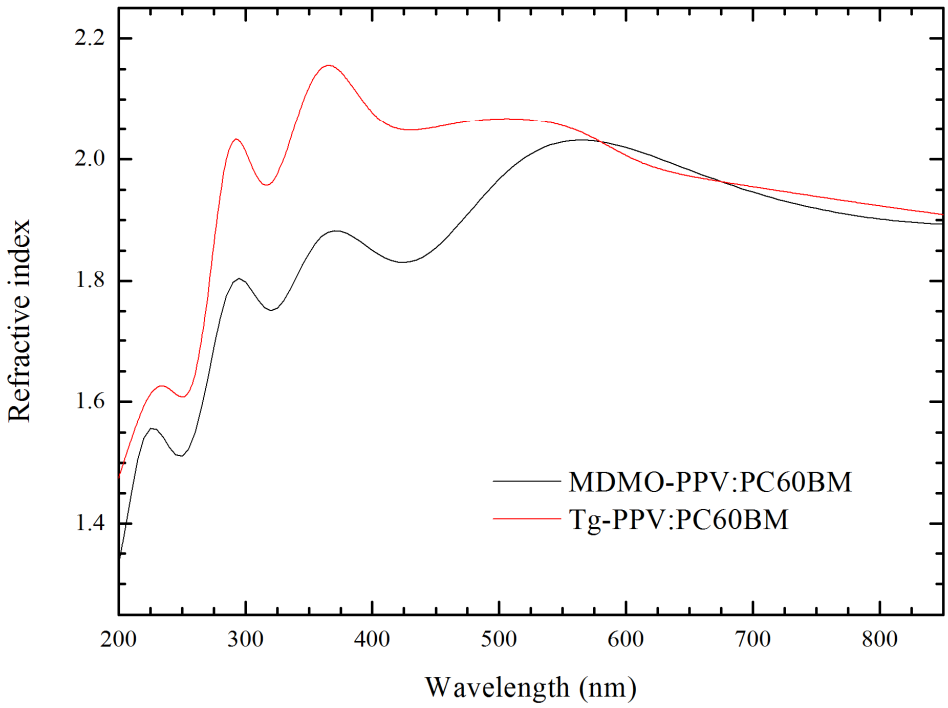

Fig. B) Index of refraction of MDMO-PPV:PC_{60}BM 1:4 and Tg-PPV:PC_{60}BM 1:4

Appendix No 6.

EQE – limits

Low detection limit of EQE determination from measured photocurrents are given by these parameters: incident light intensity, light wavelength range, and low detection limit of photocurrent. Plot on *Fig C)* shows the detection range of apparatus for spectrally resolved photocurrent experiments and low determination limits of EQE

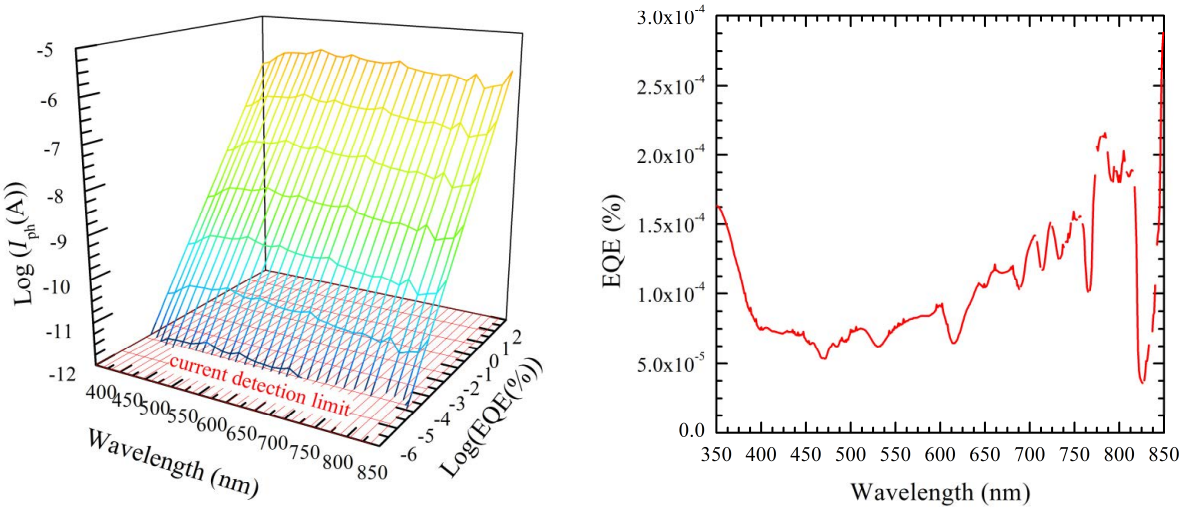

Fig. C): The plots represent the detection range of apparatus for spectrally resolved photocurrent measurements at integral incident light intensity 1 mW/cm^2, in the wavelength range 350–850 nm, currents in range 10^{-12}–10^{-2} A. The lowest values of EQE, which can be calculated from photocurrent measurement, is in the 10^{-4} % order of magnitude

Appendix No 7.

Electroluminiscence quantum efficiency

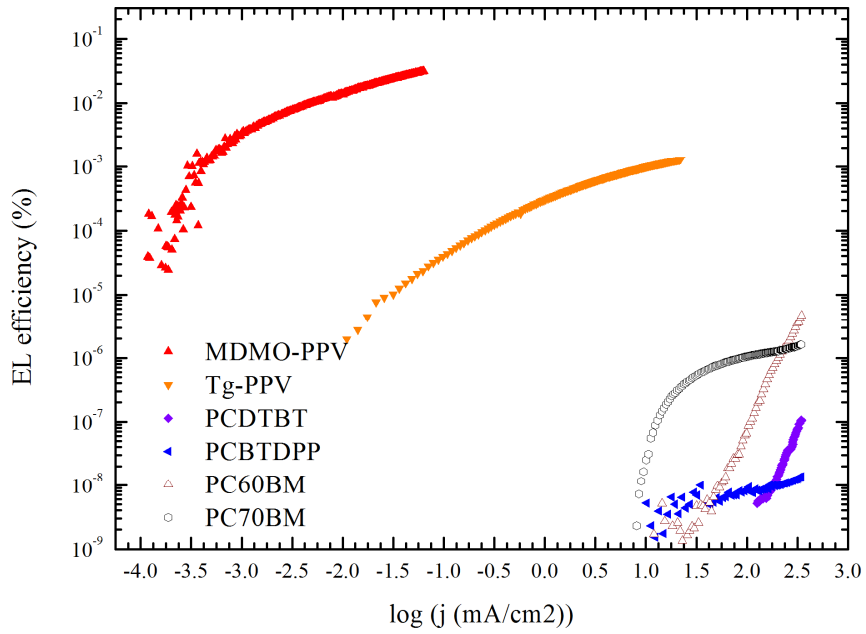

Fig. D) Electroluminescence efficiency of pristine materials

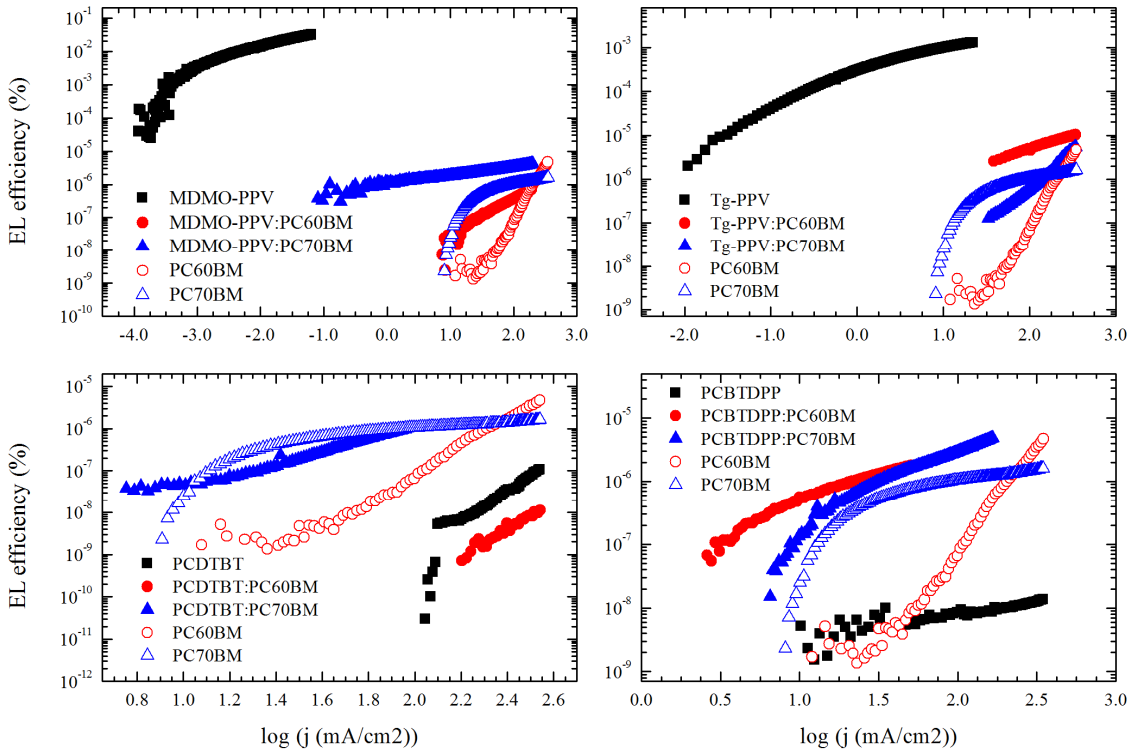

Fig. E) Electroluminescence efficiency of polymer:fullerene blends compared with pristine materials..

Appendix No 8.

Table of calculated values j_{rad}, j_{SC} and V_{OC} from EQE spectra.

Table compares values calculated directly from EQE spectra obtained from spectrally resolved photocurrent measurement and from the EQE spectra expanded beyond the detection limits of photocurrent measurements, where the edge of the EQE spectra was calculated from the emission spectra (electroluminescence or photoluminescence emission).

	Real		EQE			+ EQE IR spectrum					
Active layer	j_{SC} (mA/cm²)	V_{OC} (V)	j_{rad0} (mA/cm²)	V_{OCrad} (V)	j_{SCint} (mA/cm²)	j_{rad0}EL (mA/cm²)	V_{OCrad}EL (V)	j_{SCint}EL (mA/cm²)	j_{rad0}PL (mA/cm²)	V_{OCrad}PL (V)	j_{SCint}PL (mA/cm²)
$PC_{70}BM$	0.27	0.59	$2.26\cdot10^{-18}$	1.01	0.1215	$1.62\cdot10^{-17}$	0.97	0.1215	$3.27\cdot10^{-17}$	0.94	0.1216
$PC_{60}BM$	0.04	0.40	$5.92\cdot10^{-15}$	0.75	0.0303	$5.69\cdot10^{-17}$	0.93	0.0305	$3.62\cdot10^{-15}$	0.77	0.0303
MDMO-PPV	0.01	1.053	$5.60\cdot10^{-25}$	1.30	0.0102	$3.12\cdot10^{-23}$	1.19	0.0102	$3.38\cdot10^{-23}$	1.19	0.0102
MDMO-PPP:$PC_{60}BM$	1.32	0.74	$8.73\cdot10^{-18}$	0.95	0.9228	$2.30\cdot10^{-13}$	0.75	0.9268	$1.11\cdot10^{-14}$	0.83	0.9233
MDMO-PPV:$PC_{70}BM$	1.78	0.87	$1.63\cdot10^{-18}$	1.00	1.3101	$7.53\cdot10^{-14}$	0.79	1.3151	$1.19\cdot10^{-14}$	0.84	1.3127
Tg-PPV	$3\cdot10^{-4}$	1.09	$1.09\cdot10^{-26}$	1.32	$2.06\cdot10^{-5}$	$2.33\cdot10^{-24}$	1.18	$2.06\cdot10^{-5}$	$2.40\cdot10^{-24}$	1.18	$2.06\cdot10^{-5}$
Tg-PPV:$PC_{60}BM$	2.18	0.73	$3.60\cdot10^{-17}$	0.93	2.0115	$4.35\cdot10^{-13}$	0.75	2.0175	$1.63\cdot10^{-12}$	0.72	2.0174
Tg-PPV:$PC_{70}BM$	3.81	0.73	$3.76\cdot10^{-18}$	1.01	2.959	$1.60\cdot10^{-14}$	0.85	2.9528			
PCDTBT	0.03	0.98	$3.42\cdot10^{-21}$	1.12	0.04133	$2.45\cdot10^{-19}$	1.01	0.0435	$4.45\cdot10^{-19}$	1.00	0.04137
PCDTBT:$PC_{60}BM$	7.9	0.69	$3.51\cdot10^{-18}$	1.09	0.09481	$1.47\cdot10^{-14}$	0.87	0.09573	$2.44\cdot10^{-14}$	0.86	0.09587
PCDTBT:$PC_{70}BM$	11.7	0.75	$1.85\cdot10^{-18}$	1.11	1.312	$1.01\cdot10^{-13}$	0.83	1.357	$1.93\cdot10^{-14}$	0.89	1.314
PCBTDPP	0.04	0.65	$1.10\cdot10^{-18}$	0.98	0.03217	$1.24\cdot10^{-16}$	0.86	0.03217			
PCBTDPP:$PC_{60}BM$	4.6	0.70	$1.31\cdot10^{-15}$	0.92	2.26267	$8.19\cdot10^{-11}$	0.73	2.29	$4.72\cdot10^{-12}$	0.71	2.28
PCBTDPP:$PC_{70}BM$	6.3	0.60	$1.84\cdot10^{-16}$	0.98	4.42	$1.21\cdot10^{-12}$	0.75	4.53	$2.11\cdot10^{-12}$	0.71	4.51

Appendix No 9.

The surface roughness

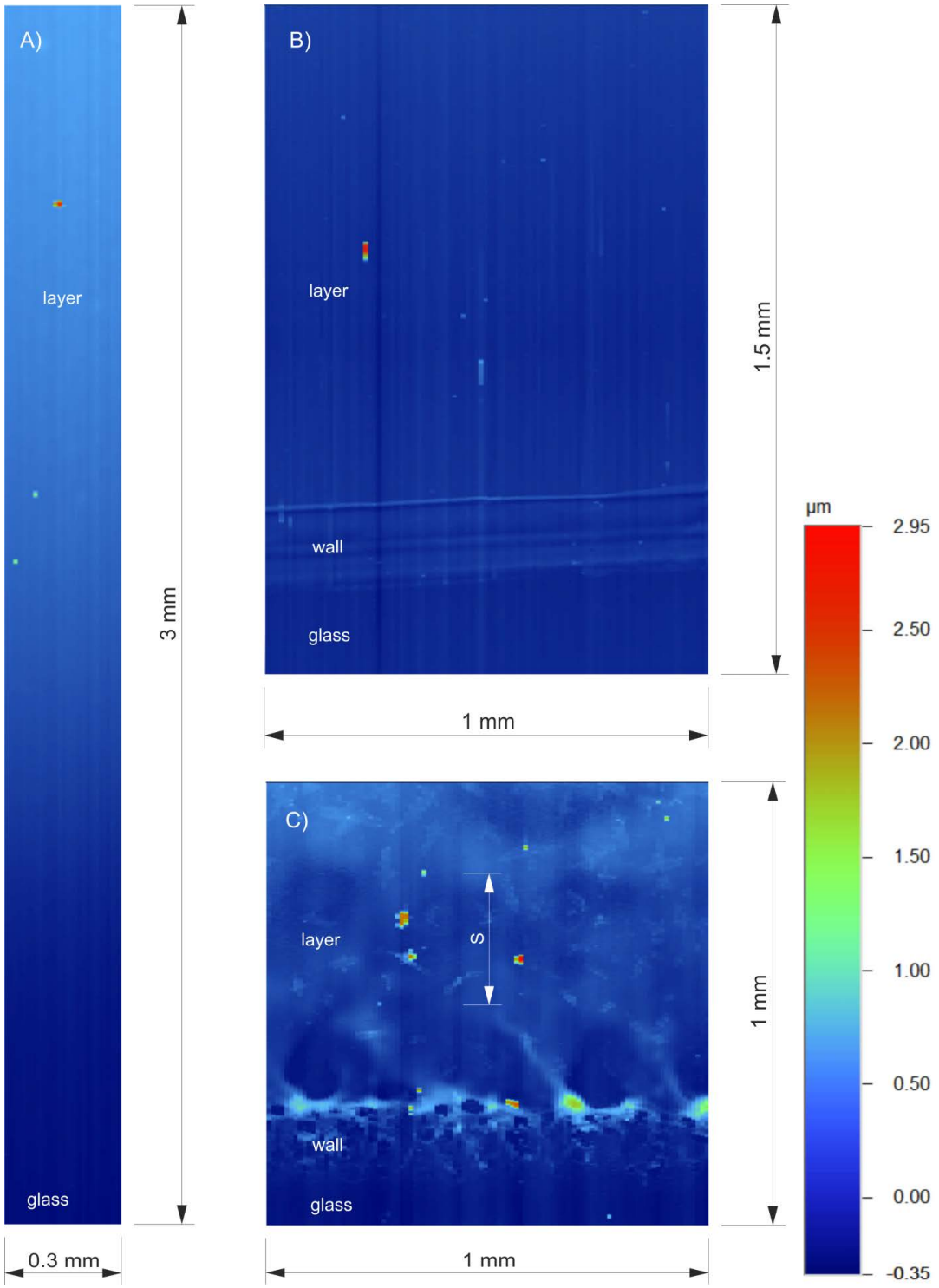

Fig. F) Surface maps of thin layers prepared employing A) electrophoretic deposition, B) spin-coating and C) inkjet printing. Vertical lines along the direction of scanning are artefacts of measurements.

The surface roughness of active layers prepared by different deposition methods: spin-coating, inkjet printing, electrophoretic deposition was studied by mechanical profilometry. Roughness of layers has significant influence on quality of other preparared layers (transport layers, electrodes) as well as on stability and functionality of whole optoelectrical devices.

Samples were analysed in the direction from clean substrate to deposed layer. Profilometry measurements provided surface profile maps, which are shown on *Fig F)*. Spin-coated layer as well as electrophoretically deposed layer were found to be texture-free under the conditions of the measurement (the resolution was in tens of nanometres order), inkjet printed layer was found textured according to previous expectation.

Surface roughness was characterized by calculation of average roughness parameter R_a.

$$R_a = \frac{1}{l}\int_0^l |Z(x)|dx$$

where l is the evaluation length and Z is the distance from meanline [184]. For illustration see *Fig. G)*:

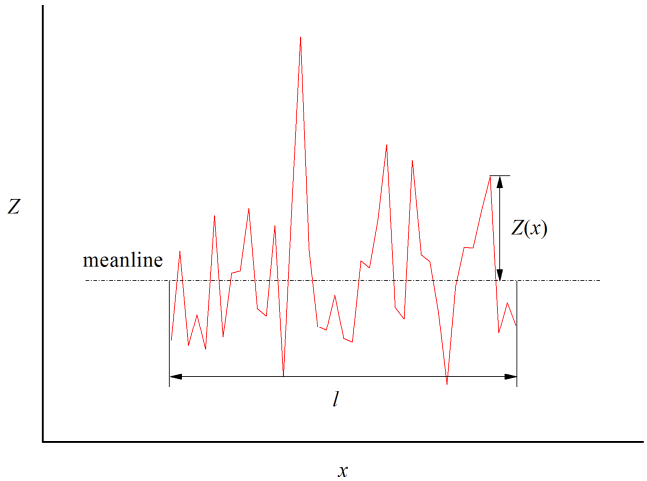

Fig. G) Graphical illustration of parameters Z(x) and l used to calculation of arithmetic average roughness R_a.

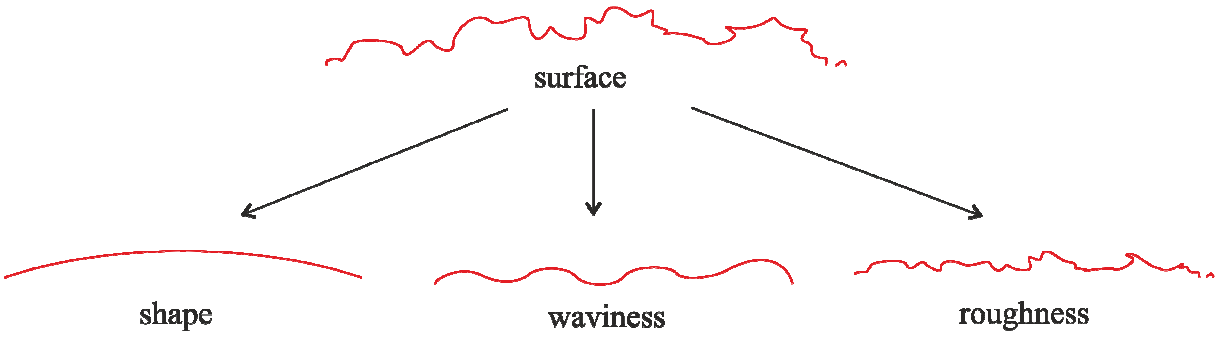

Fig. H) Scheme illustrates general approach of data analyses obtained from measurement. Surface is described by shape, waviness and roughness.

The determination of R_a parameter requires definition of surface shape and surface texture, for illustration see *Fig H)*. Approximated surface shape of prepared layers is plotted by the red line on *Fig I)*, which shows 2D profile of layers.

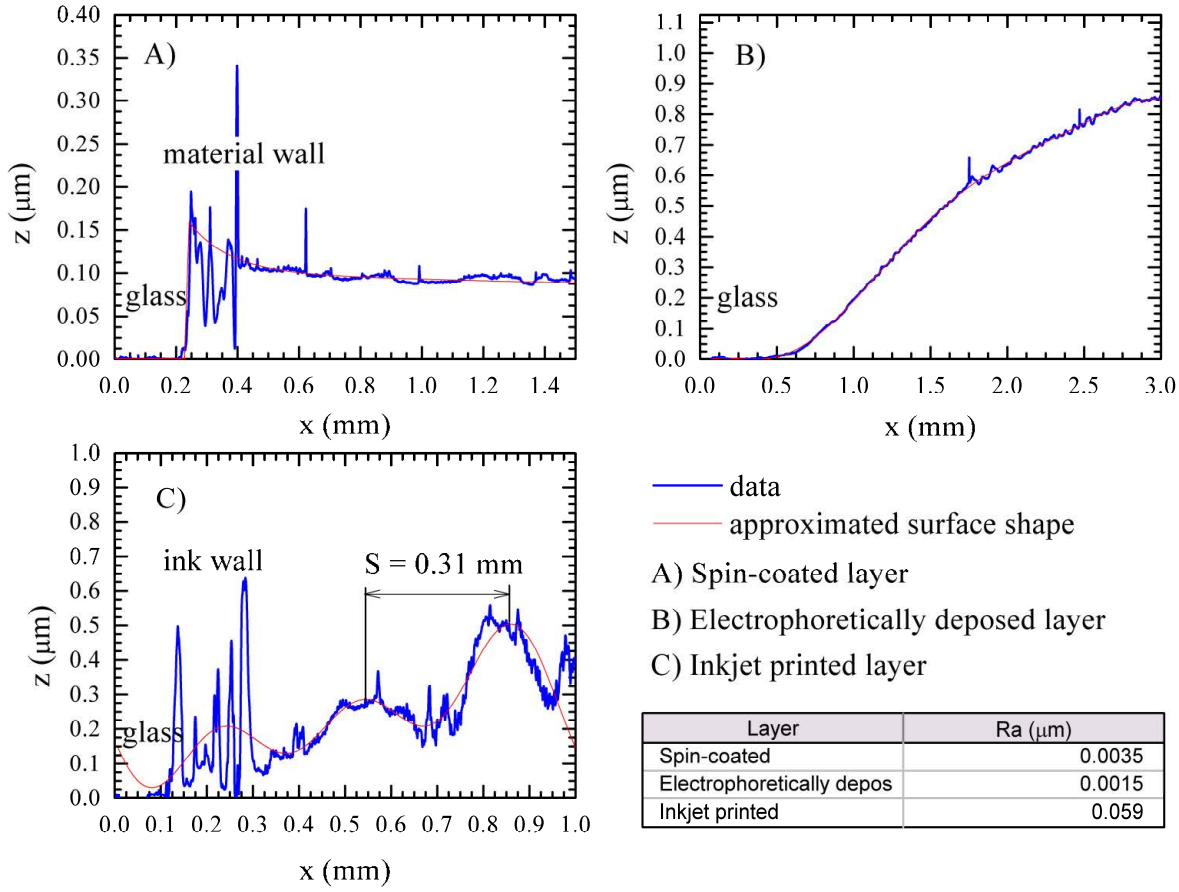

Layer	Ra (µm)
Spin-coated	0.0035
Electrophoretically depos	0.0015
Inkjet printed	0.059

Fig. I) Plots of thin layers surfaces profiles and table containing values of R_a (arithmetic average roughness) describing surface roughness.

Spin-coated layers are characterized by the layer thickness grow from the centre to the edge of layer. The profile of electrophoretically deposed layers is driven by the shape of the opposite electrode during deposition. In our cases, layers have grown faster on the substrate edge as well as layer thicknesses have grown slower at the level of suspension than in the volume of suspense during deposition. Plot on *Fig I)* shows the profile from a suspension level site, therefore the gradual increase of thickness was recorded.

Inkjet printed layer texture can be described by surface waviness, when Fourier threshold filter was applied to determination of centre elements spacing *S*. Value of *S* was found 310 nm.

Fig I) is including the table with calculated R_a parameter for each layer, after subtracting of shape and waviness of layers [184]. R_a was determined from data located behind the material wall. Electrophoretically deposed layer is the smoothest according to R_a parameter, nevertheless the R_a value of spin-coated layer is in the same order of magnitude, which is on the device detection limit. Therefore, it can be considered that the difference is only a result of statistics and both layers are similarly smooth. R_a value in the case of inkjet printed layer is one order magnitude higher than for the other layers, which is clear evidence of enhanced roughness of this layer surface.